NASA Technical Paper 1786

Low-Speed Aerodynamic Characteristics of a 17-Percent-Thick Medium-Speed Airfoil Designed for General Aviation Applications

Robert J. McGhee and William D. Beasley
Langley Research Center
Hampton, Virginia

National Aeronautics
and Space Administration

**Scientific and Technical
Information Branch**

1980

SUMMARY

An investigation was conducted in the Langley Low-Turbulence Pressure Tunnel to determine the low-speed two-dimensional aerodynamic characteristics of a 17-percent-thick medium-speed airfoil designed for general aviation applications. The results are compared with data for the 17-percent-thick low-speed airfoil and the 13-percent-thick medium-speed airfoil. Theoretical predictions of the drag-rise characteristics for the medium-speed airfoil are also provided. The tests were conducted over a Mach number range from 0.10 to 0.32, a chord Reynolds number range from 2.0×10^6 to 12.0×10^6, and an angle-of-attack range from about -8° to 20°.

The results of the investigation indicate that maximum section lift coefficients at a Mach number of 0.15 increased from about 1.6 to 2.0 as the Reynolds number increased from about 2.0×10^6 to 12.0×10^6. Stall characteristics were of the trailing-edge type and were docile at all Reynolds numbers. The application of a roughness strip near the leading edge of the airfoil decreased the maximum section lift coefficient as much as 0.04 over the test Reynolds number range. Increasing the Mach number from 0.10 to 0.32 at a constant Reynolds number of 6.0×10^6 decreased the maximum section lift coefficient about 0.03. The magnitude of the quarter-chord pitching-moment coefficient was decreased about 25 percent, and the drag coefficient decreased at all lift coefficients (fixed transition) for the 17-percent-thick medium-speed airfoil compared with the 17-percent-thick low-speed airfoil. The predominant effects of increasing airfoil thickness from 13 percent to 17 percent for the medium-speed airfoils were to decrease the maximum section lift coefficient and to increase the drag coefficient at all lift coefficients (fixed transition).

INTRODUCTION

Research on advanced-aerodynamics-technology airfoils for general aviation applications has received considerable attention over the last several years at the Langley Research Center. An initial family of low-speed airfoils was developed; this research is summarized in reference 1. Recently, the general aviation industry indicated a requirement for airfoils which provide higher cruise Mach numbers than the low-speed airfoils and which still retain good high-lift low-speed characteristics. These medium-speed airfoils have been designed to fill the gap between the low-speed airfoils and the supercritical airfoils for application on light general aviation aircraft. Reference 2 reports the results of a 13-percent-thick medium-speed airfoil designed for a lift coefficient of 0.30 and a Mach number of 0.72.

The present investigation was conducted to determine the low-speed aerodynamic characteristics of a 17-percent-thick medium-speed airfoil designed for a lift coefficient of 0.30, a Reynolds number of 14.0×10^6, and a Mach number of 0.68. This airfoil is designated as MS(1)-0317. In addition, the results are compared with data for the 17-percent-thick low-speed airfoil (LS(1)-0417)

and the 13-percent-thick medium-speed airfoil (MS(1)-0313). Theoretical predictions of the drag-rise characteristics for the medium-speed airfoil are also provided.

The investigation was performed in the Langley Low-Turbulence Pressure Tunnel over a Mach number range from 0.10 to 0.32. The Reynolds number, based on the airfoil chord, varied from about 2.0×10^6 to 12.0×10^6, and the geometric angle of attack varied from about -8° to 20°.

SYMBOLS

Values are given in both SI and U.S. Customary Units. The measurements and calculations were made in U.S. Customary Units.

c_p pressure coefficient, $\dfrac{p_\ell - p_\infty}{q_\infty}$

c airfoil chord, cm (in.)

c_c section chord-force coefficient, $\oint c_p \, d\left(\frac{z}{c}\right)$

c_d section profile-drag coefficient, $\int_{\text{Wake}} c_d' \, d\left(\frac{h}{c}\right)$

c_d' point-drag coefficient

c_ℓ section lift coefficient, $c_n \cos \alpha - c_c \sin \alpha$

c_m section pitching-moment coefficient about quarter-chord point,

$$-\oint c_p\left(\frac{x}{c} - 0.25\right) d\left(\frac{x}{c}\right) + \oint c_p \frac{z}{c} \, d\left(\frac{z}{c}\right)$$

c_n section normal-force coefficient, $-\oint c_p \, d\left(\frac{x}{c}\right)$

h vertical distance in wake profile, cm (in.)

M free-stream Mach number

p static pressure, Pa (lb/ft^2)

q dynamic pressure, Pa (lb/ft^2)

R Reynolds number based on free-stream conditions and airfoil chord

x airfoil abscissa, cm (in.)

z airfoil ordinate, cm (in.)

z_c mean camber line ordinate, cm (in.)

z_t mean thickness, cm (in.)

α geometric angle of attack, deg

Subscripts:

ℓ local point on airfoil

max maximum

∞ free-stream conditions

Abbreviations:

LS(1) low-speed, first series

MS(1) medium-speed, first series

AIRFOIL DESIGNATION

A sketch of the section shape for the 17-percent-thick medium-speed airfoil is shown in figure 1. The airfoil is designated in the form MS(1)-0317. MS(1) indicates medium speed (first series). The next two digits designate the airfoil design lift coefficient in tenths (0.30), and the last two digits designate the airfoil maximum thickness in percent chord (17).

AIRFOIL DEVELOPMENT

The intention of medium-speed airfoil development was to combine the best features of low-speed and supercritical airfoil technology; this airfoil development is discussed in detail in reference 2. The design objective of the medium-speed airfoils was to increase the cruise Mach number of the low-speed airfoils while retaining their good high-lift, low-speed characteristics. This 17-percent-thick medium-speed airfoil was designed for a lift coefficient of 0.30, a Reynolds number of 14.0×10^6, and a Mach number of 0.68. The airfoil shape was changed iteratively until the design pressure distribution was obtained. (See fig. 2.) The computer program of reference 3 was used to predict the results of various airfoil modifications.

The design pressure distributions for the 13-percent and 17-percent medium-speed airfoils are compared in figure 2. Note that for the 17-percent-thick airfoil, which has higher induced velocities, the start of the aft upper-surface pressure recovery is located at about 0.50c, compared with about 0.60c for the 13-percent airfoil. This is required in order to keep the aft pressure gradient gradual enough to avoid separation for the thicker airfoil. The thickness dis-

tribution and camber line for the 17-percent medium-speed airfoil are shown in figure 3, and the airfoil design coordinates are presented in table I.

MODEL, APPARATUS, AND PROCEDURE

Model

The airfoil model was constructed with a metal core around which plastic fill and two thin layers of fiberglass were used to form the contour of the airfoil. The model had a chord of 61 cm (24 in.) and a span of 91 cm (36 in.) and was equipped with both upper- and lower-surface orifices located 5 cm (2 in.) off the midspan. The airfoil surface was sanded in the chordwise direction with No. 400 dry silicon carbide paper to provide a smooth aerodynamic finish. The model contour accuracy was generally within ±0.10 mm (0.004 in.).

Wind Tunnel

The Langley Low-Turbulence Pressure Tunnel (ref. 4) is a closed-throat, single-return tunnel which can be operated at stagnation pressures from 1.0 to 10.0 atm (1 atm = 101.3 kPa) with tunnel-empty test-section Mach numbers up to 0.42 and 0.22, respectively. The maximum Reynolds number is about 49.0×10^6 per meter (15.0×10^6 per foot) at a free-stream Mach number of about 0.22. The tunnel test section is 91 cm (3 ft) wide and 229 cm (7.5 ft) high.

Hydraulically actuated circular plates provided positioning and attachment for the two-dimensional model. The plates are 102 cm (40 in.) in diameter, rotate with the airfoil, and are flush with the tunnel wall. The airfoil ends were attached to rectangular model-attachment plates (fig. 4), and the airfoil was mounted so that the center of rotation for the circular plates was at 0.25c on the model reference line. The air gaps in the tunnel walls between the rectangular plates and the circular plates were sealed with metal seals.

Wake Survey Rake

A fixed wake survey rake (fig. 5) at the model midspan was mounted from the tunnel sidewall and located 1 chord length behind the trailing edge of the airfoil. The wake rake used 0.15-cm (0.06-in.) diameter total-pressure tubes and 0.32-cm (0.125-in.) diameter static-pressure tubes. The total-pressure tubes were flattened to 0.10 cm (0.04 in.) for 0.61 cm (0.24 in.) from the tip of the tube. Each static-pressure tube had four flush orifices drilled 90° apart; these orifices were located 8 tube diameters from the tip of the tube and in the plane of measurement for the total-pressure tubes.

Instrumentation

Measurements of the static pressures on the airfoil surfaces and the wake-rake pressures were made by an automatic pressure-scanning system using variable-capacitance precision transducers. Basic tunnel pressures were measured with

precision quartz manometers. Angle of attack was measured with a calibrated digital shaft encoder operated by a pinion gear and rack attached to the circular model-attachment plates. Data were obtained by a high-speed acquisition system and recorded on magnetic tape.

TESTS AND METHODS

The airfoil was tested at free-stream Mach numbers from 0.10 to 0.32 over an angle-of-attack range from about -8° to 20°. Reynolds number based on the airfoil chord was varied from about 2.0×10^6 to 12.0×10^6. The airfoil was tested both in the smooth condition (natural transition) and with roughness located on both upper and lower surfaces at 0.075c. The roughness was sized for each Reynolds number according to the technique described in reference 5. The roughness was sparsely distributed and consisted of granular-type strips 0.13 cm (0.05 in.) wide which were attached to the surfaces with clear lacquer.

The static-pressure measurements at the airfoil surface were reduced to standard pressure coefficients and machine integrated to obtain section normal-force and chord-force coefficients as well as section pitching-moment coefficients about the quarter-chord point. Section profile-drag coefficients were computed from the wake-rake total and static pressures by the method reported in reference 6.

An estimate of the standard low-speed wind-tunnel boundary corrections (ref. 7) amounted to a maximum of about 2 percent of the measured coefficients; these corrections have not been applied to the data. An estimate of the displacement of the effective center of a total-pressure tube in a velocity gradient on the values of c_d showed these effects to be negligible (ref. 6).

PRESENTATION OF RESULTS

The test conditions are summarized in table II. The results of this investigation have been reduced to coefficient form and are presented in the following figures:

DISCUSSION OF RESULTS

Section Characteristics

Lift.- Figure 9(a) shows that the lift-curve slope for the 17-percent medium-speed airfoil in a smooth condition (natural boundary-layer transition) varied from about 0.11 to 0.12 per degree for the Reynolds numbers investigated (M = 0.15). The angle of attack for zero lift coefficient was about -3°. Maximum lift coefficients increased from about 1.60 to 2.0 as the Reynolds number was increased from 2.0×10^6 to 12.0×10^6. The largest effect of Reynolds number on maximum lift coefficient occurred for Reynolds numbers below 6.0×10^6. The stall characteristics of the airfoil are of the trailing-edge type, as shown by the lift data of figure 9(a) and the pressure data of figure 14. The nature of the stall is docile for all Reynolds numbers tested.

The addition of a narrow roughness strip at 0.075c (fig. 8) resulted in the expected decambering effect because of the increase in boundary-layer thickness. The lift coefficient at $\alpha = 0^\circ$ decreased about 0.04 at the lower Reynolds numbers, but only small changes occurred at the higher Reynolds numbers. The roughness strip decreased the $c_{l,max}$ performance of the airfoil as much as 0.04 for the test Reynolds number range (fig. 19).

The effects of Mach number on the airfoil lift characteristics at a Reynolds number of 6.0×10^6 with roughness located at 0.075c are shown in figure 11(a). Increasing the Mach number from 0.10 to 0.32 resulted in the expected Prandtl-Glauert increase in lift-curve slope, a decrease in the angle of attack for a stall of about 2.5°, and a decrease in $c_{l,max}$ of about 0.03.

The lift data for the 17-percent-thick low- and medium-speed airfoils are compared in figure 12 for Reynolds numbers from 2.0×10^6 to 6.0×10^6 and are summarized in figure 18. The design lift coefficients for the low-speed and medium-speed airfoils were 0.40 and 0.30, respectively. The data indicate that the linearity of the lift curve is extended to higher angles of attack for the medium-speed airfoil and that both airfoils develop about the same $c_{l,max}$ at the lower Reynolds numbers. This result is attributed to reduced upper-surface boundary-layer separation for the medium-speed airfoil, as illustrated by the pressure-data comparison of figure 16(b). At the higher Reynolds numbers (fig. 18), a decrease in $c_{l,max}$ of about 0.06 is shown for the medium-speed airfoil compared with the low-speed airfoil for airfoils without roughness. Figure 18 also illustrates two interesting features of the Reynolds number effect on $c_{l,max}$ for the 17-percent low- and medium-speed airfoils. The irregular variation of $c_{l,max}$ with Reynolds number at the lower Reynolds numbers and the sensitivity of $c_{l,max}$ to roughness for the low-speed airfoil have been improved for the medium-speed airfoil design.

The lift data for the 13-percent-thick and 17-percent-thick medium-speed airfoils are compared in figure 13 for Reynolds numbers from 2.0×10^6 to 12.0×10^6 and are summarized in figures 19 and 20. The predominant effect of increasing the airfoil thickness is to decrease $c_{l,max}$ about 0.10 at Reynolds numbers from 2.0×10^6 to 6.0×10^6. At the higher Reynolds numbers, only small effects of airfoil thickness on $c_{l,max}$ performance are shown. Figure 19 also indicates that the sensitivity of $c_{l,max}$ to roughness is somewhat greater for the thicker airfoil. The effects of Mach number on $c_{l,max}$ for both airfoils are shown in figure 20 for a Reynolds number of 6.0×10^6. Increasing the Mach number results in similar decreases in $c_{l,max}$ for both airfoils up to about $M = 0.28$. However, above $M = 0.28$, the 13-percent airfoil indicates a larger decrease in $c_{l,max}$, compared with the 17-percent airfoil.

Pitching moment.- The pitching-moment-coefficient data of figures 8, 9, and 10 illustrate the expected positive increments in c_m due to decreasing the Reynolds number or adding roughness at a constant Reynolds number. This result is typical of the decambering effect associated with boundary-layer thickening for aft-loaded airfoils. At a Reynolds number of 6.0×10^6, increasing the Mach number from 0.10 to 0.32 (fig. 11(c)) shows small effects on the pitching-moment data to about $\alpha = 8^\circ$. At the higher angles of attack, a positive increment in c_m is shown.

The pitching-moment data for the 17-percent-thick low- and medium-speed airfoils are compared in figure 12. A reduction in the magnitude of c_m of about 25 percent throughout the c_l range is indicated for the medium-speed airfoil. This result is important because of the expected reduced trim penalties for the medium-speed airfoil at cruise conditions. Comparison of

the data for the 13-percent-thick and 17-percent-thick medium-speed airfoils in figure 13 shows essentially no effect of thickness on the pitching-moment characteristics.

Drag.- The design pressure distribution for the medium-speed airfoil (fig. 2) shows that a favorable pressure gradient exists only back to about 0.10c on the upper and lower surfaces at a Mach number of 0.68. The low-speed (M = 0.15) pressure data (fig. 14) show that a pressure peak develops at about 0.06c on the upper surface of the airfoil at a lift coefficient of about 0.30. Thus, the pressure distributions are not conducive to long runs of laminar flow. Since natural transition usually occurs near the leading edge of airfoils for general aviation aircraft due to roughness of construction or insect remains gathered in flight, the discussion of the drag data is limited to data obtained with fixed transition at 0.075c.

The profile-drag coefficient at design lift ($c_l = 0.30$) decreased from about 0.0116 at $R = 2.0 \times 10^6$ to about 0.0090 at $R = 12.0 \times 10^6$. (See fig. 10(b) and fig. 21.) This drag reduction is associated with the related decrease in boundary-layer thickness and the accompanying reduction in skin-friction drag. There are only small effects of Mach number on c_d (fig. 11(b)) over a Mach number range from 0.10 to 0.32.

The drag data for the 17-percent-thick low- and medium-speed airfoils are compared in figure 12 for Reynolds numbers from 2.0×10^6 to 6.0×10^6 with fixed transition at 0.075c. A decrease in drag coefficient at all lift coefficients is shown for the medium-speed airfoil. The small decrease in drag coefficients for the medium-speed airfoil at low lift coefficients is associated with the reduced aft upper-surface pressure gradient (fig. 16(a)) and resulting boundary-layer development. The large decrease in drag coefficients at the higher lift coefficients for the medium-speed airfoil is a result of less separation on the airfoil, as illustrated in figure 16(b).

The drag data for the 13-percent-thick and 17-percent-thick medium-speed airfoils are compared in figure 13 for Reynolds numbers from 2.0×10^6 to 12.0×10^6 with fixed transition at 0.075c. Increasing the airfoil thickness results in the expected increase in drag coefficient throughout the lift coefficient range. At the design lift coefficient of 0.30, increases in c_d of about 0.0015 ($R = 2.0 \times 10^6$) and 0.0008 ($R = 12.0 \times 10^6$) are indicated by increasing the airfoil thickness from 13 to 17 percent.

Theoretically calculated drag-rise characteristics (ref. 3) for the 13- and 17-percent-thick medium-speed airfoils at design conditions are shown in figure 22. Boundary-layer transition was specified at $x/c = 0.04$ for the calculations to ensure a turbulent boundary-layer development on the airfoils. The estimated drag-rise Mach numbers are about 0.76 and 0.72 for the 13- and 17-percent airfoils, respectively.

Pressure Distributions

The chordwise pressure data of figure 14 illustrate the effects of angle of attack for several Reynolds numbers. As the angle of attack is increased,

upper-surface trailing-edge separation is first indicated by the approximate constant-pressure region on the airfoil. Additional increases in angle of attack result in this constant-pressure region moving forward along the airfoil. At maximum lift, trailing-edge separation is present over approximately 20 to 30 percent of the airfoil chord, depending on the Reynolds number. The airfoil stall is of the trailing-edge type, and the stall characteristics are docile at all Reynolds numbers.

The effects of Mach number on the chordwise pressure data at a Reynolds number of 6.0×10^6 for angles of attack of 8° and 14° are illustrated in figure 15. Increasing the Mach number from 0.10 to 0.32 results in the expected Prandtl-Glauert increase in the value of C_p at $\alpha = 8^\circ$ (fig. 15(a)). However, at $\alpha = 14^\circ$ (fig. 15(b)), this same Mach number increase results in an increase in the extent of upper-surface trailing-edge separation of about 0.05c. This result is attributed to the increased upper-surface pressure gradient, which has an adverse effect on the resulting boundary-layer development.

Comparisons of the pressure data for the 17-percent-thick low- and medium-speed airfoils at a Mach number of 0.15 and a Reynolds number of 4.0×10^6 are shown in figure 16. Note the substantial decrease in the aft upper-surface pressure gradient for the medium-speed airfoil (fig. 16(a)). This reduced pressure gradient has a favorable effect on the airfoil boundary-layer development (reduced thickness) and results in a small decrease in drag coefficient at low lift coefficients (see fig. 12). At the higher lift coefficients, this reduced pressure gradient decreases the amount of upper-surface trailing-edge separation for the medium-speed airfoil. For example, at a lift coefficient of 1.60 (fig. 16(b)), the medium-speed airfoil exhibits about 0.10c less separation than the low-speed airfoil.

The pressure data for the 13-percent-thick and 17-percent-thick medium-speed airfoils at a Mach number of 0.15 and a Reynolds number of 4.0×10^6 are compared in figure 17. The pressure data at $\alpha = 0^\circ$ (fig. 17(a)) illustrate the increase in upper- and lower-surface velocities due to increased airfoil thickness. Note that the aft upper-surface pressure gradient is about the same for the two airfoils. The effect of thickness on the extent of upper-surface trailing-edge separation is illustrated at $\alpha = 16^\circ$ in figure 17(c). The 13-percent medium-speed airfoil exhibits about 0.15c less separation compared with the 17-percent airfoil.

CONCLUDING REMARKS

Wind-tunnel tests have been conducted to determine the low-speed two-dimensional aerodynamic characteristics of a 17-percent-thick medium-speed airfoil designed for general aviation applications. The results were compared with those for the 17-percent-thick low-speed airfoil and the 13-percent-thick medium-speed airfoil. Theoretical predictions of the drag-rise characteristics for this airfoil are also provided. The tests were conducted in the Langley Low-Turbulence Pressure Tunnel over a Mach number range from 0.10 to 0.32. The chord Reynolds number was varied from about 2.0×10^6 to 12.0×10^6. The following results were determined from this investigation:

1. Maximum section lift coefficients at a Mach number of 0.15 increased from about 1.6 to 2.0 as the Reynolds number was increased from about 2.0×10^6 to 12.0×10^6.

2. Stall characteristics were of the trailing-edge type and were docile at all Reynolds numbers.

3. The application of a roughness strip near the leading edge of the airfoil decreased the maximum section lift coefficient as much as 0.04 over the test Reynolds number range.

4. Increasing the Mach number from 0.10 to 0.32 at a constant Reynolds number of about 6.0×10^6 decreased the maximum section lift coefficient about 0.03.

5. The magnitude of the quarter-chord pitching-moment coefficient was decreased about 25 percent, and the drag coefficient decreased at all lift coefficients (fixed transition) for the 17-percent-thick medium-speed airfoil compared with the 17-percent-thick low-speed airfoil.

6. The predominant effects of increasing airfoil thickness from 13 percent to 17 percent for the medium-speed airfoils were to decrease the maximum section lift coefficient and to increase the drag coefficient at all lift coefficients (fixed transition).

Langley Research Center
National Aeronautics and Space Administration
Hampton, VA 23665
November 25, 1980

REFERENCES

1. McGhee, Robert J.; Beasley, William D.; and Whitcomb, Richard T.: NASA Low- and Medium-Speed Airfoil Development. NASA TM-78709, 1979.

2. McGhee, Robert J.; and Beasley, William D.: Low-Speed Aerodynamic Characteristics of a 13-Percent-Thick Medium-Speed Airfoil Designed for General Aviation Applications. NASA TP-1498, 1979.

3. Bauer, Frances; Garabedian, Paul; Korn, David; and Jameson, Antony: Supercritical Wing Sections II. Volume 108 of Lecture Notes in Economics and Mathematical Systems, Springer-Verlag, 1975.

4. Von Doenhoff, Albert E.; and Abbott, Frank T., Jr.: The Langley Two-Dimensional Low-Turbulence Pressure Tunnel. NACA TN 1283, 1947.

5. Braslow, Albert L.; and Knox, Eugene C.: Simplified Method for Determination of Critical Height of Distributed Roughness Particles for Boundary-Layer Transition at Mach Numbers From 0 to 5. NACA TN 4363, 1958.

6. Pankhurst, R. C.; and Holder, D. W.: Wind-Tunnel Technique. Sir Isaac Pitman & Sons, Ltd. (London), 1965.

7. Pope, Alan; and Harper, John J.: Low-Speed Wind Tunnel Testing. John Wiley & Sons, Inc., c.1966.

TABLE I.- MS(1)-0317 AIRFOIL COORDINATES

x/c	z/c, upper	z/c, lower
0.00000	0.00099	0.00099
.00200	.01248	-.00857
.00500	.01950	-.01366
.01250	.03099	-.02105
.02500	.04322	-.02866
.03750	.05210	-.03423
.05000	.05893	-.03865
.07500	.06840	-.04541
.10000	.07511	-.05058
.12500	.08033	-.05477
.15000	.08454	-.05817
.17500	.08805	-.06099
.20000	.09096	-.06330
.22500	.09339	-.06527
.25000	.09536	-.06685
.27500	.09694	-.06812
.30000	.09815	-.06909
.32500	.09901	-.06978
.35000	.09952	-.07021
.37500	.09972	-.07036
.40000	.09956	-.07019
.42500	.09909	-.06967
.45000	.09826	-.06880
.47500	.09700	-.06755
.50000	.09535	-.06591
.52500	.09323	-.06389
.55000	.09073	-.06138
.57500	.08777	-.05845
.60000	.08448	-.05501
.62500	.08079	-.05106
.65000	.07672	-.04674
.67500	.07232	-.04214
.70000	.06763	-.03735
.72500	.06269	-.03255
.75000	.05755	-.02780
.77500	.05225	-.02309
.80000	.04687	-.01857
.82500	.04132	-.01433
.85000	.03576	-.01049
.87500	.03013	-.00719
.90000	.02444	-.00460
.92500	.01873	-.00289
.95000	.01302	-.00232
.97500	.00720	-.00324
1.00000	.00125	-.00597

TABLE II.- TEST CONDITIONS

M	R					Configuration
	2×10^6	4×10^6	6×10^6	9×10^6	12×10^6	
0.15	×	×	×	×	×	Smooth
.10			×			Roughness on
.15	×	×	×	×	×	Roughness on
.20			×			Roughness on
.28			×			Roughness on
.32			×			Roughness on

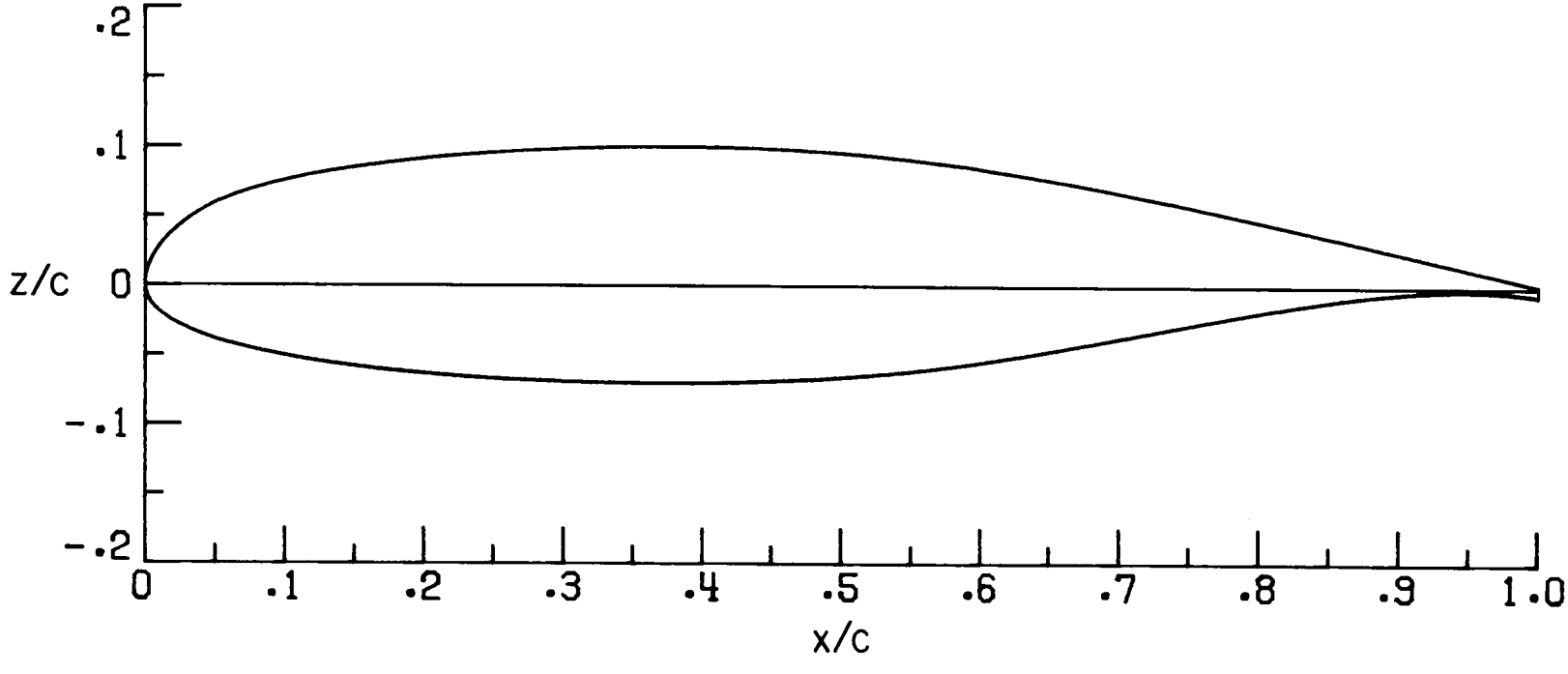

Figure 1.- Section shape for MS(1)-0317 airfoil.

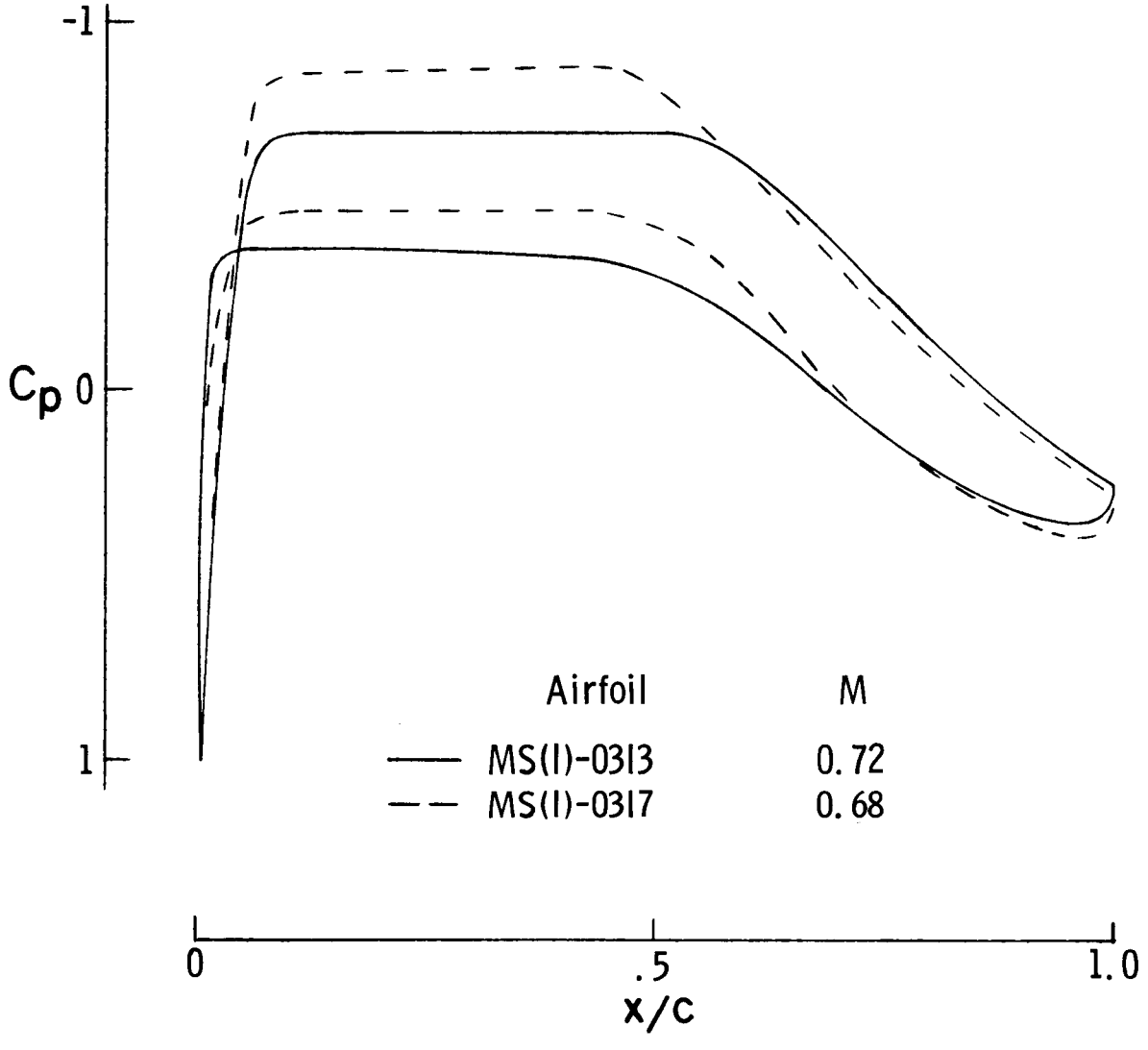

Figure 2.- Calculated pressure distributions for medium-speed airfoils. $R = 14.0 \times 10^6$; $c_l = 0.30$.

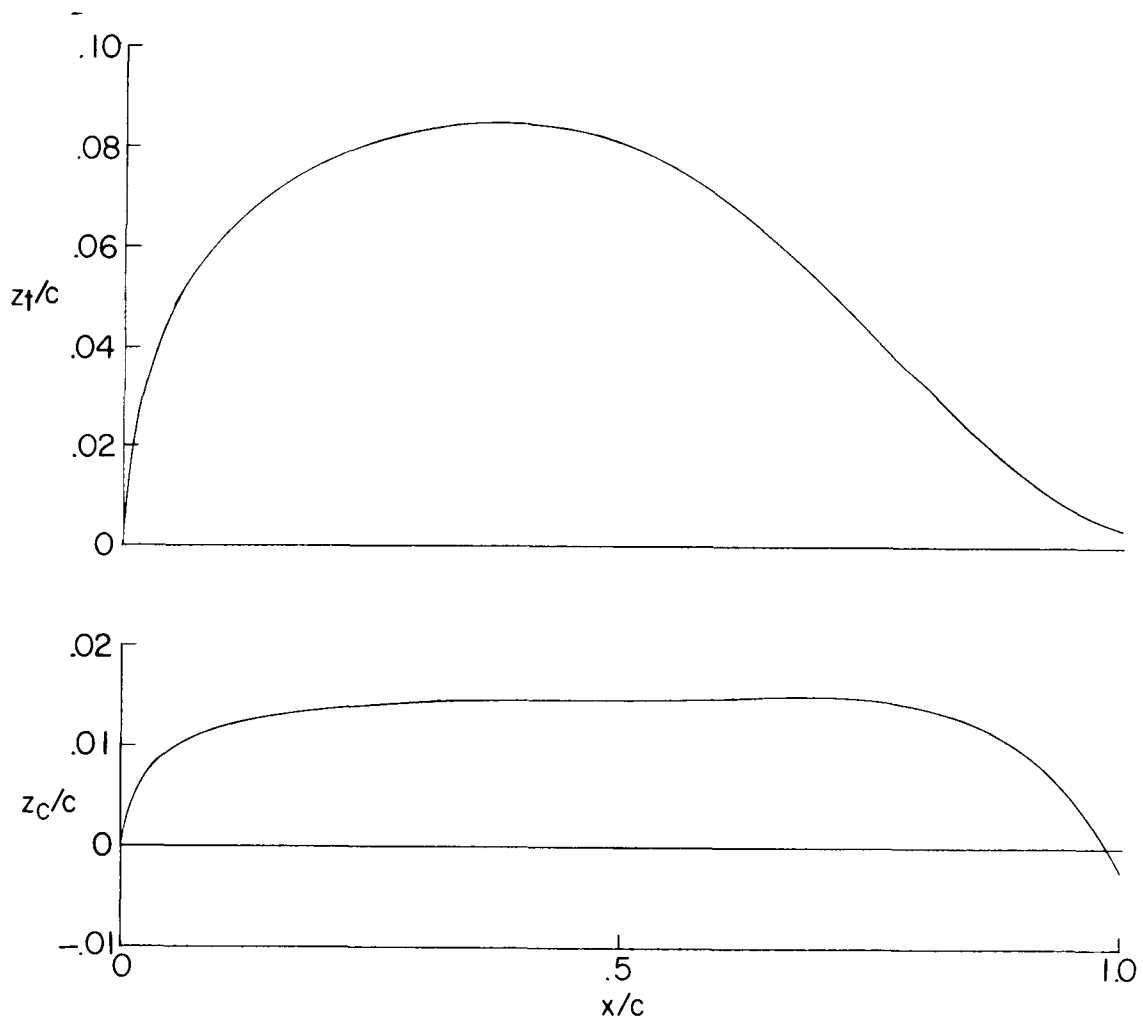

Figure 3.- Thickness distribution and camber line for MS(1)-0317 airfoil.

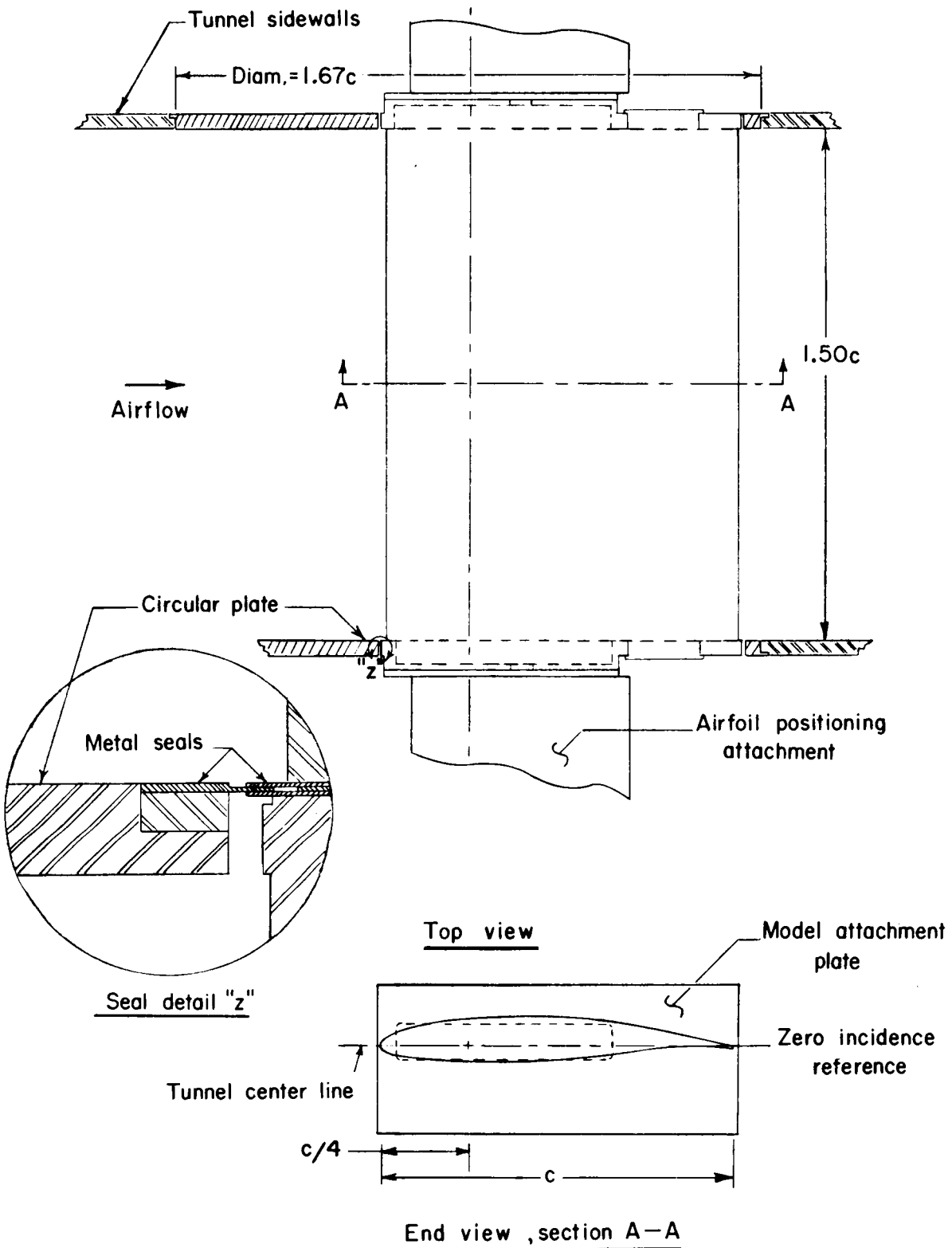

Figure 4.- Typical airfoil model mounted in wind tunnel. c = 61 cm (24 in.).

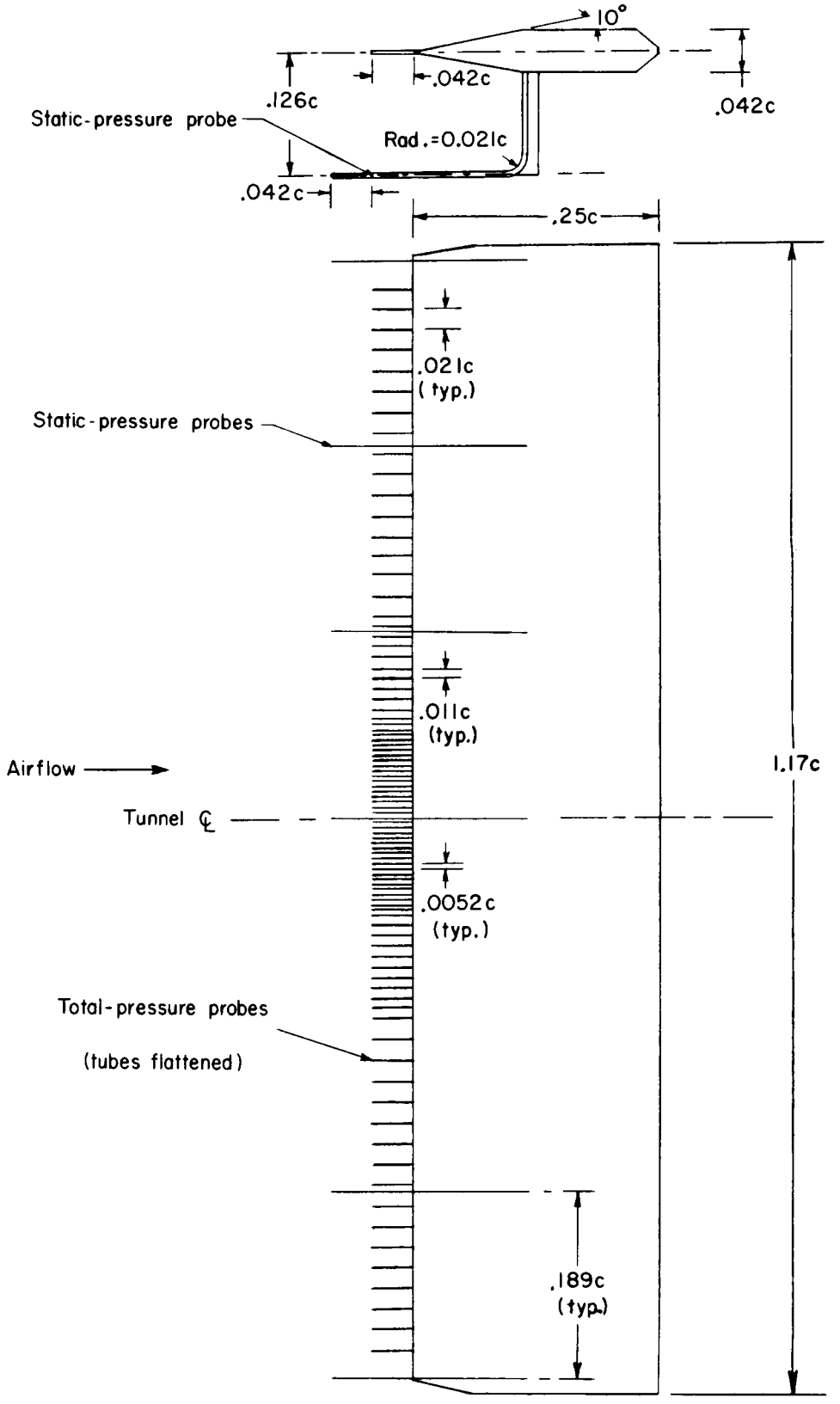

Figure 5.- Wake survey rake. c = 61 cm (24 in.).

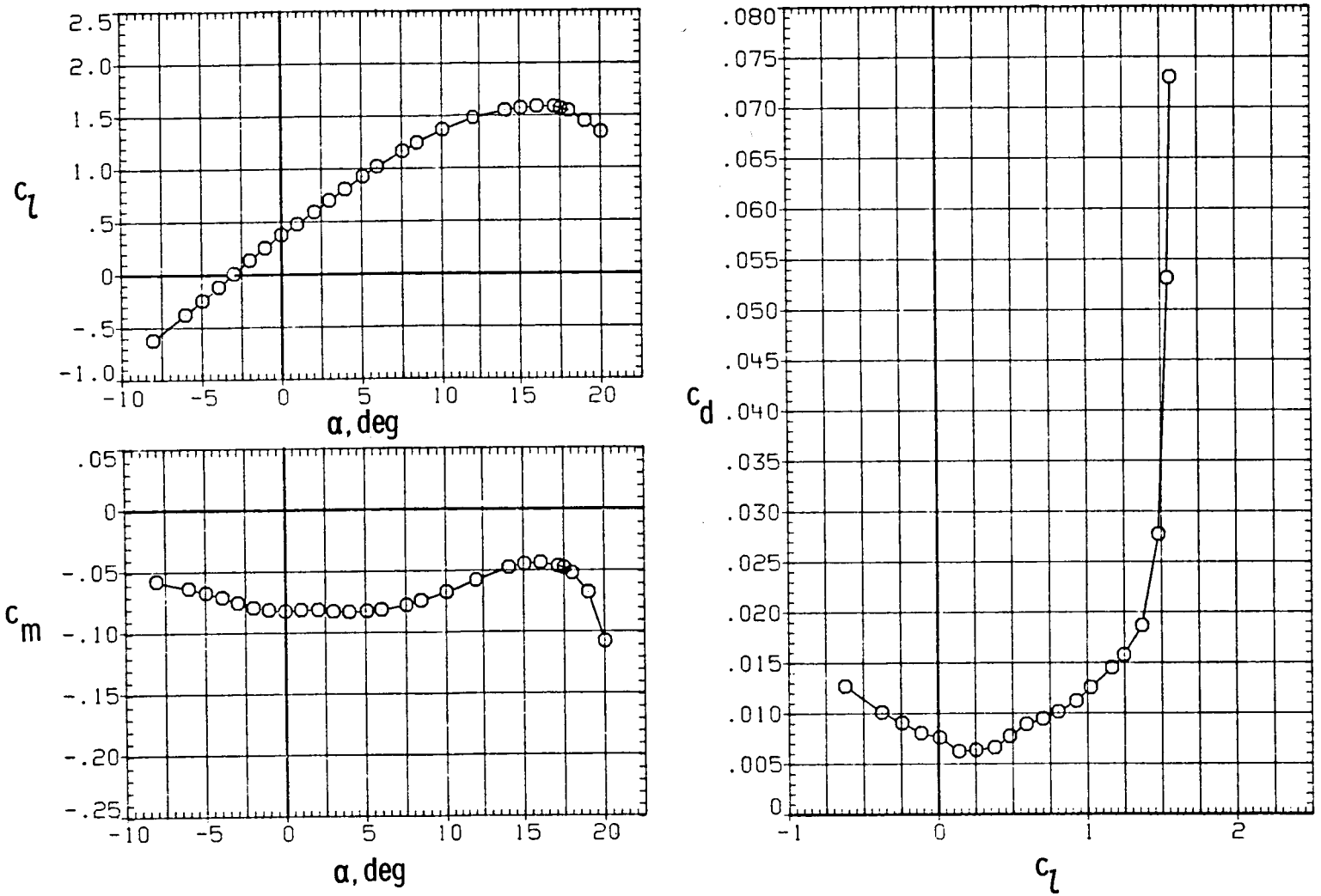

(a) $R = 2.0 \times 10^6$.

Figure 6.- Section characteristics for MS(1)-0317 airfoil. Model smooth; M = 0.15.

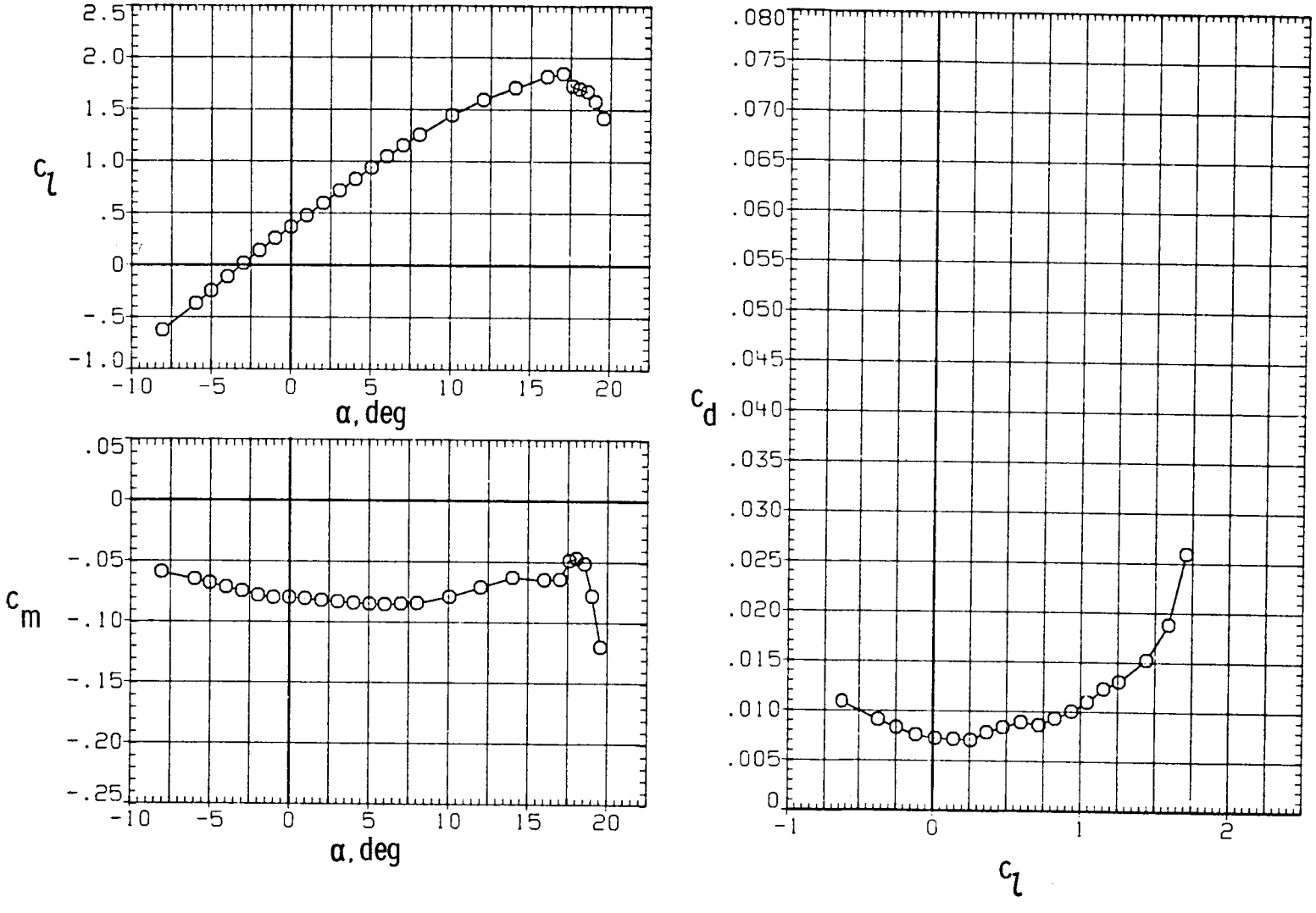

(b) $R = 4.0 \times 10^6$.

Figure 6.- Continued.

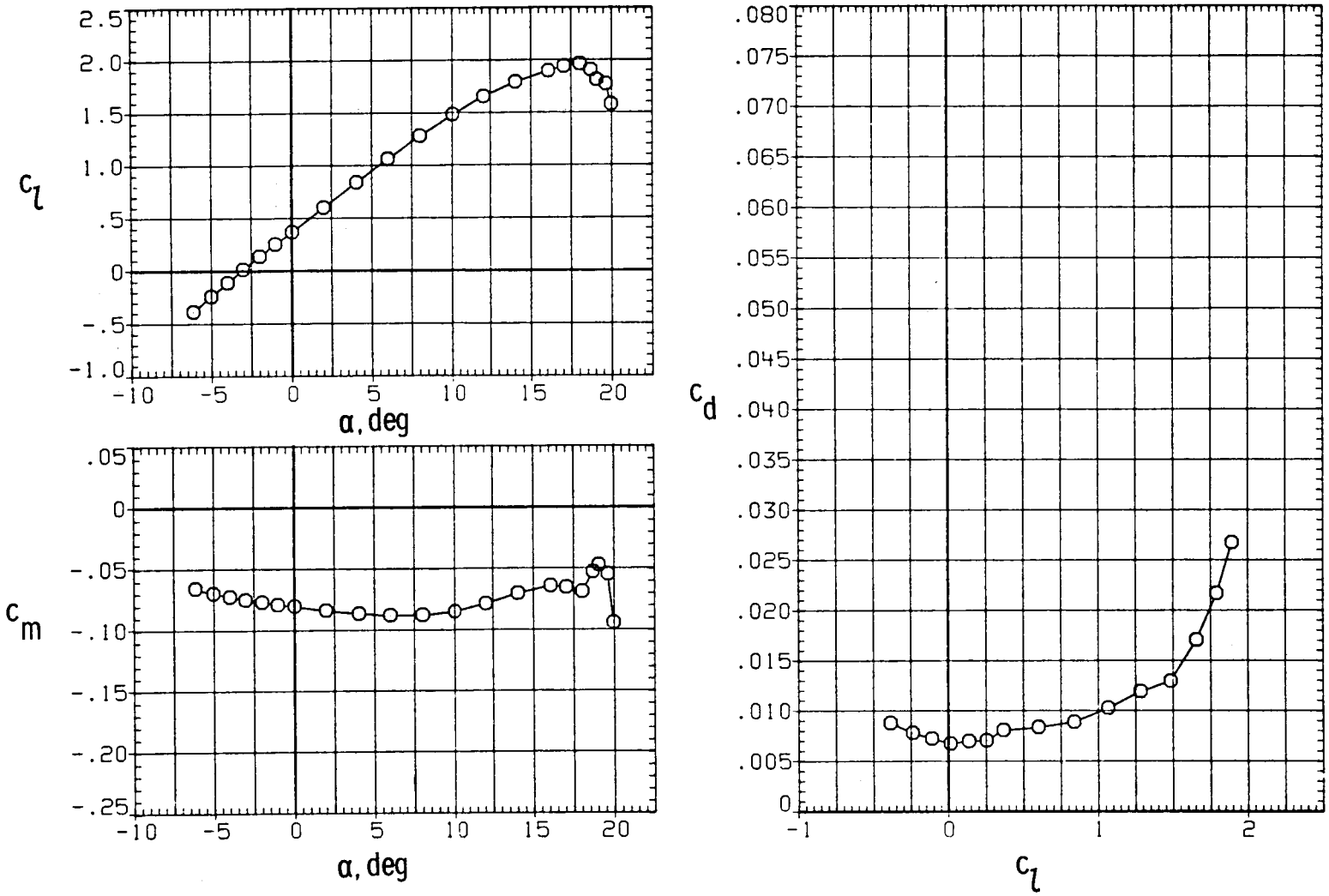

(c) $R = 6.0 \times 10^6$.

Figure 6.- Continued.

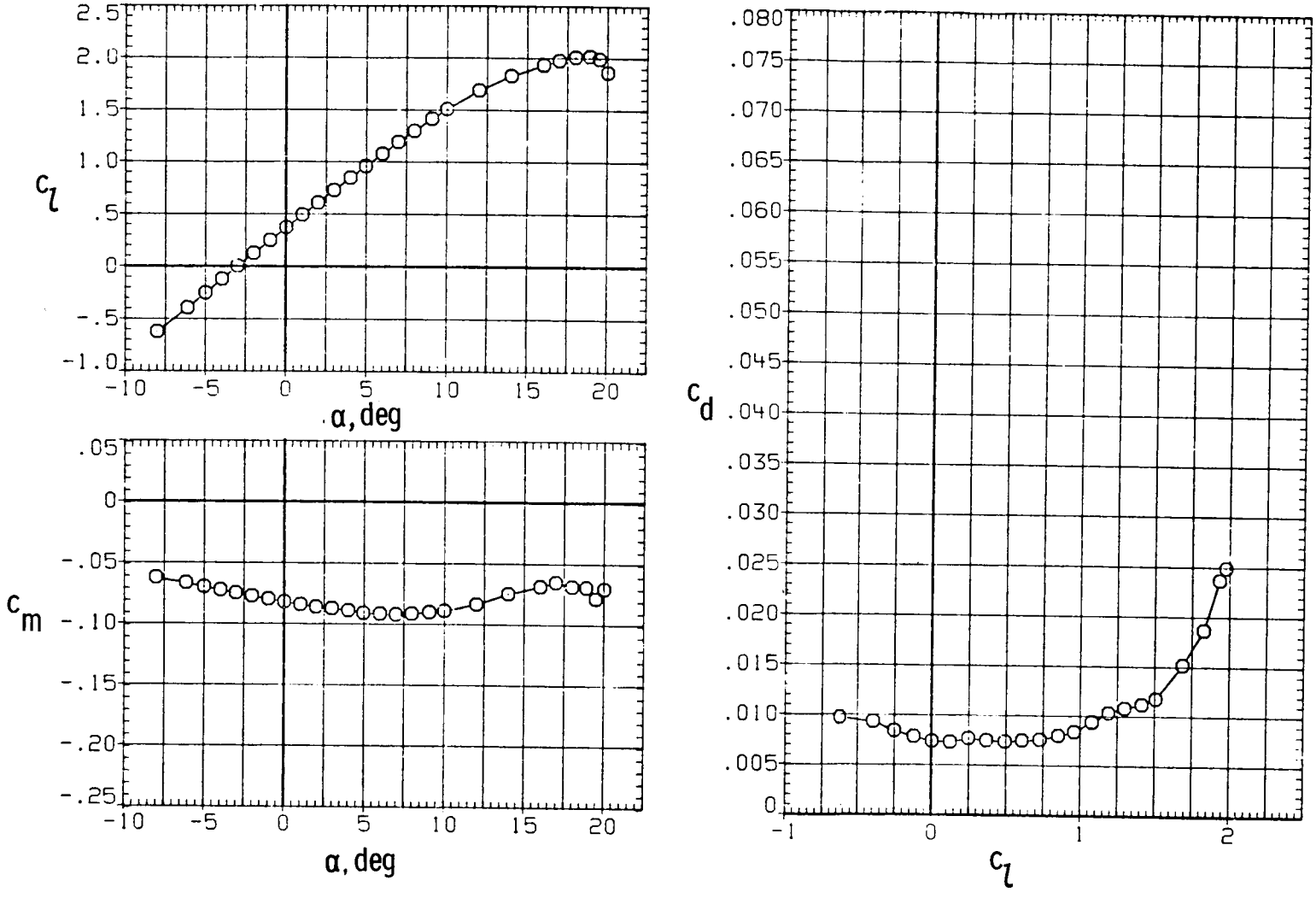

(d) $R = 9.0 \times 10^6$.

Figure 6.- Continued.

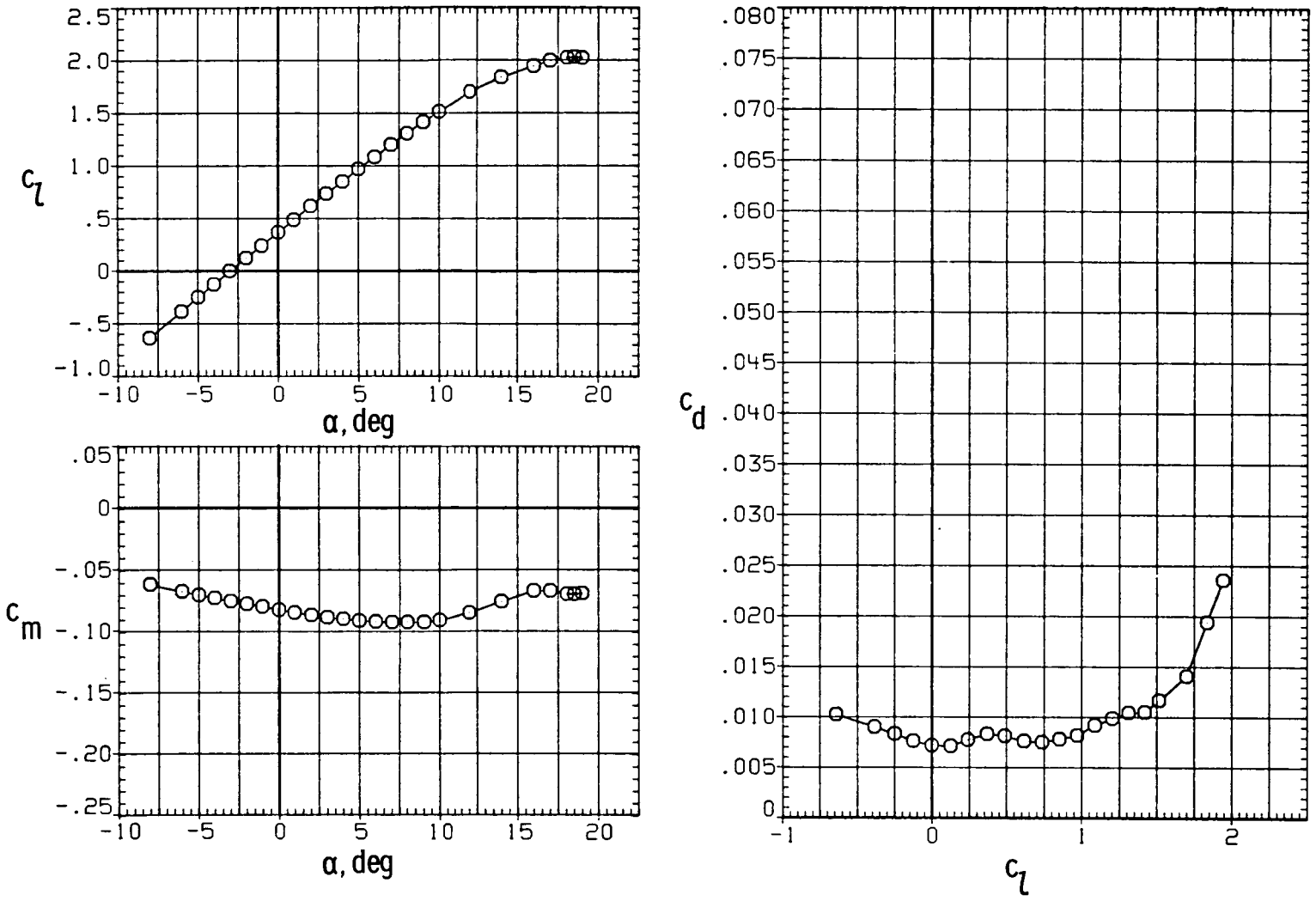

(e) $R = 12.0 \times 10^6$.

Figure 6.- Concluded.

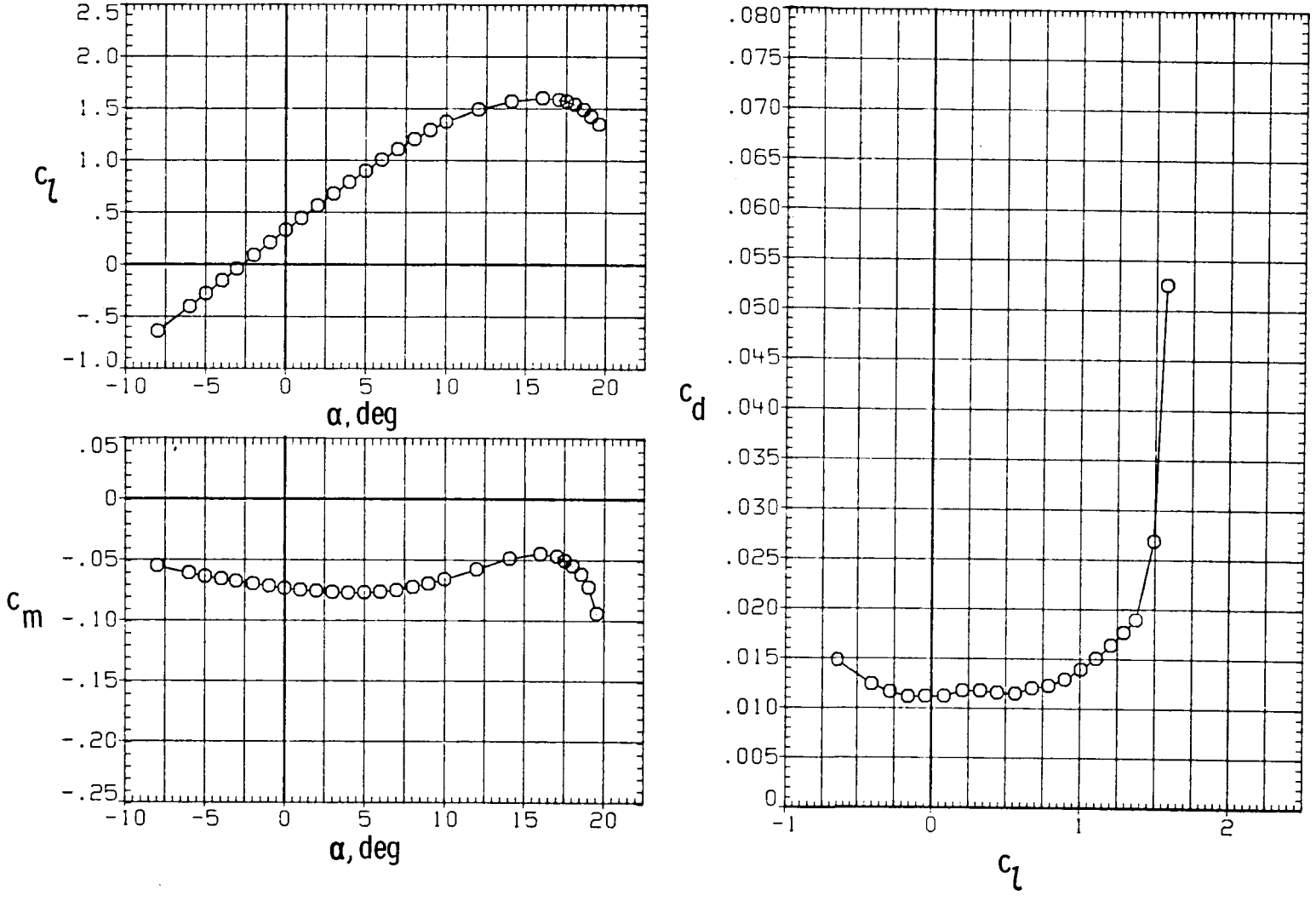

(a) M = 0.15; R = 2.0×10^6.

Figure 7.- Section characteristics for MS(1)-0317 airfoil. Roughness located at 0.075c.

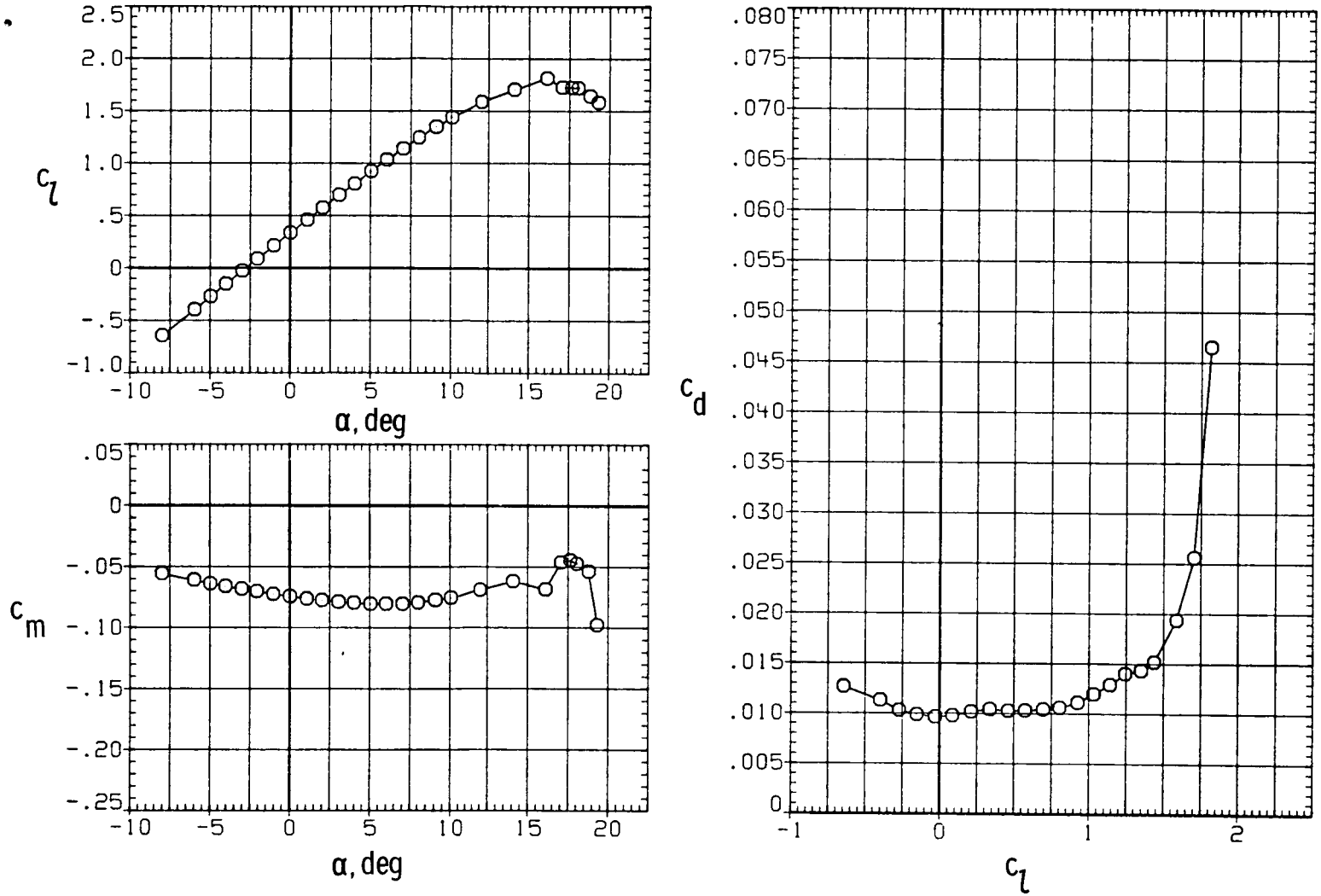

(b) M = 0.15; R = 4.0 × 10^6.

Figure 7.- Continued.

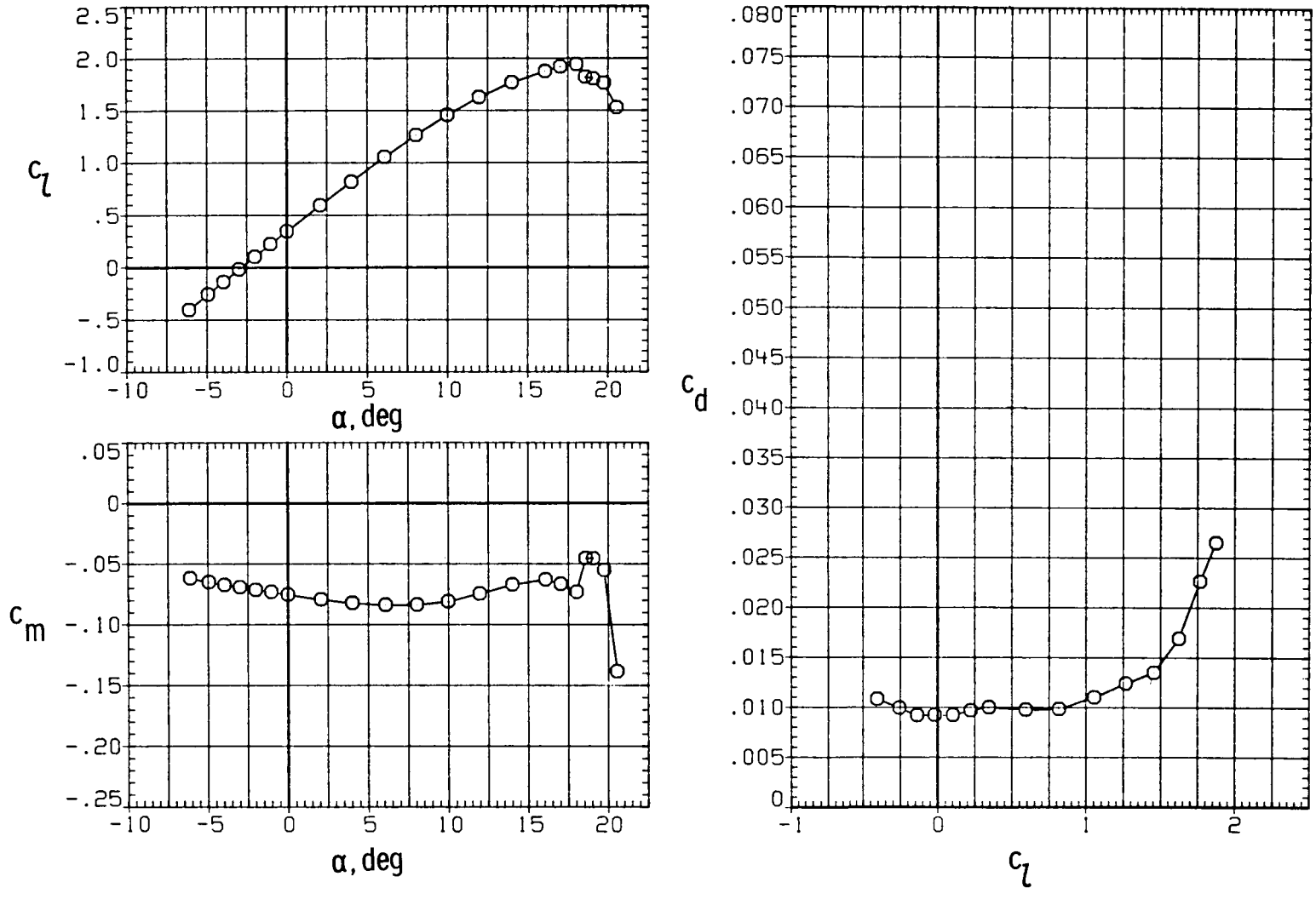

(c) M = 0.10; R = 6.0×10^6.

Figure 7.- Continued.

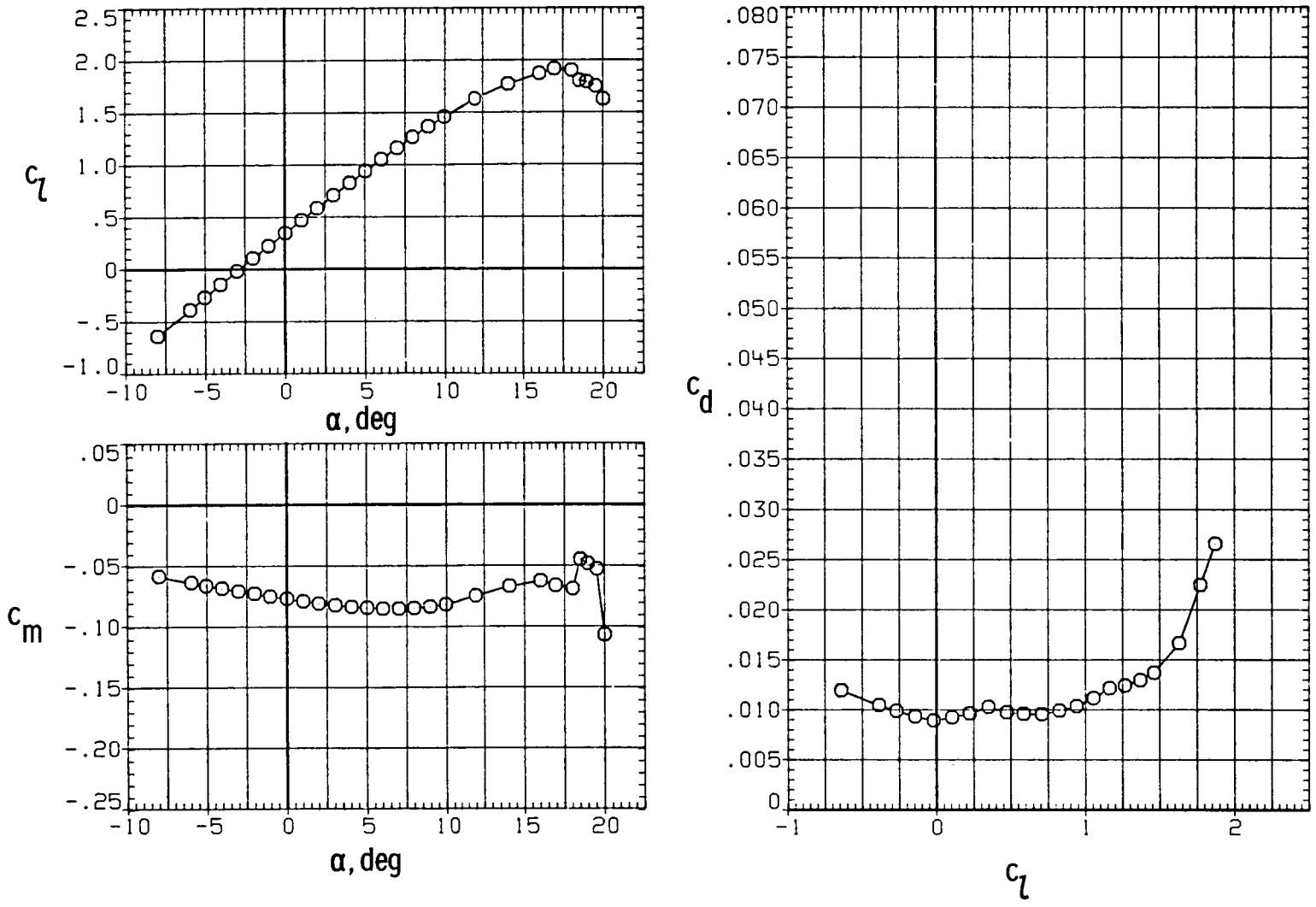

(d) M = 0.15; R = 6.0×10^6.

Figure 7.- Continued.

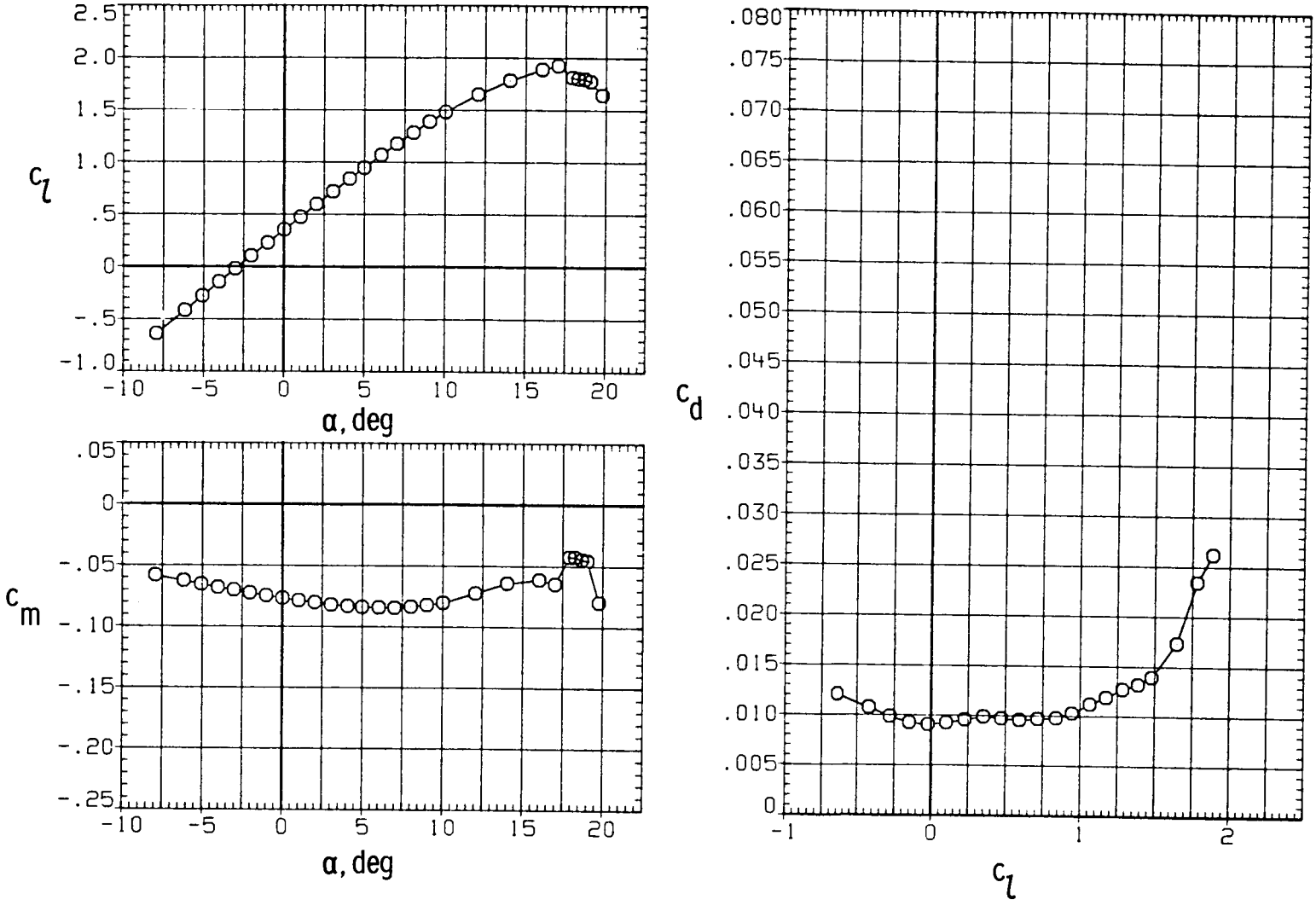

(e) M = 0.20; R = 6.0 × 10^6.

Figure 7.- Continued.

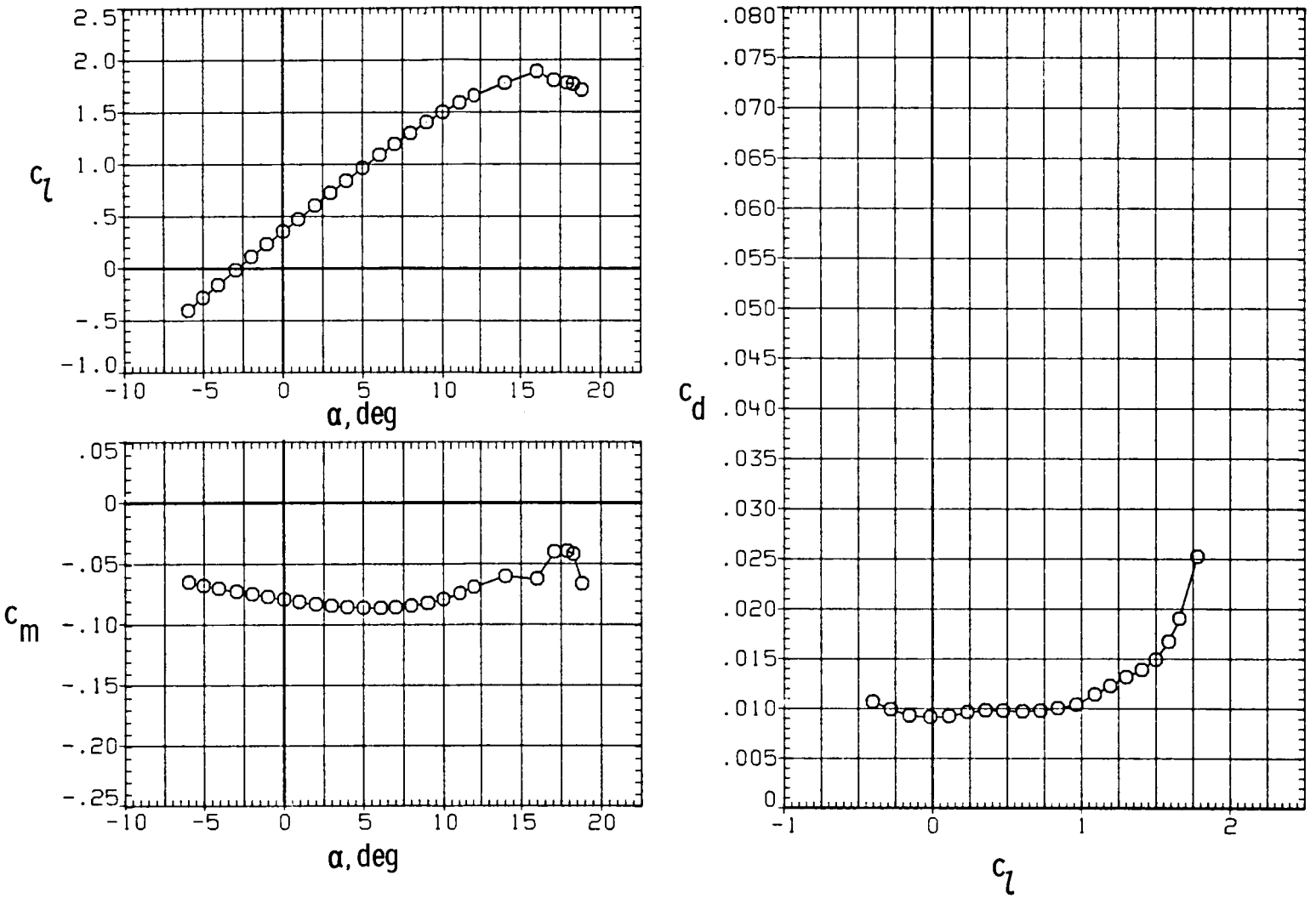

(f) M = 0.28; R = 6.0×10^6.

Figure 7.- Continued.

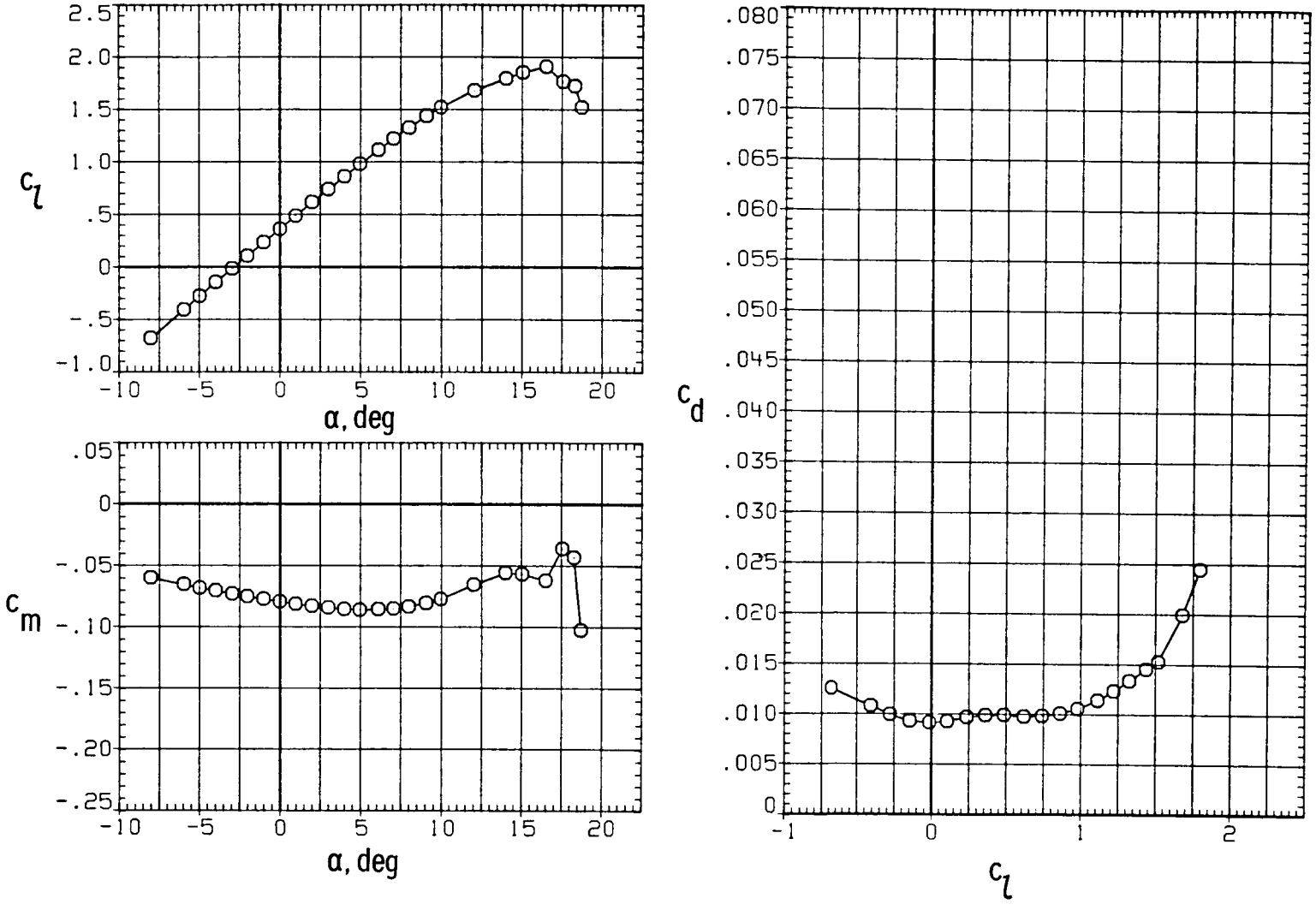

(g) M = 0.32; R = 6.0×10^6.

Figure 7.- Continued.

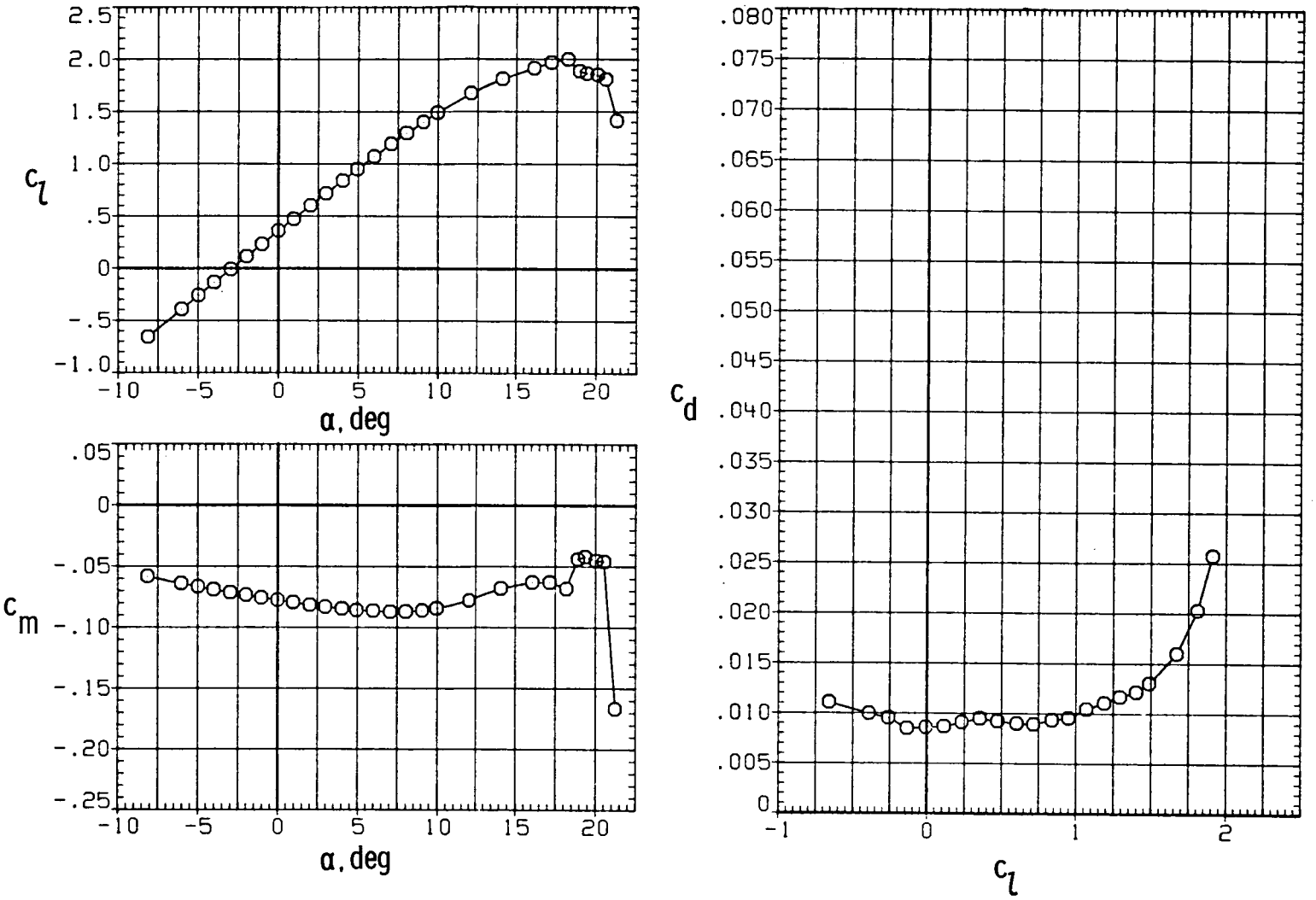

(h) M = 0.15; R = 9.0×10^6.

Figure 7.- Continued.

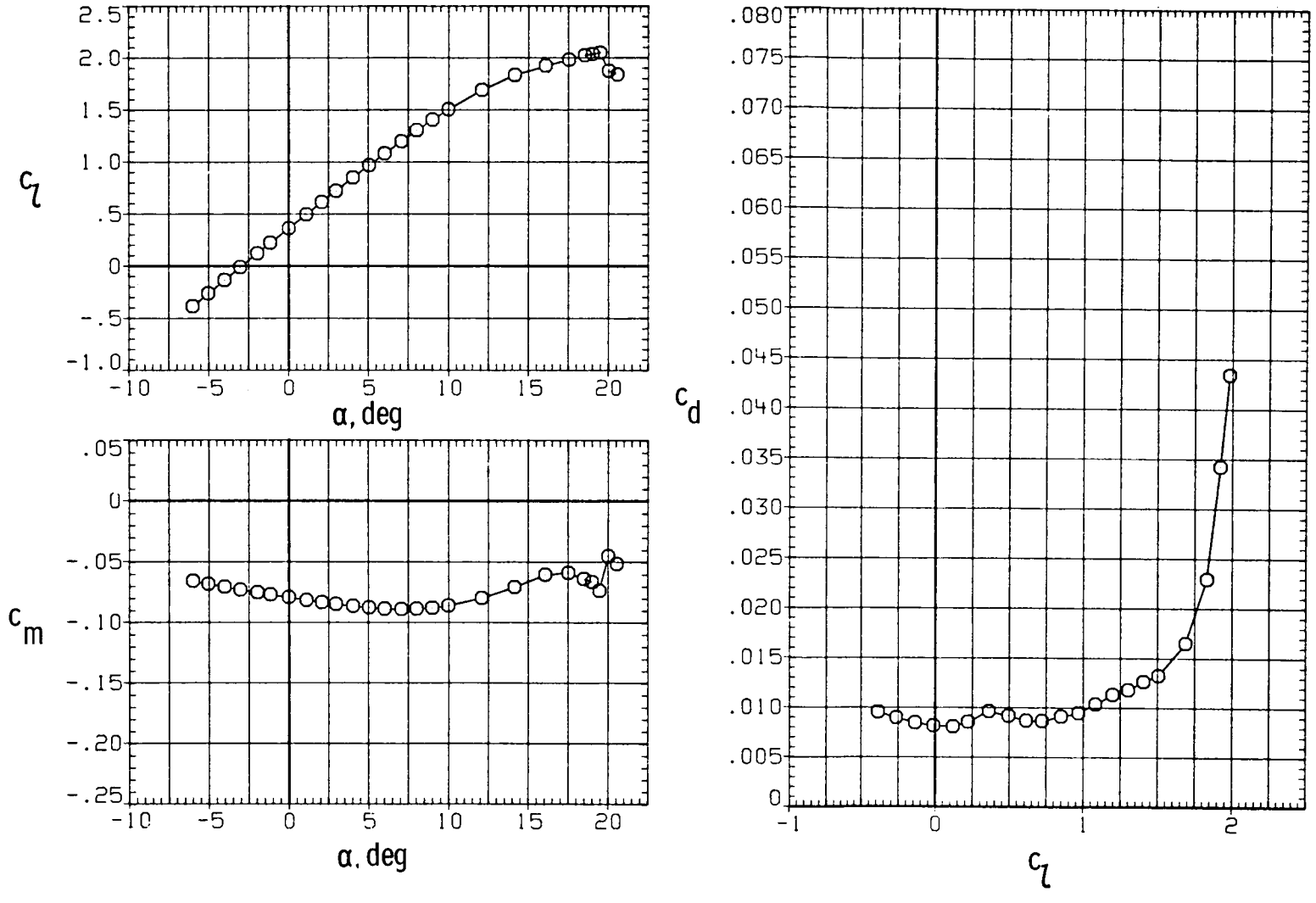

(i) M = 0.15; R = 12.0 × 10^6.

Figure 7.- Concluded.

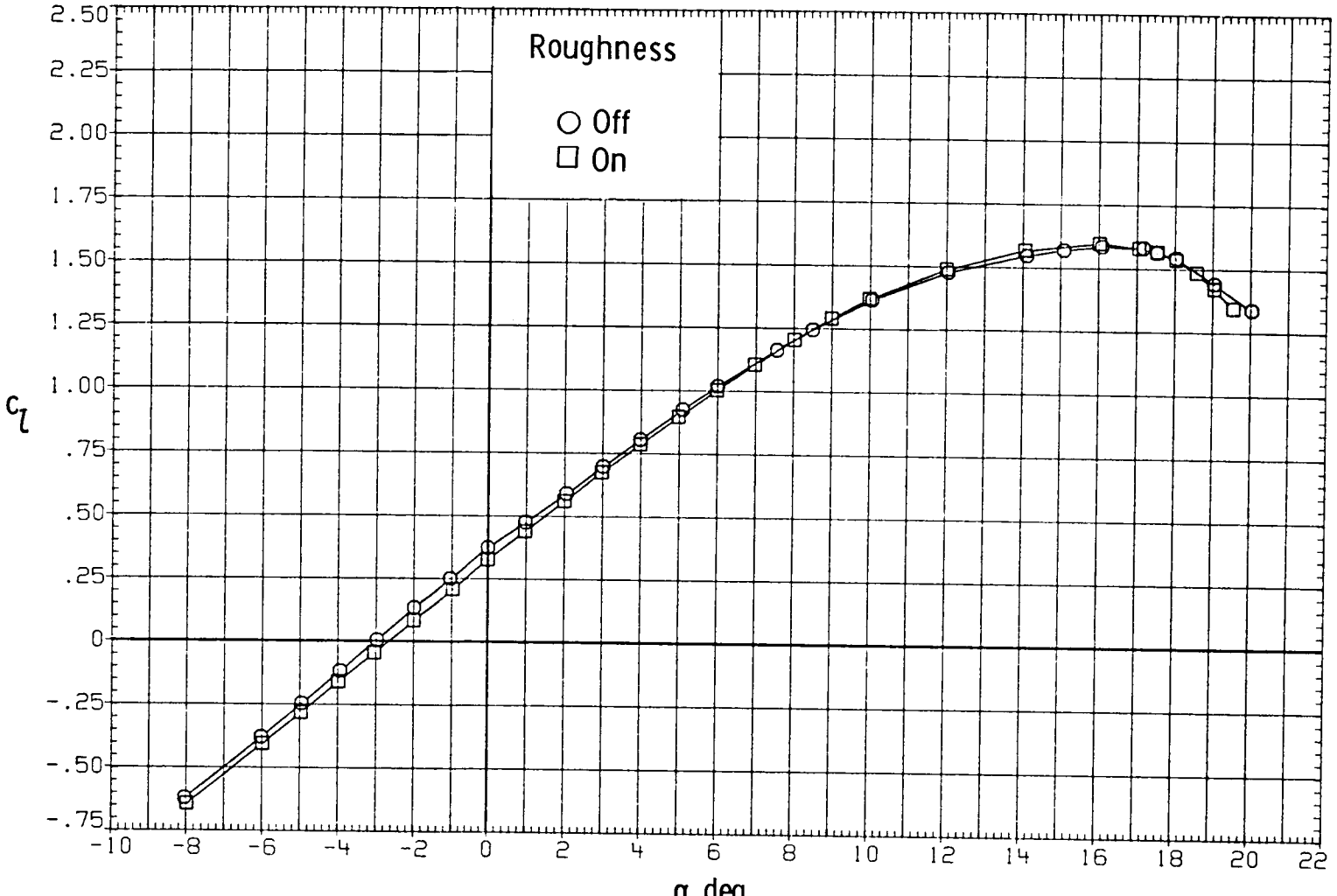

(a) $R = 2.0 \times 10^6$.

Figure 8.- Effect of roughness on section characteristics. M = 0.15.

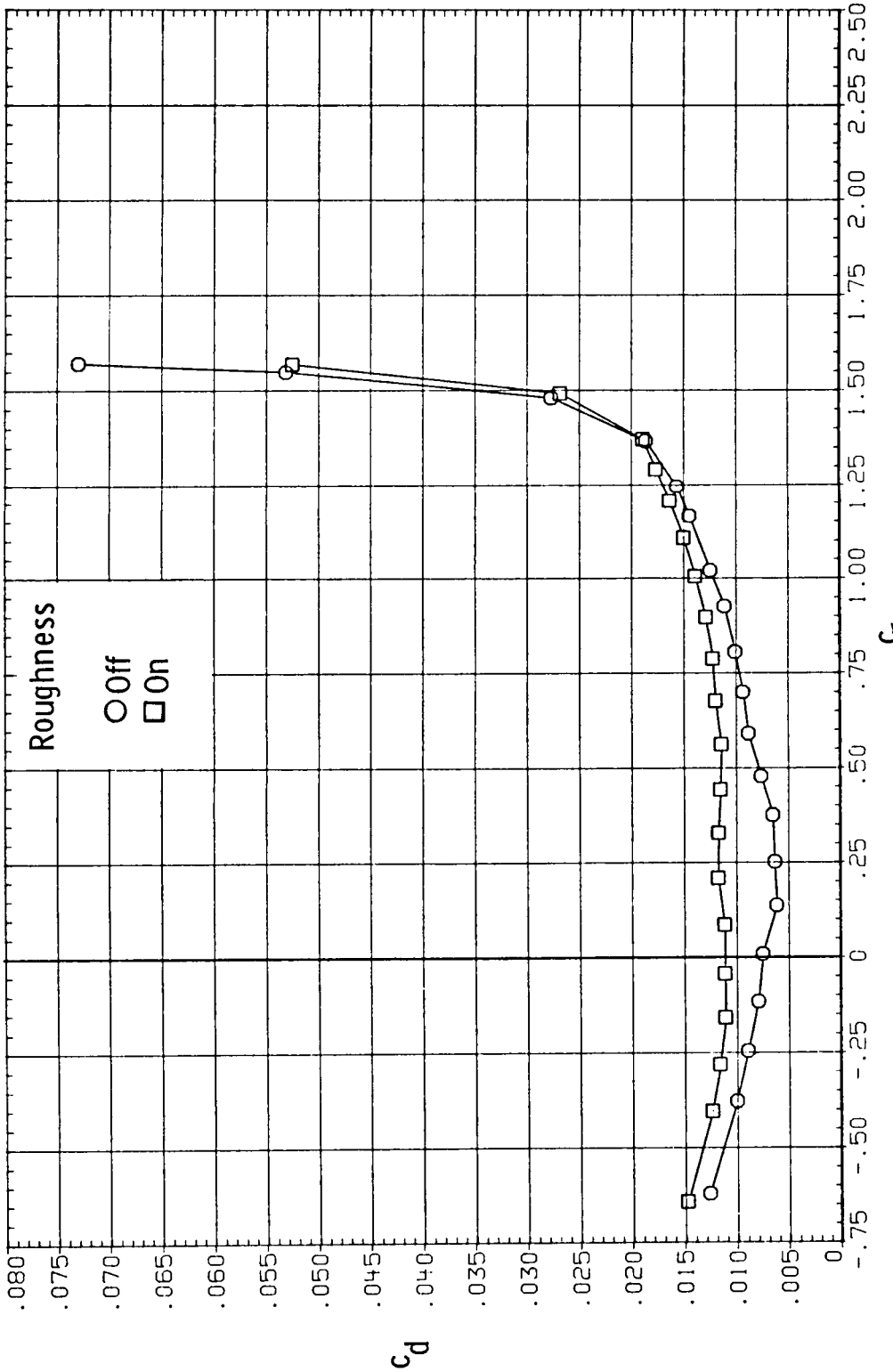

(a) $R = 2.0 \times 10^6$. Continued.

Figure 8.- Continued.

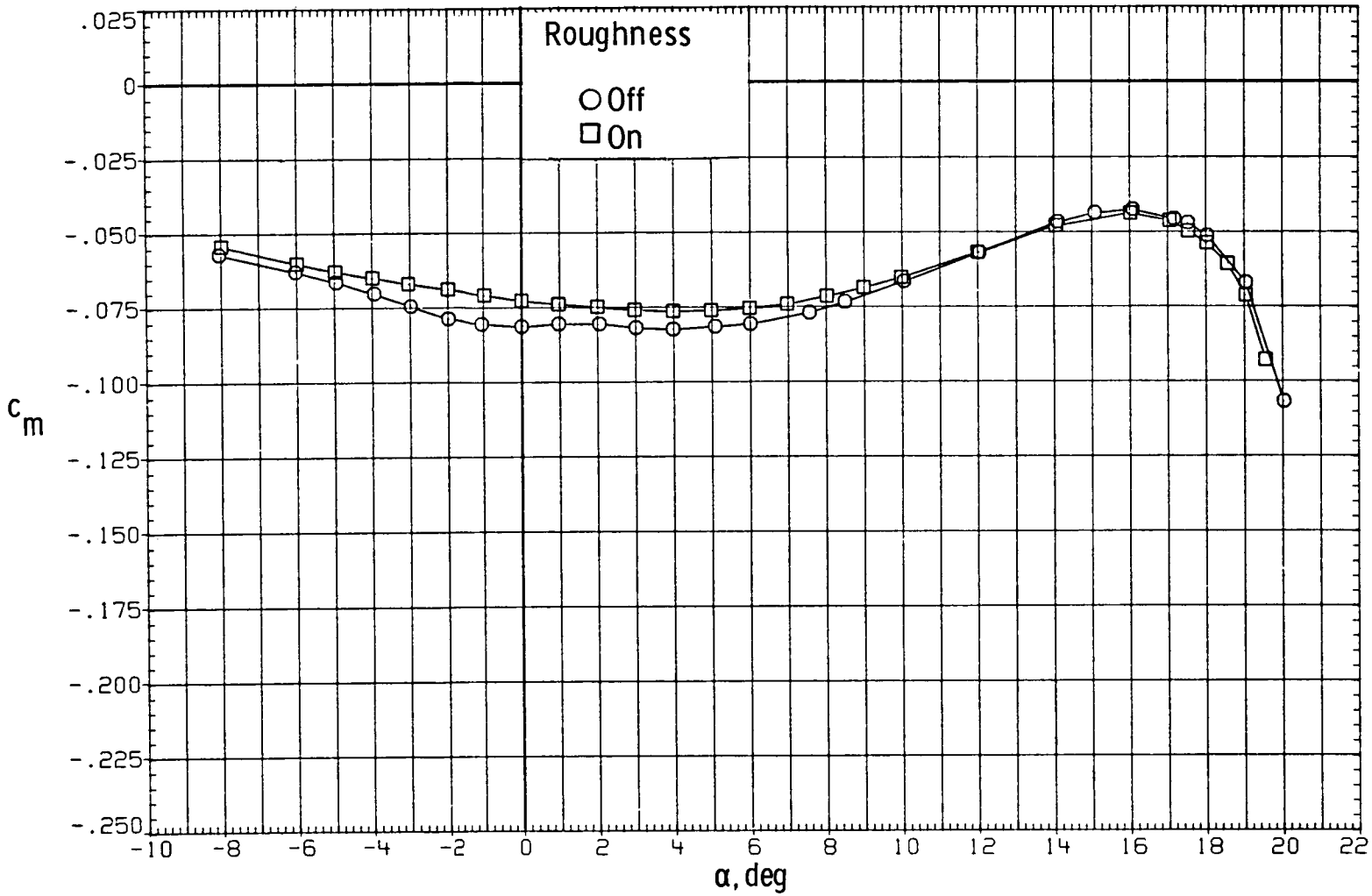

(a) $R = 2.0 \times 10^6$. Concluded.

Figure 8.- Continued.

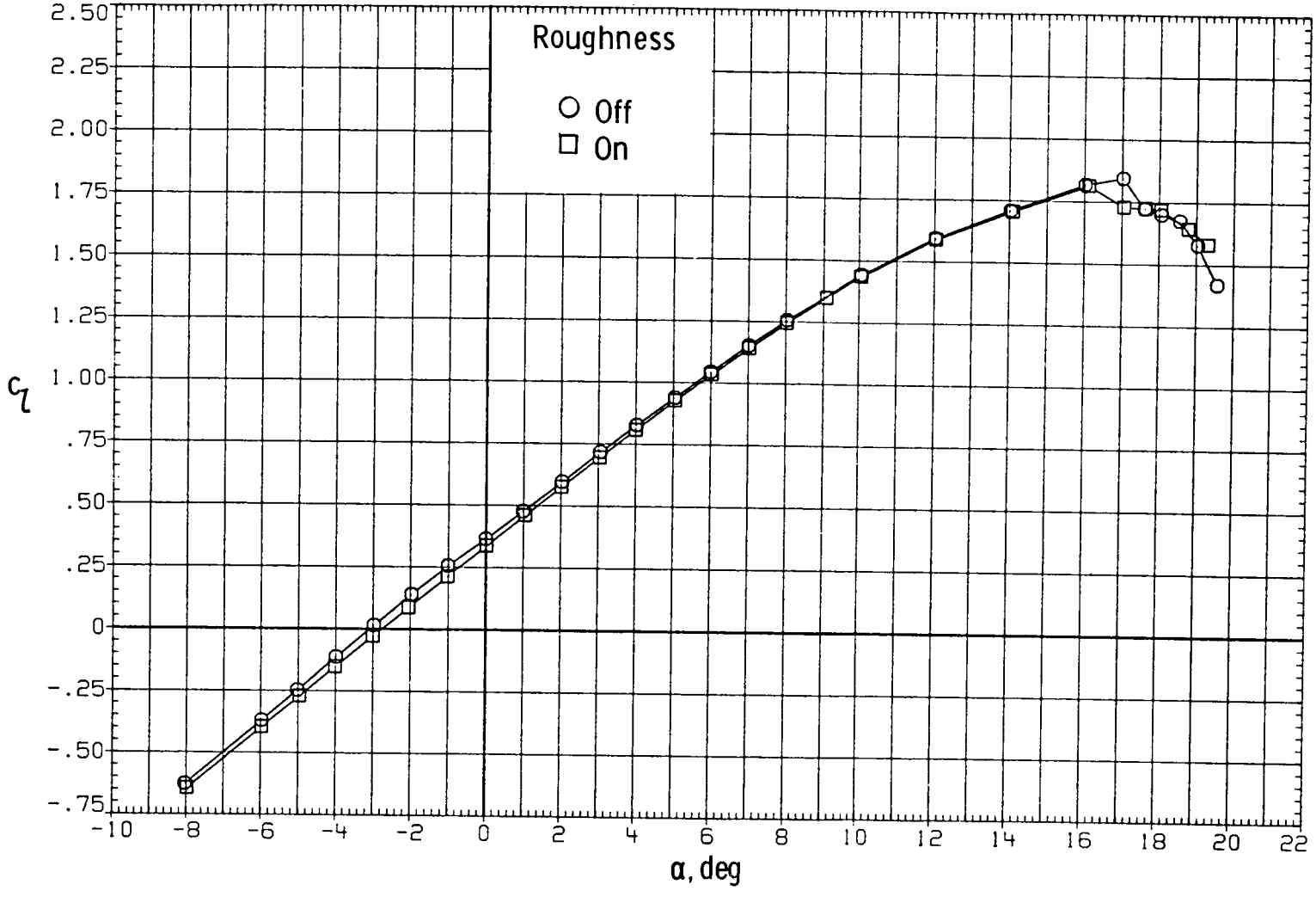

(b) $R = 4.0 \times 10^6$.

Figure 8.- Continued.

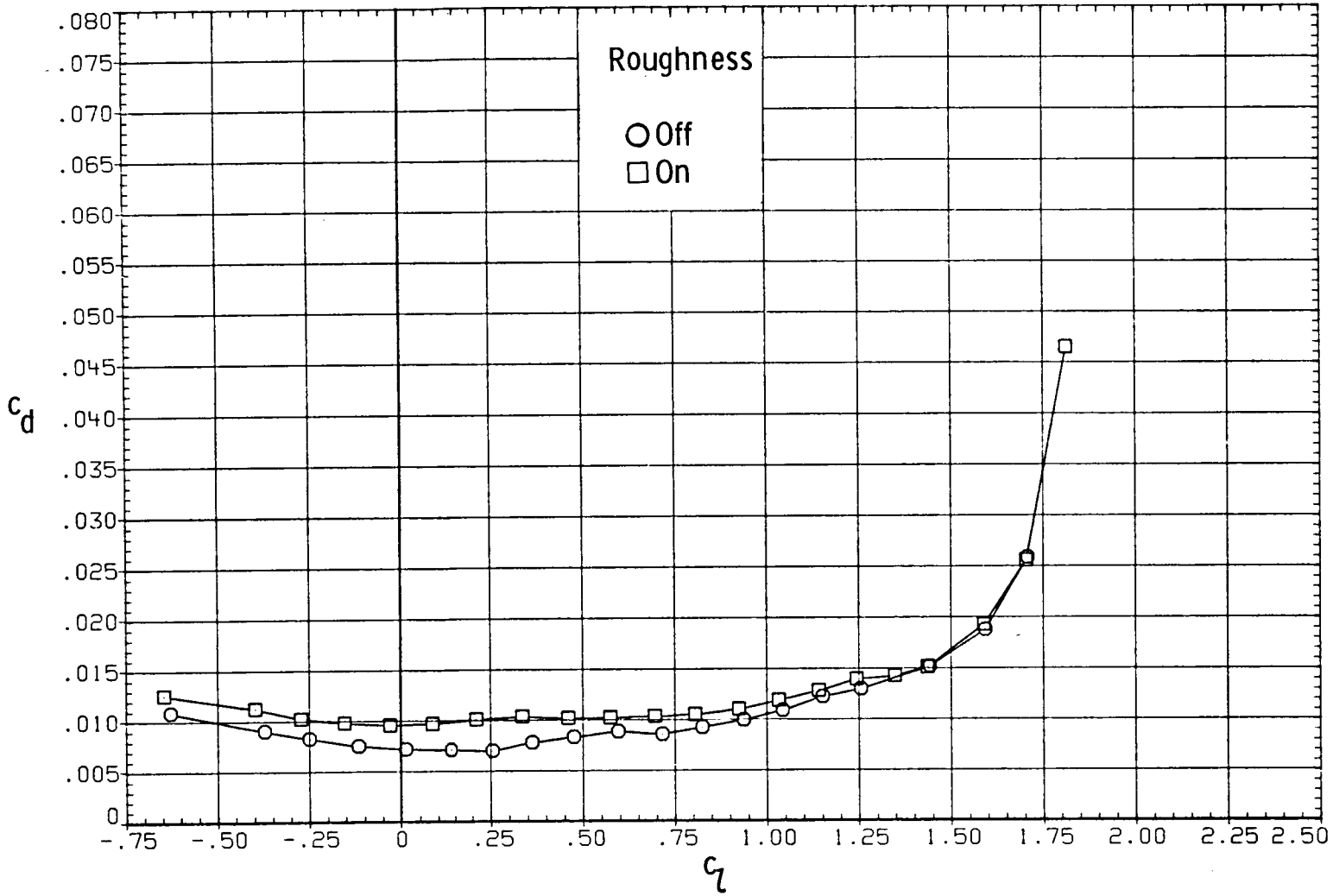

(b) $R = 4.0 \times 10^6$. Continued.

Figure 8.- Continued.

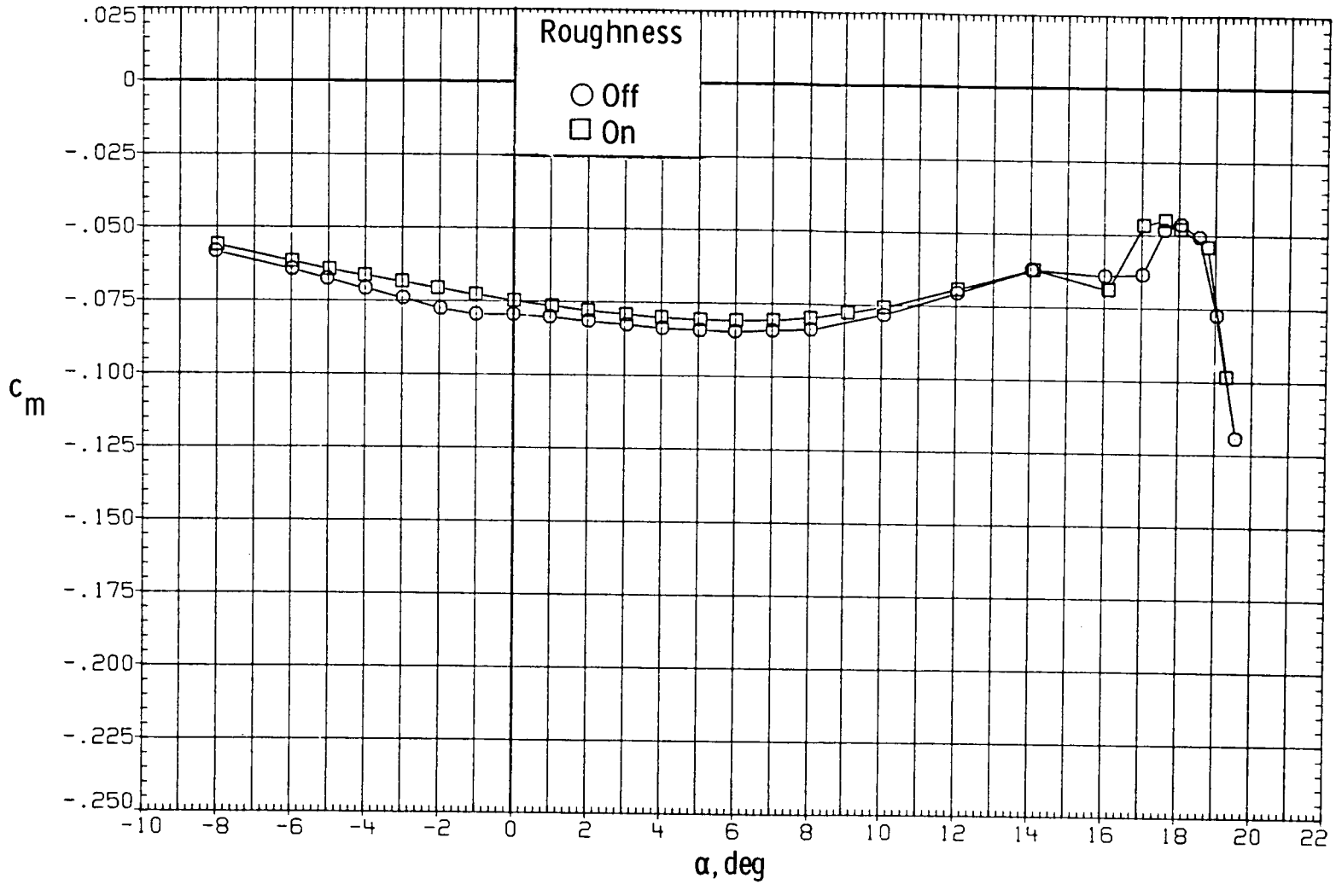

(b) $R = 4.0 \times 10^6$. Concluded.

Figure 8.- Continued.

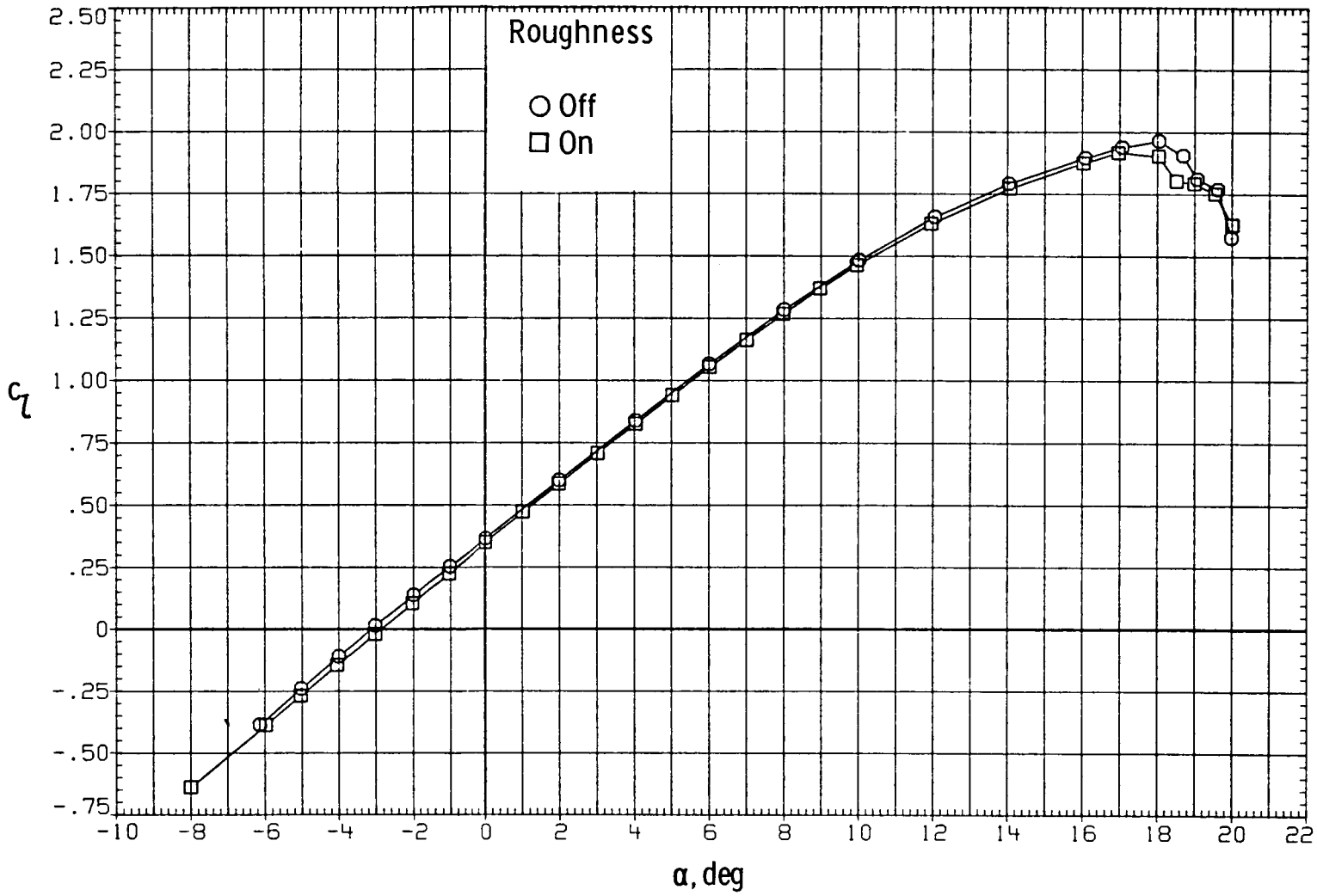

(c) $R = 6.0 \times 10^6$.

Figure 8.- Continued.

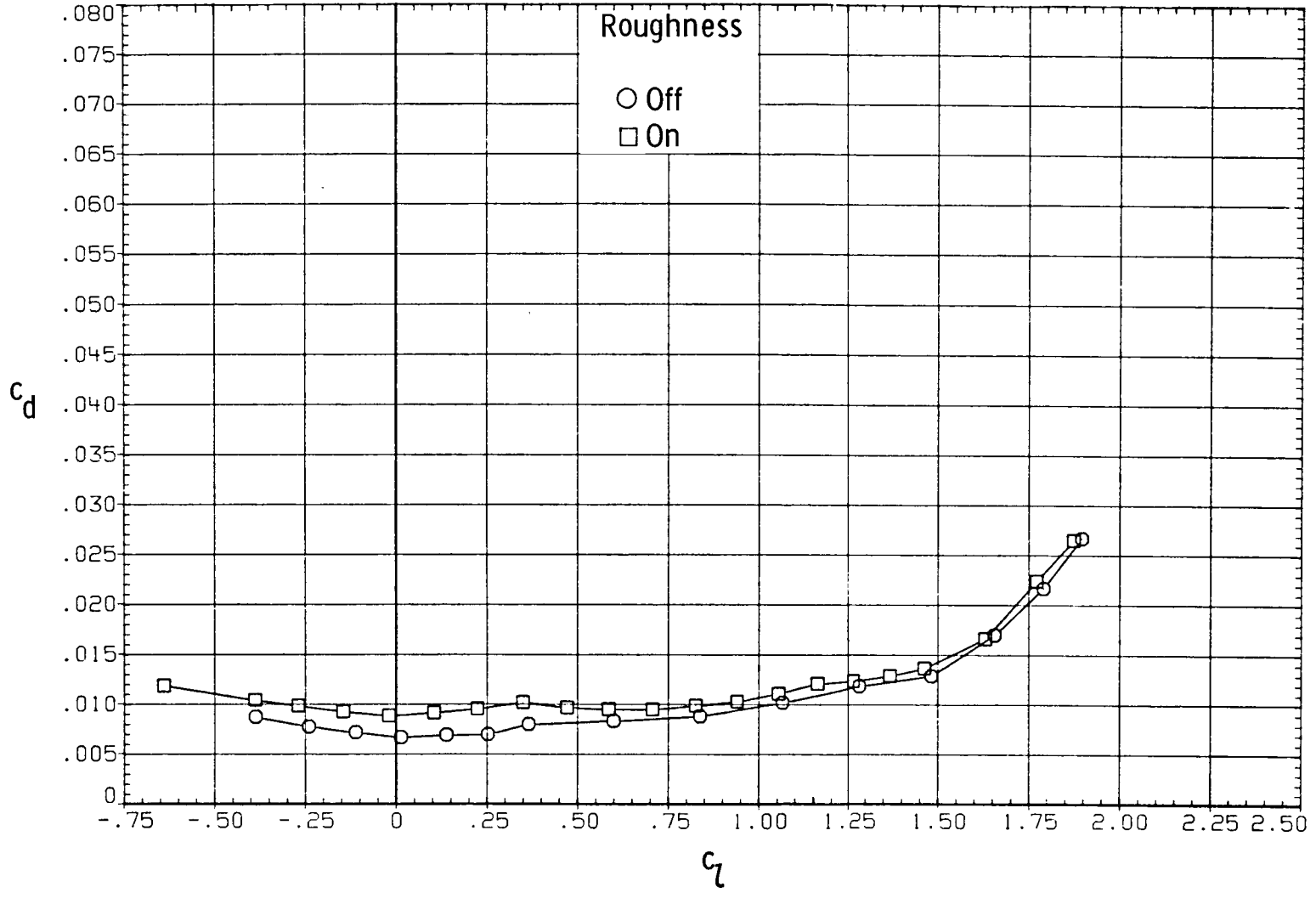

(c) $R = 6.0 \times 10^6$. Continued.

Figure 8.- Continued.

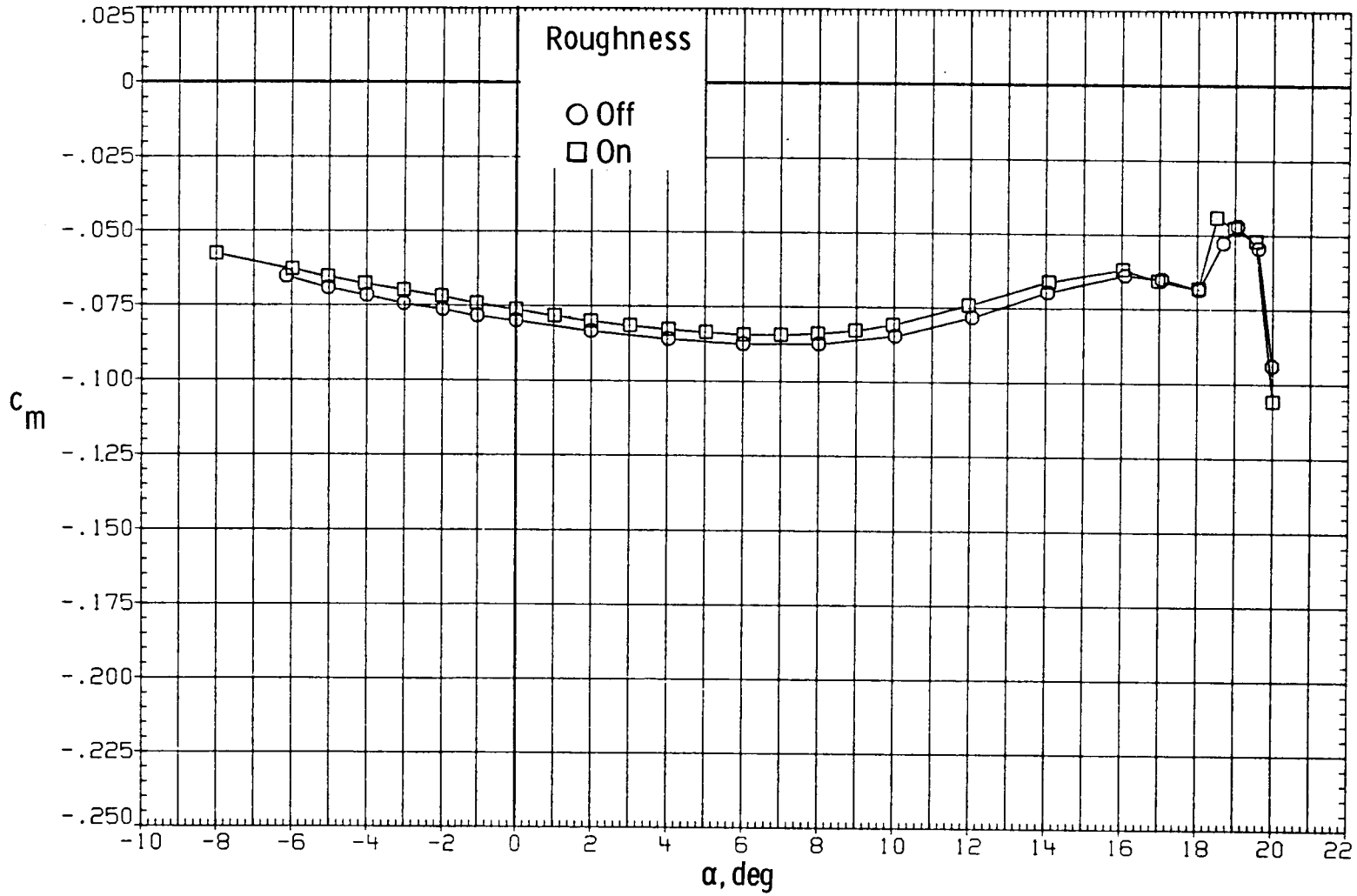

(c) R = 6.0×10^6. Concluded.

Figure 8.- Continued.

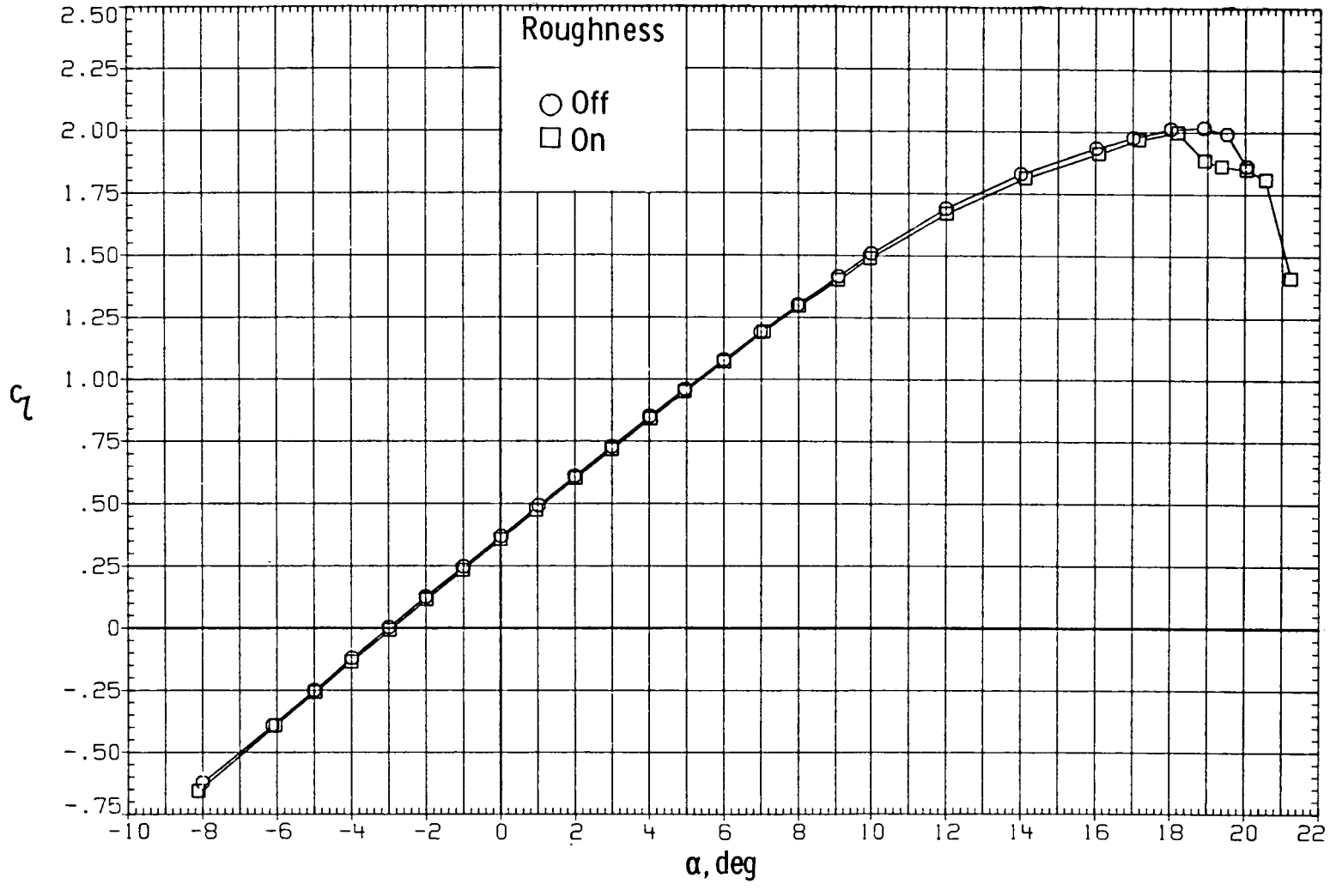

(d) $R = 9.0 \times 10^6$.

Figure 8.- Continued.

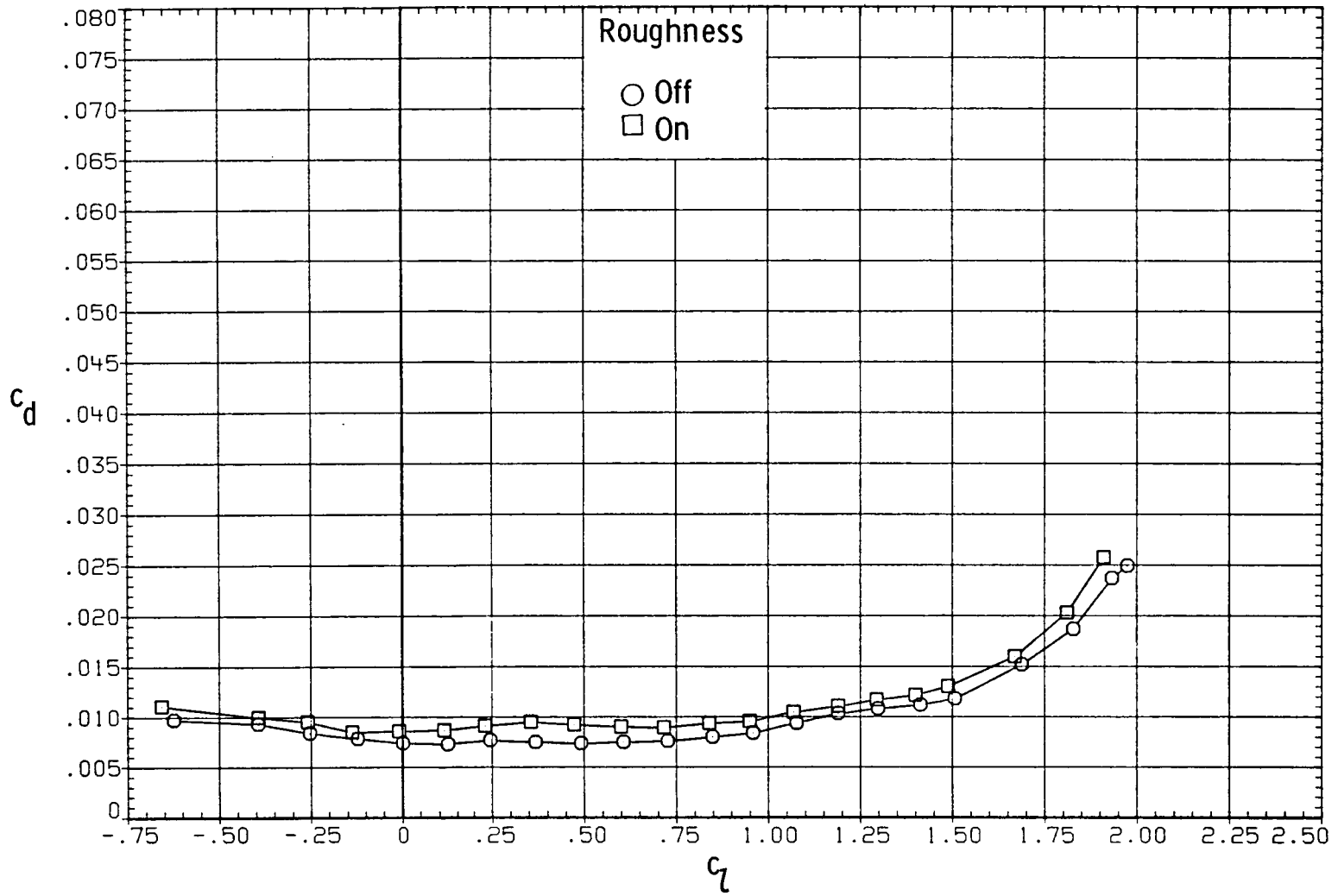

(d) $R = 9.0 \times 10^6$. Continued.

Figure 8.- Continued.

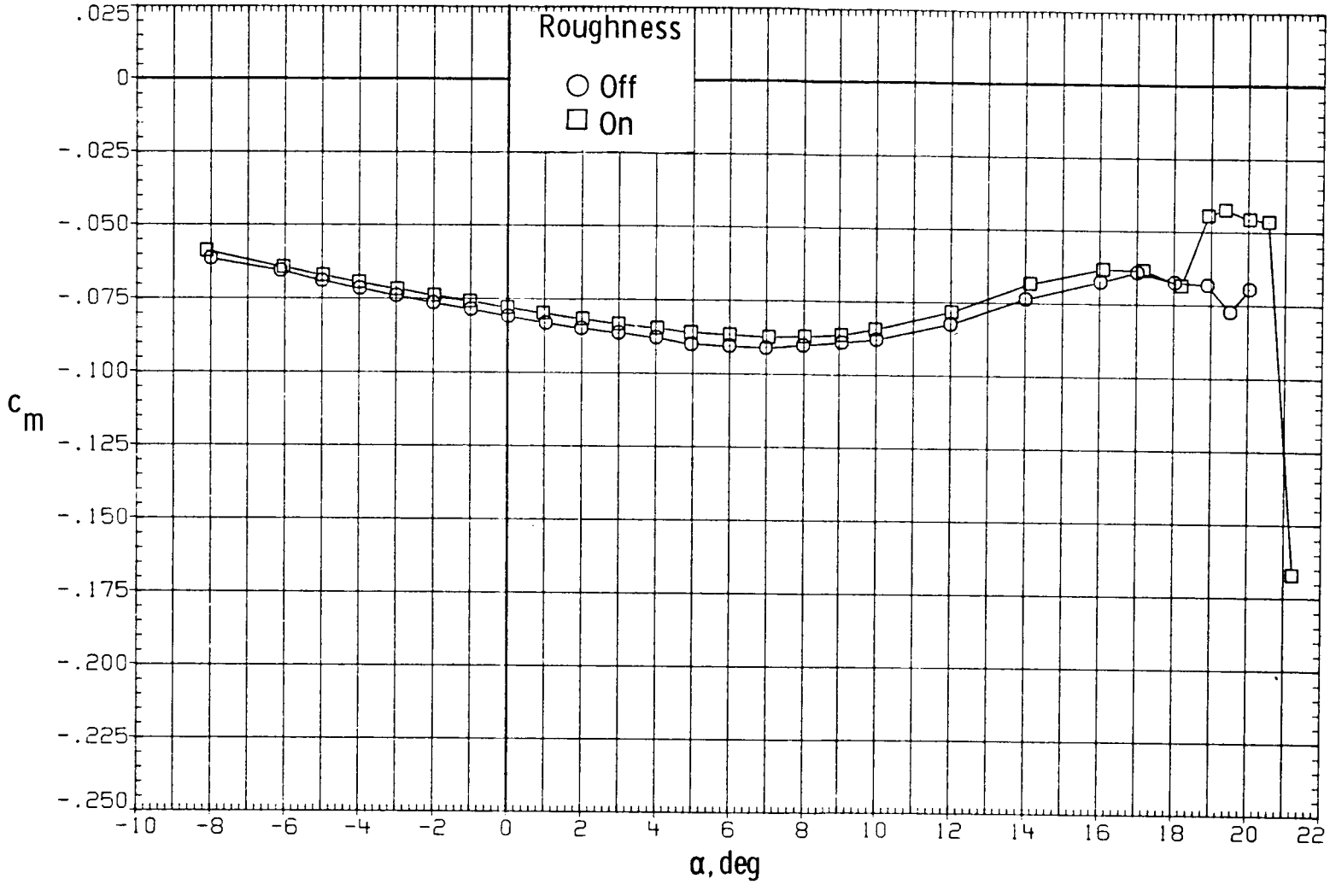

(d) $R = 9.0 \times 10^6$. Concluded.

Figure 8.- Continued.

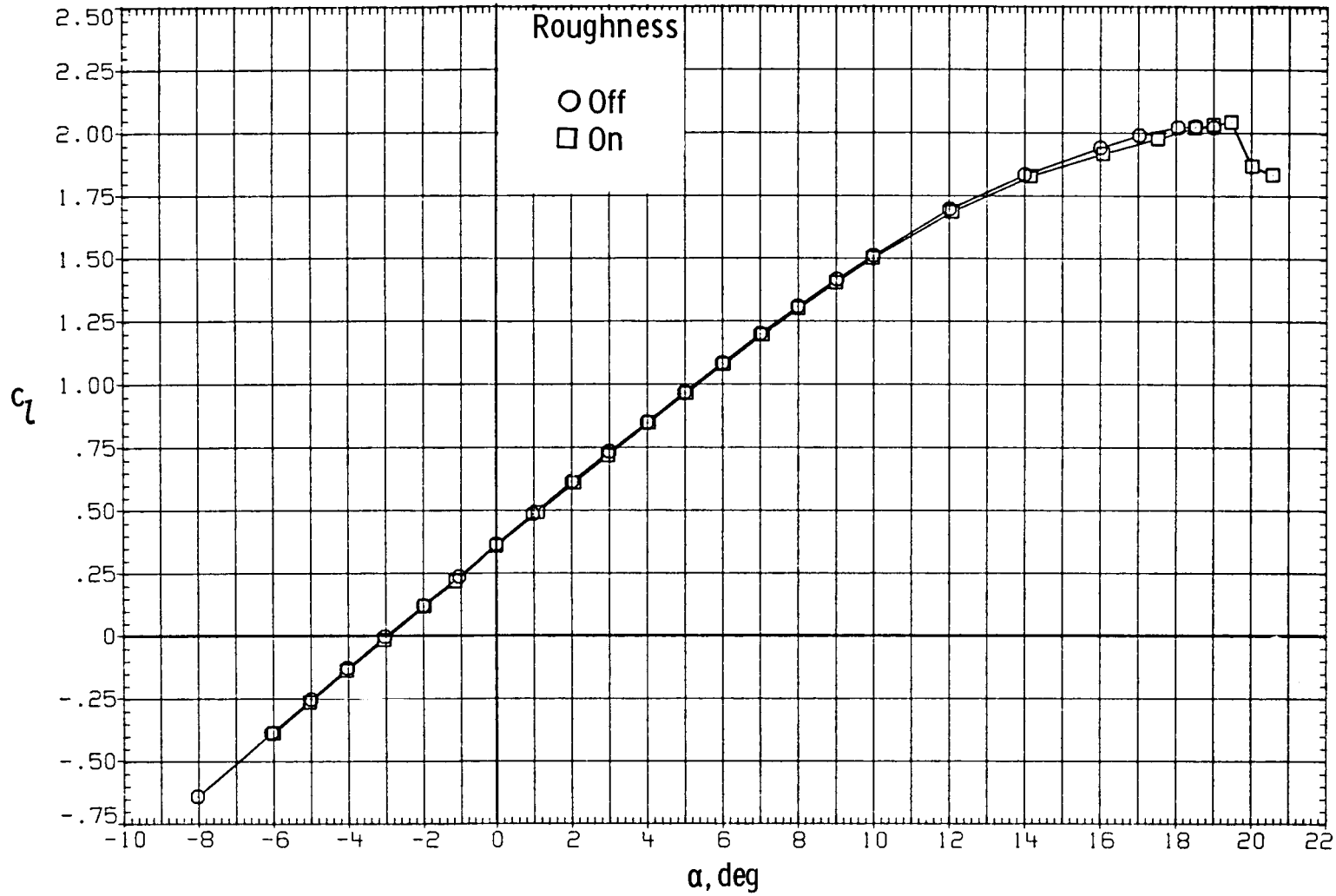

(e) $R = 12.0 \times 10^6$.

Figure 8.- Continued.

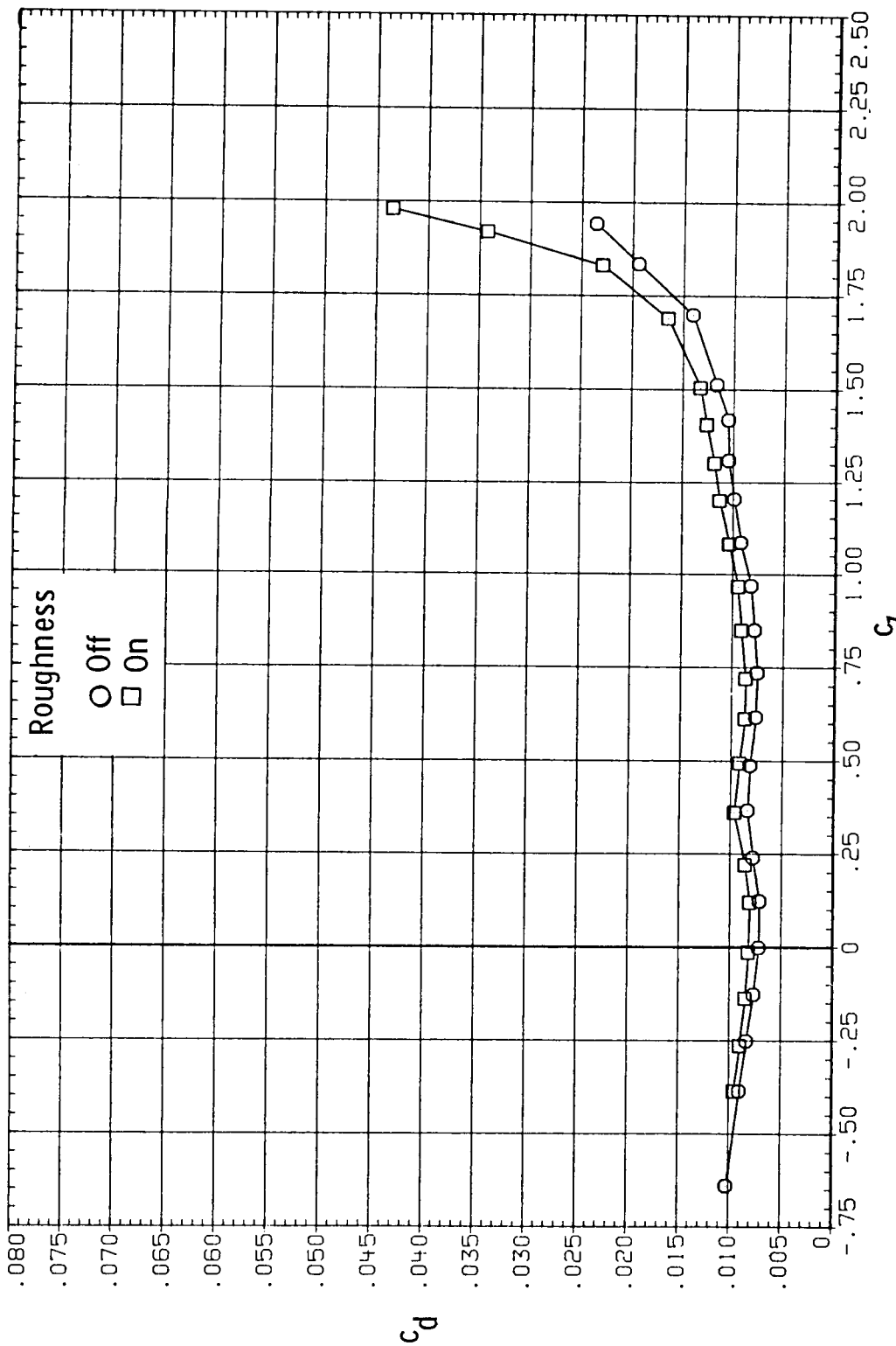

(e) $R = 12.0 \times 10^6$. Continued.

Figure 8.- Continued.

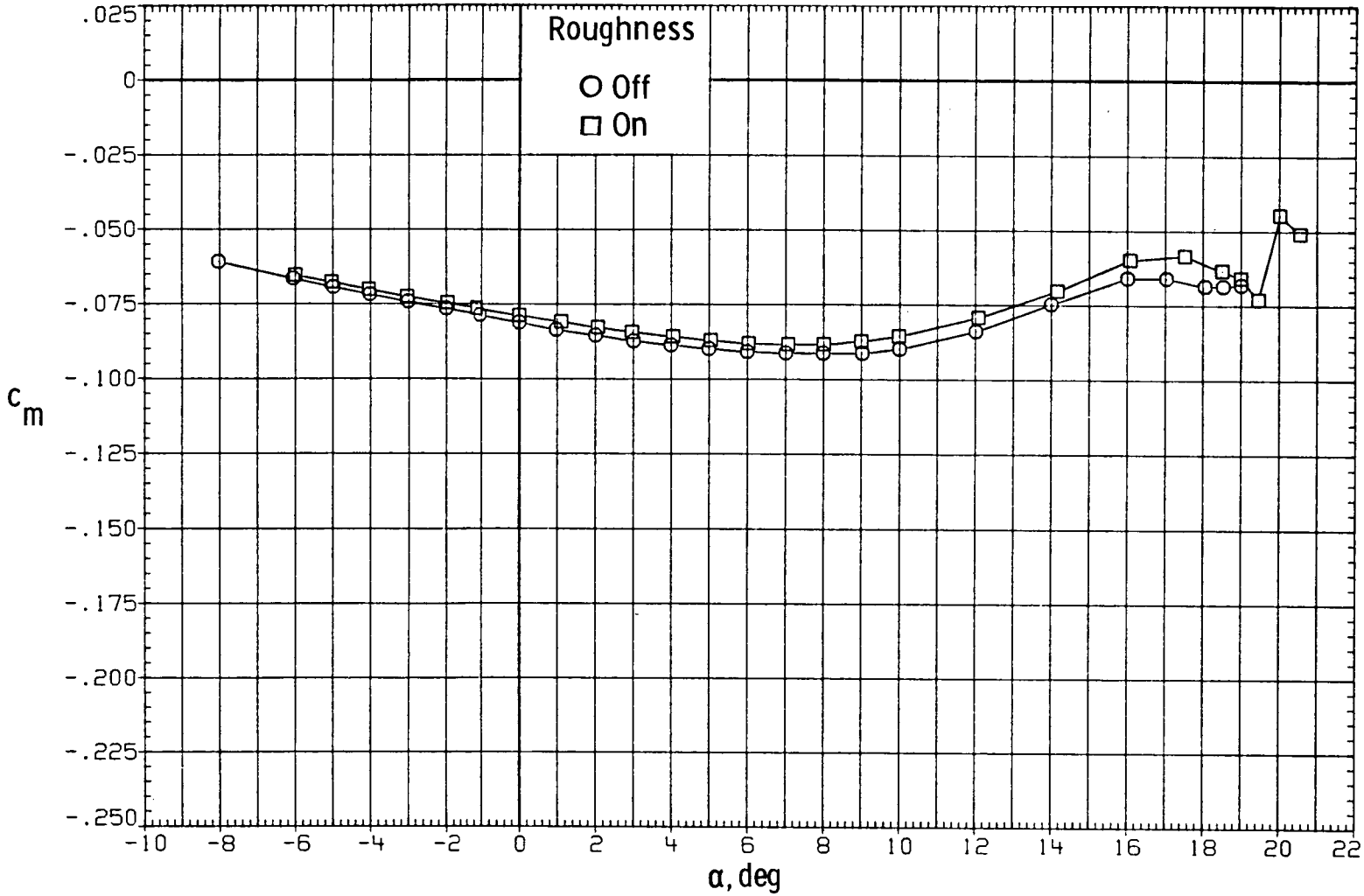

(e) $R = 12.0 \times 10^6$. Concluded.

Figure 8.- Concluded.

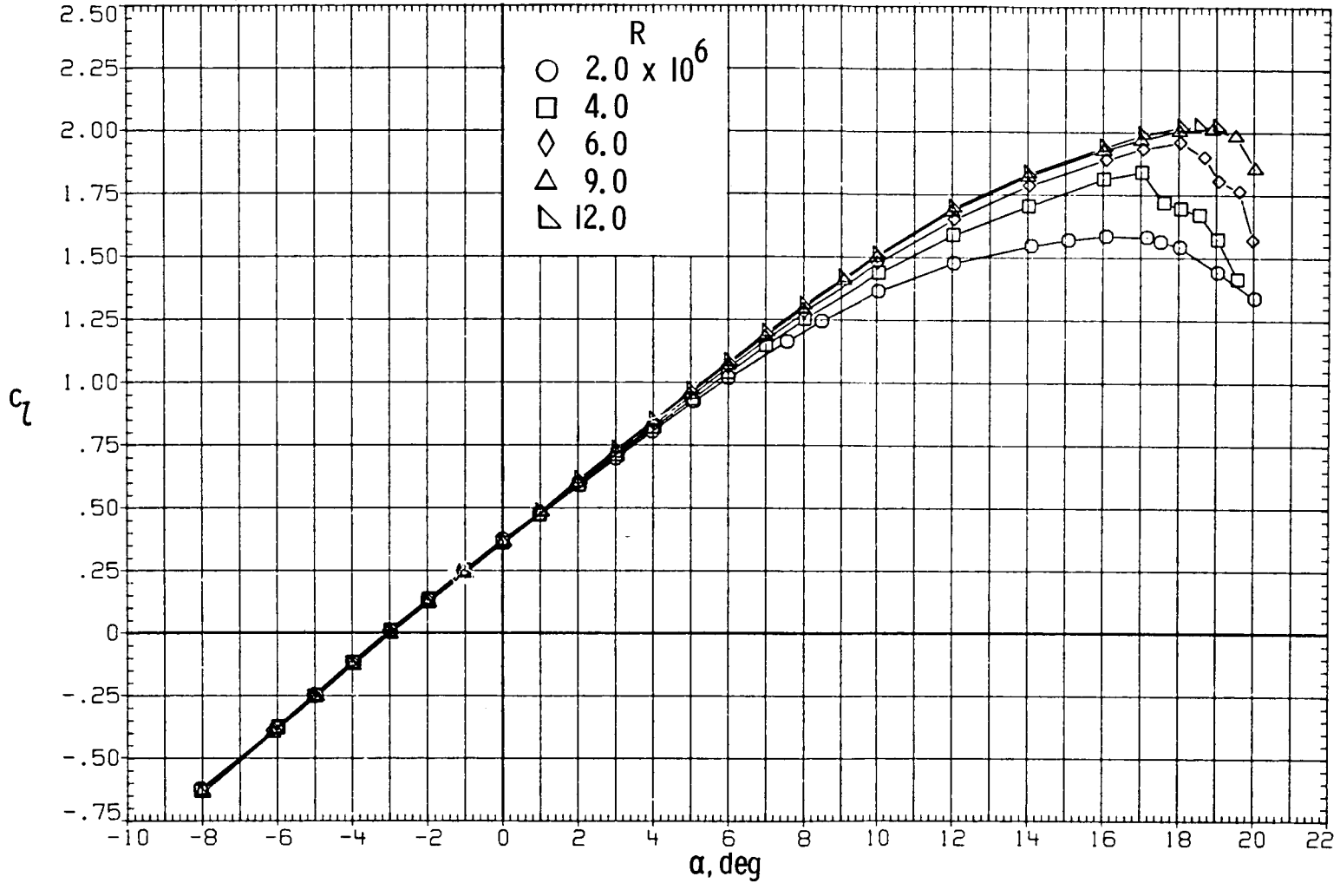

(a) Lift.

Figure 9.- Effect of Reynolds number on section characteristics. Model smooth; M = 0.15.

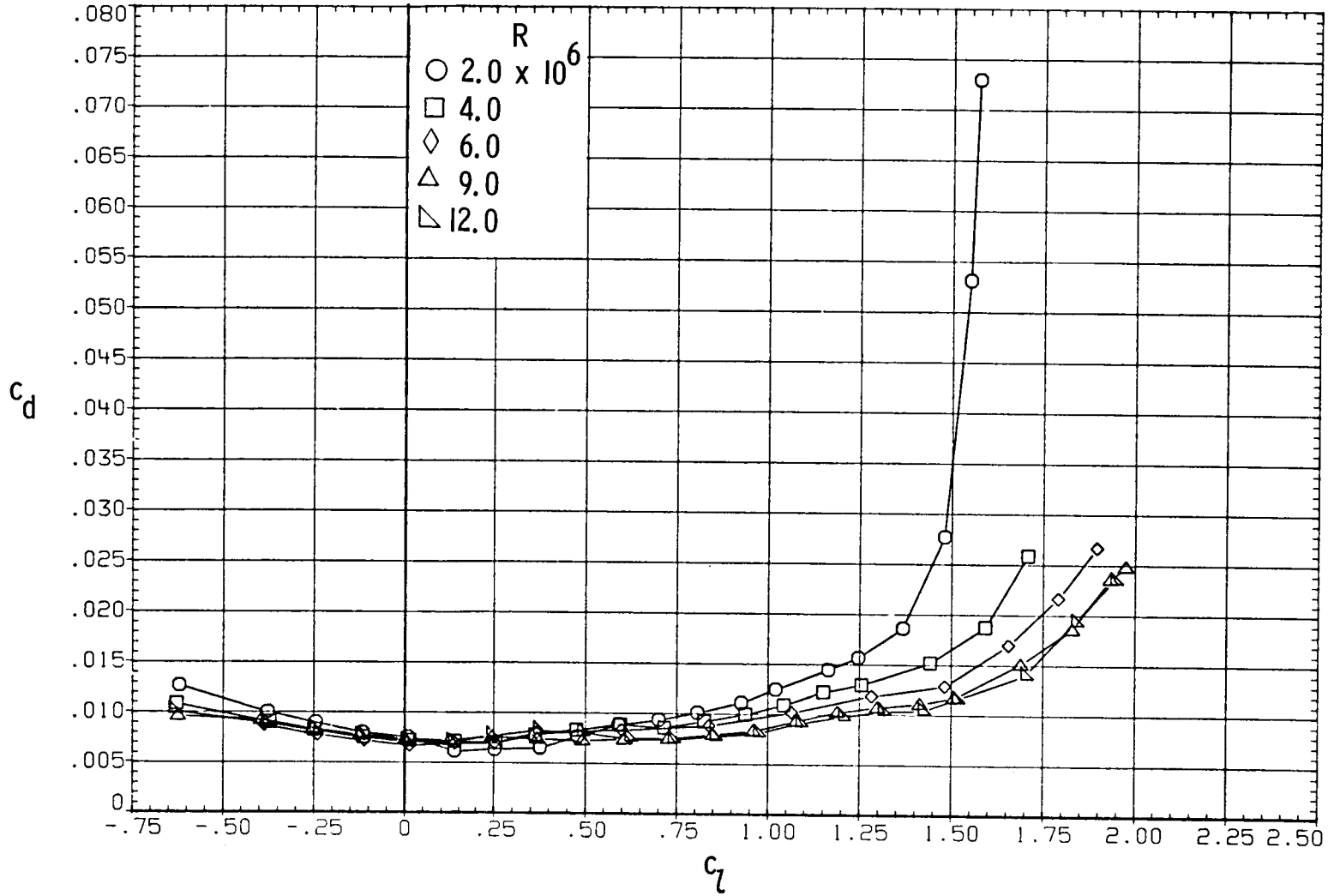

(b) Drag.

Figure 9.- Continued.

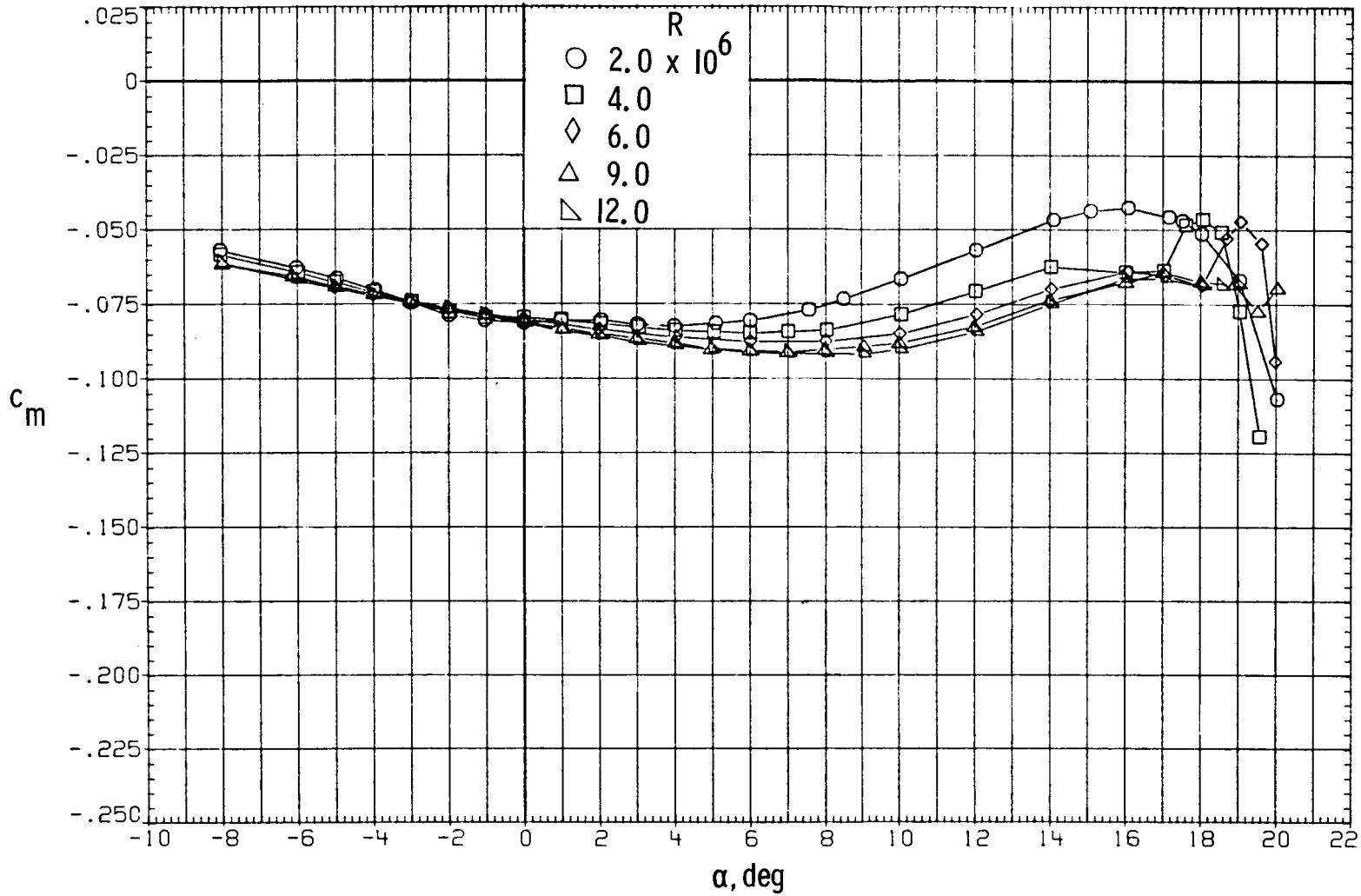

(c) Pitching moment.

Figure 9.- Concluded.

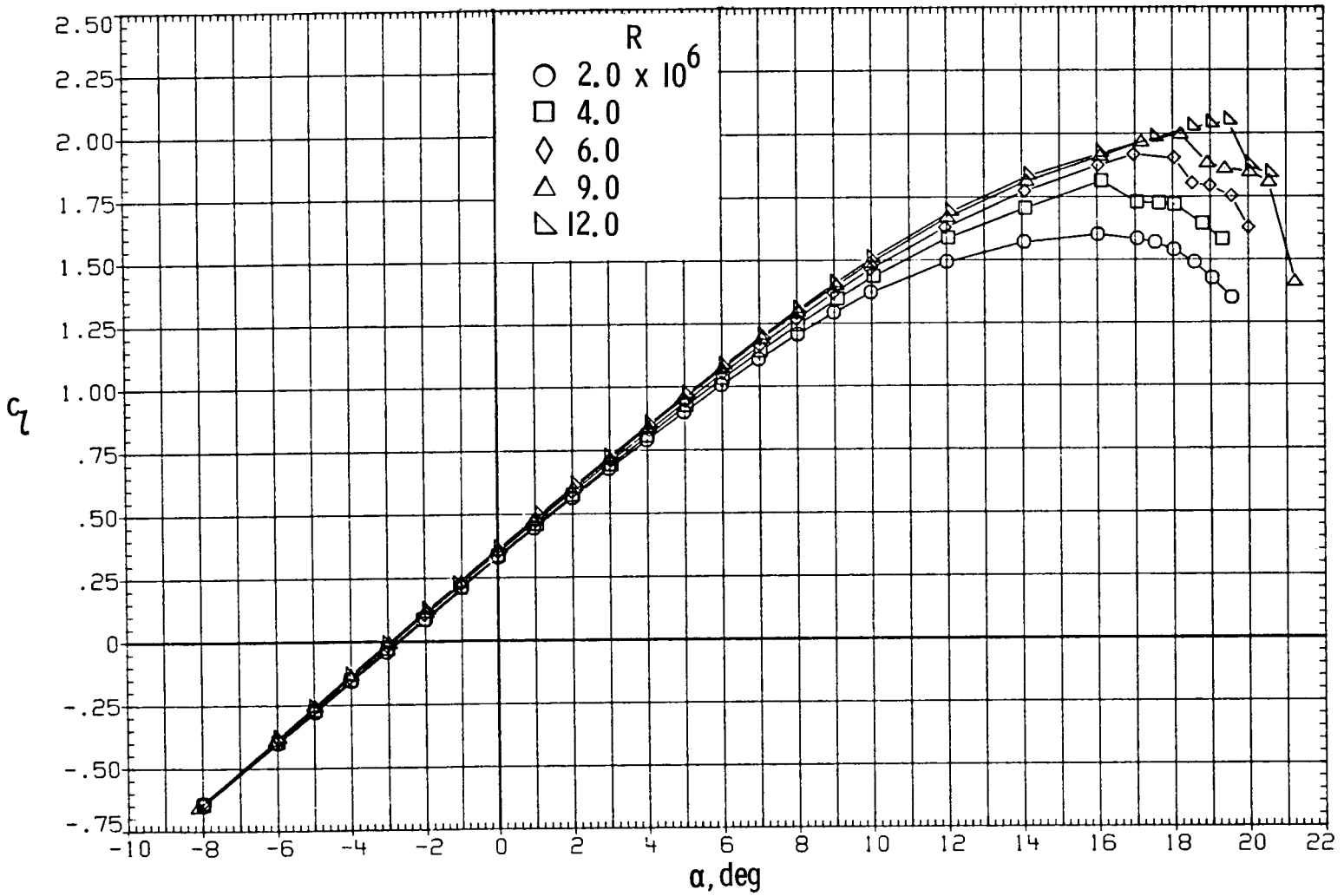

(a) Lift.

Figure 10.- Effect of Reynolds number on section characteristics. Roughness located at 0.075c; M = 0.15.

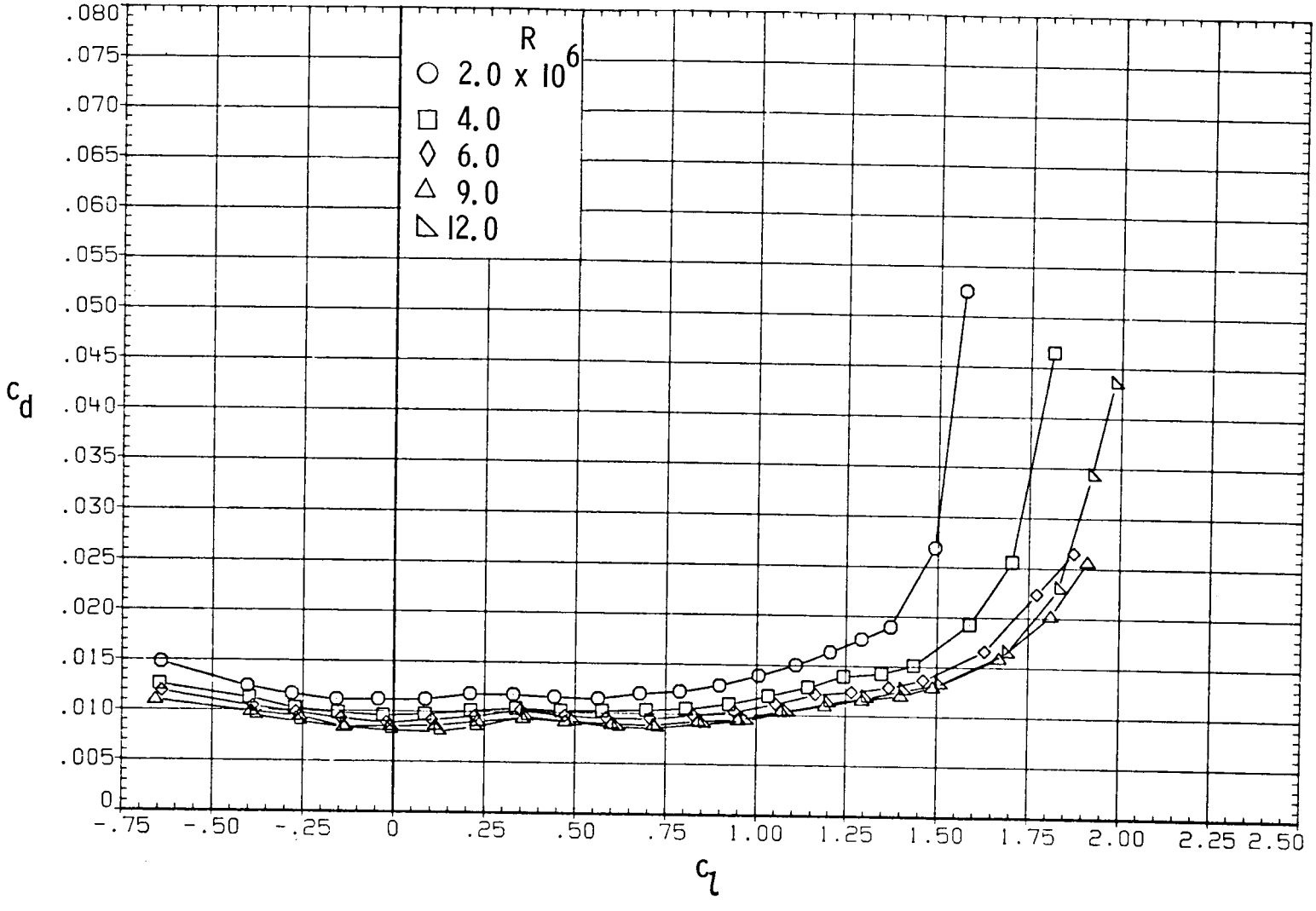

(b) Drag.

Figure 10.- Continued.

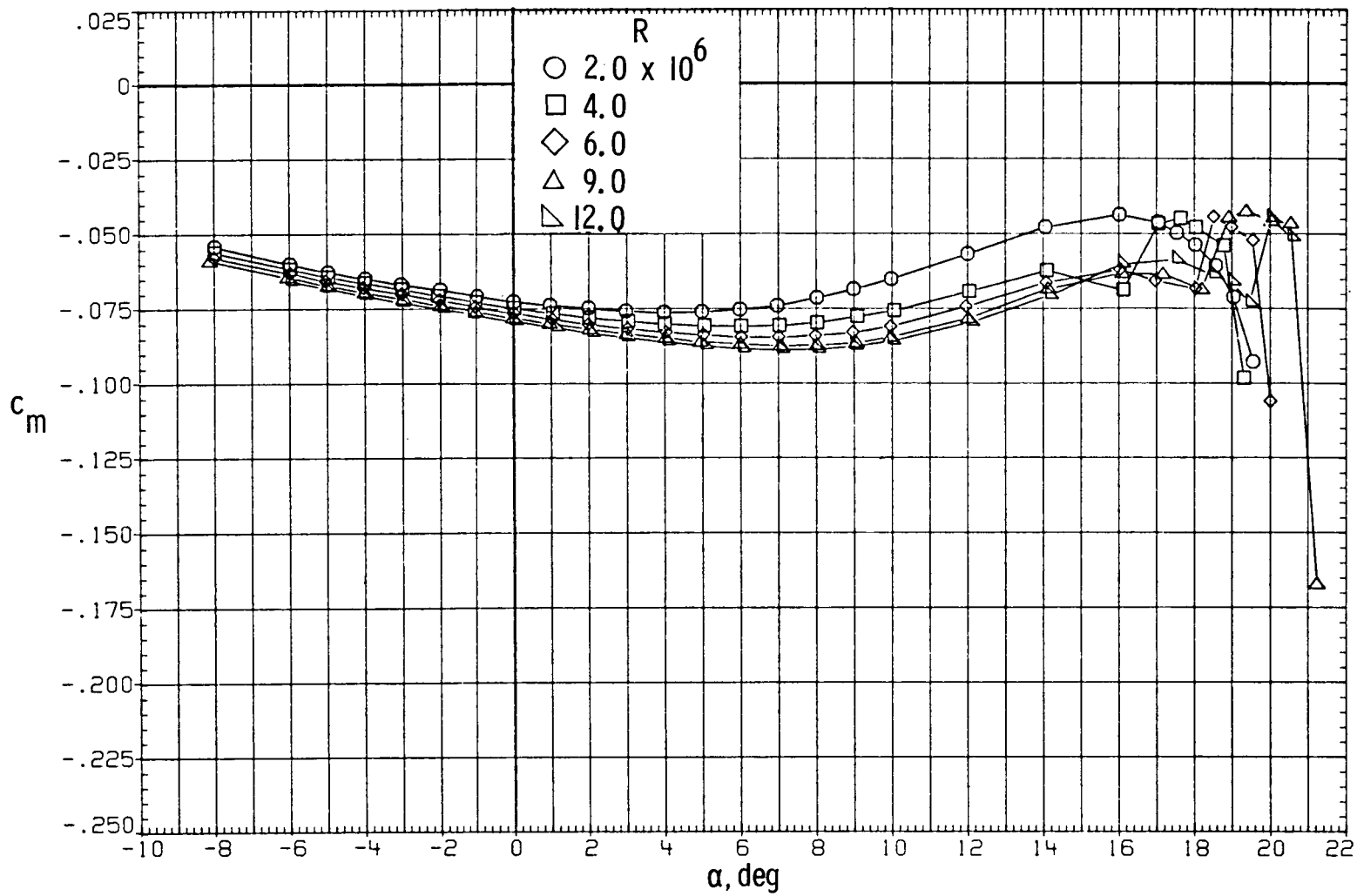

(c) Pitching moment.

Figure 10.- Concluded.

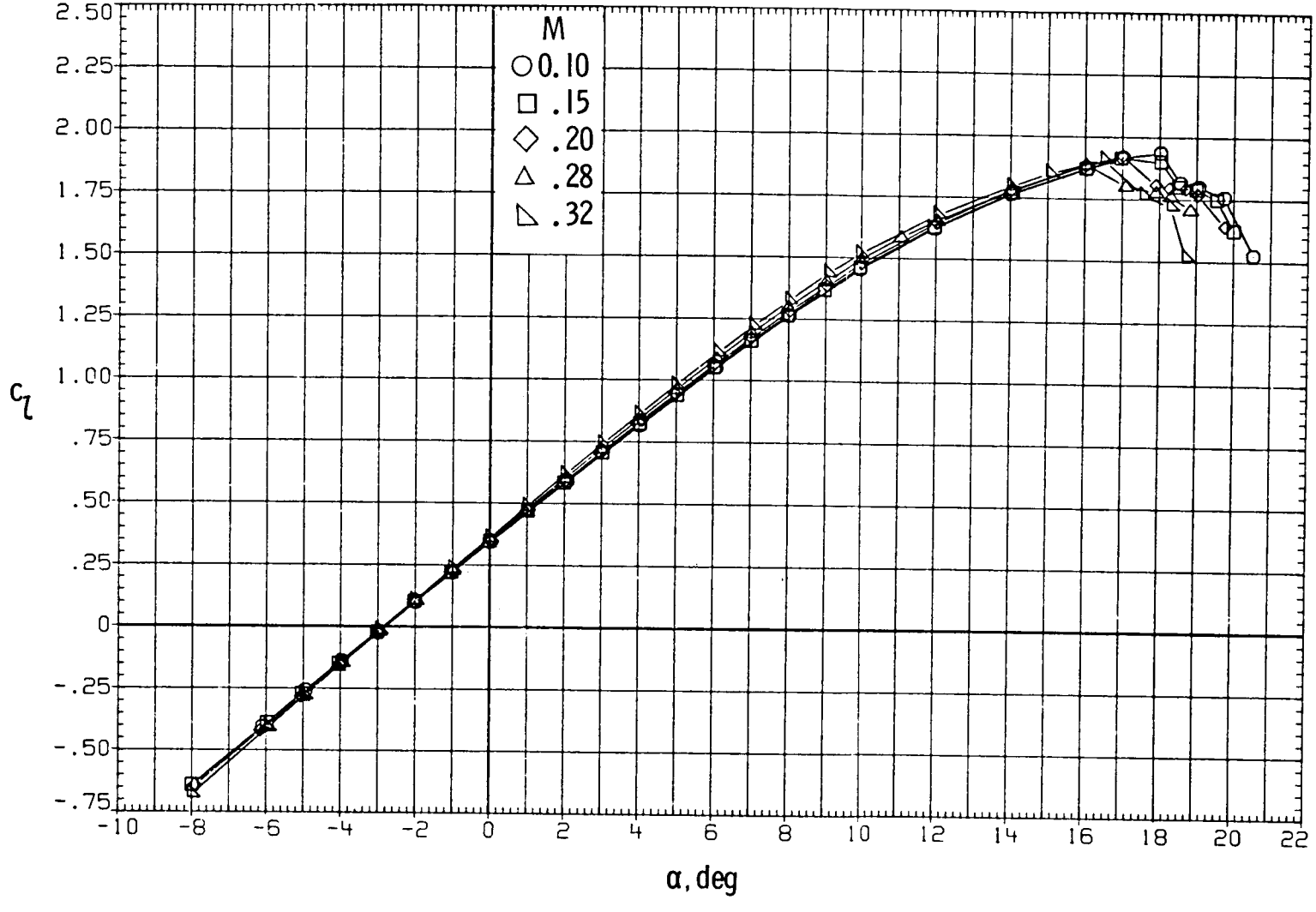

(a) Lift.

Figure 11.- Effect of Mach number on section characteristics. Roughness located at 0.075c; $R = 6.0 \times 10^6$.

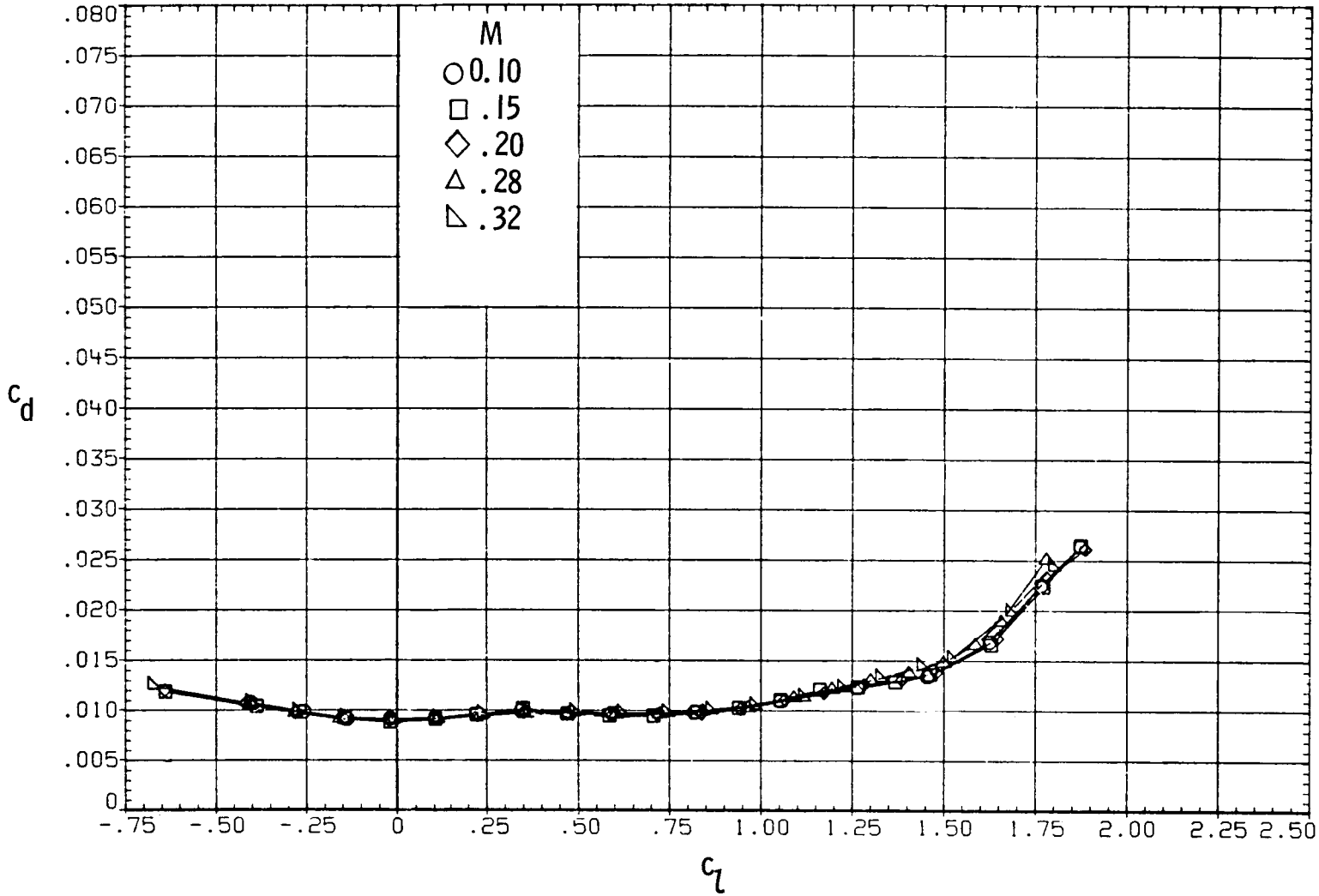

(b) Drag.

Figure 11.- Continued.

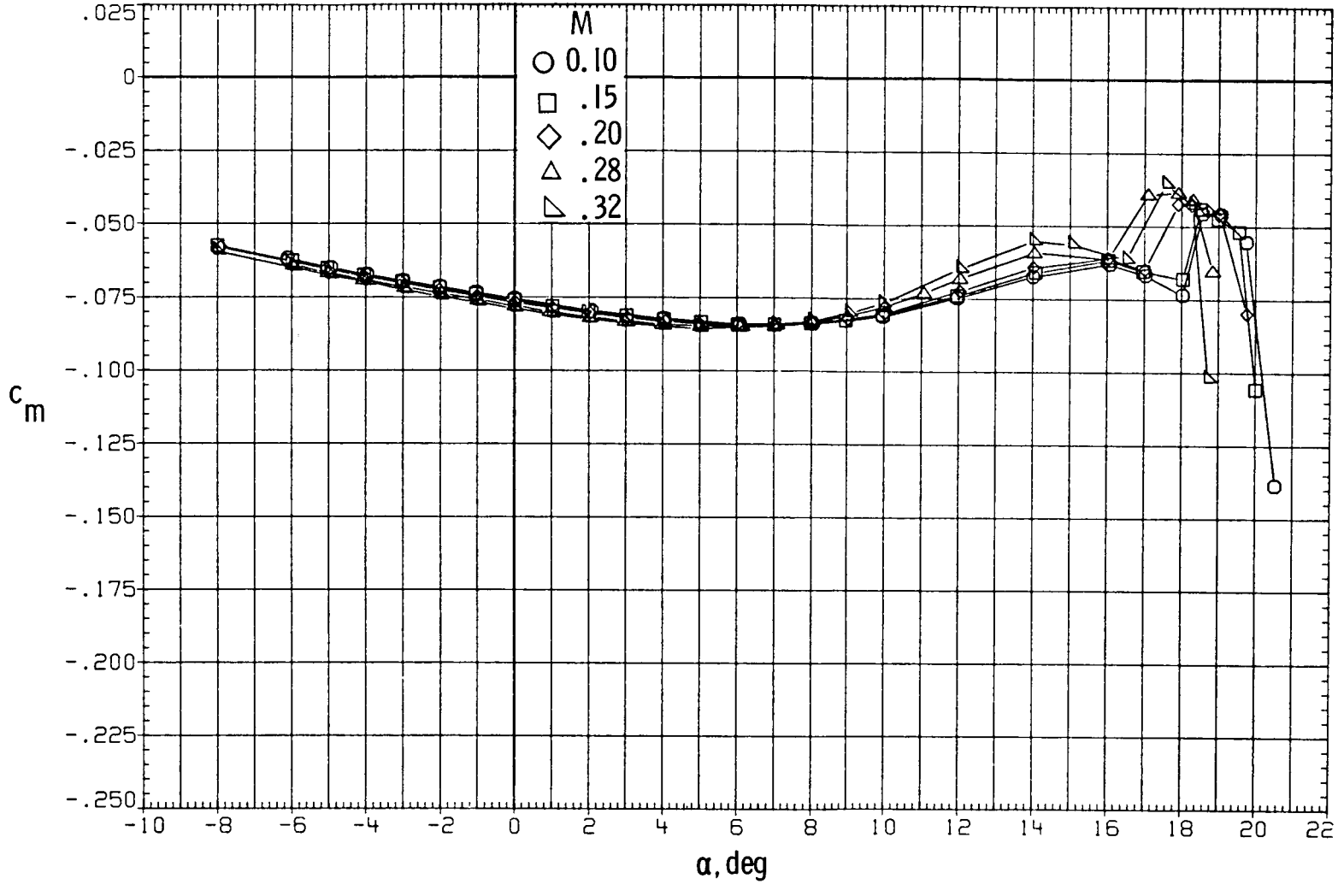

(c) Pitching moment.

Figure 11.- Concluded.

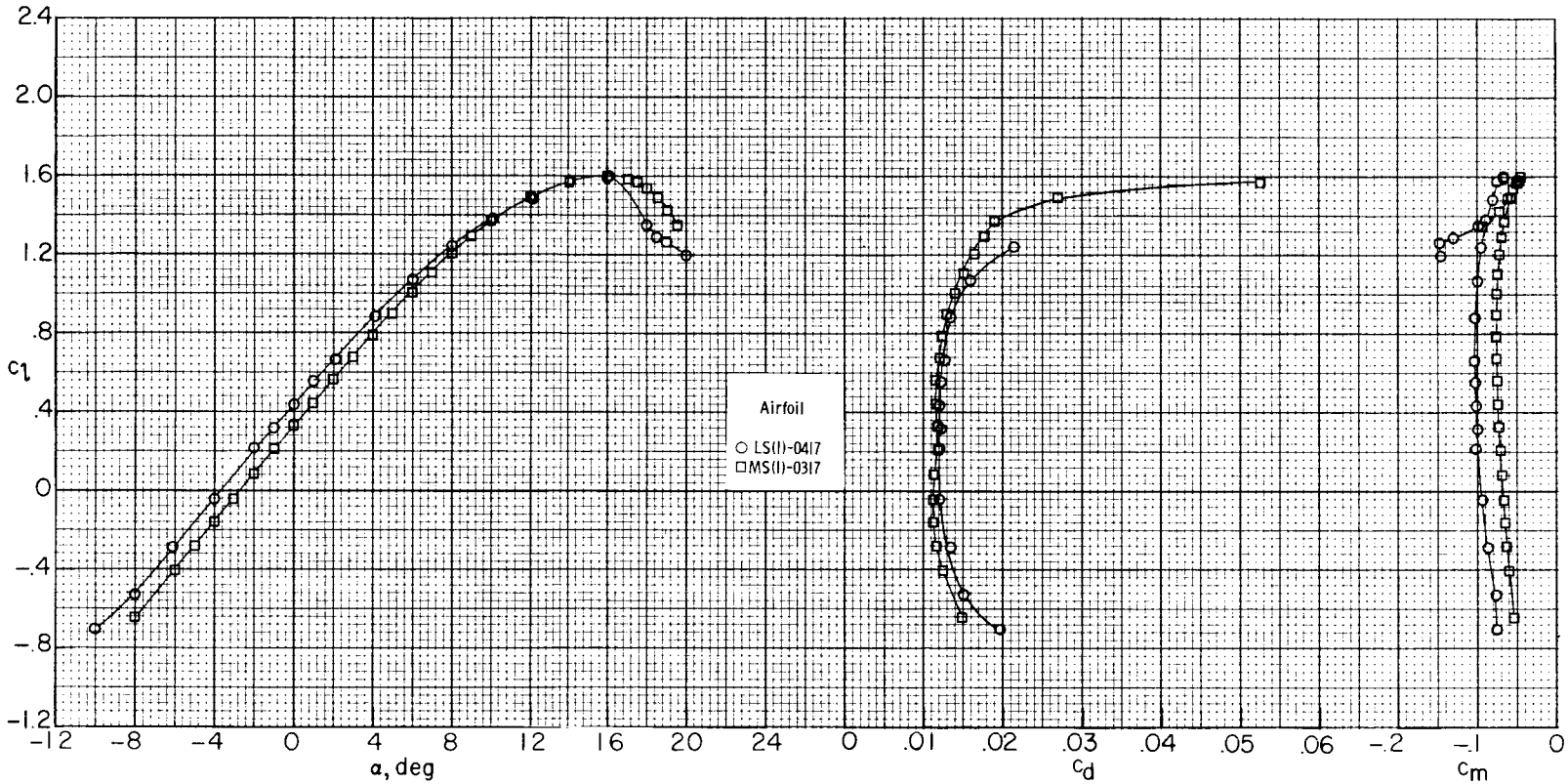

(a) $R = 2.0 \times 10^6$.

Figure 12.- Comparison of section characteristics for LS(1)-0417 and MS(1)-0317 airfoils. Roughness on; M = 0.15.

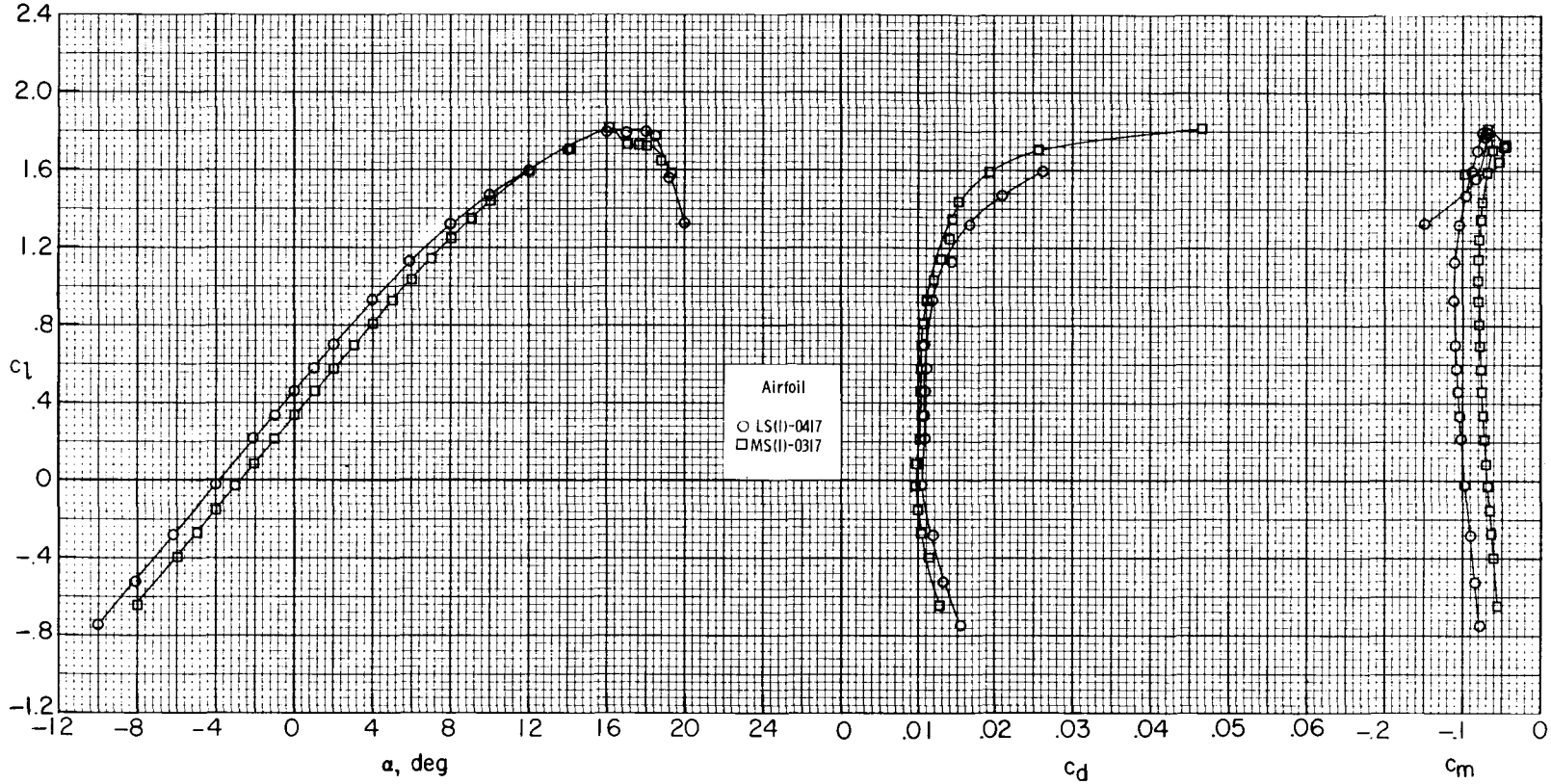

(b) $R = 4.0 \times 10^6$.

Figure 12.- Continued.

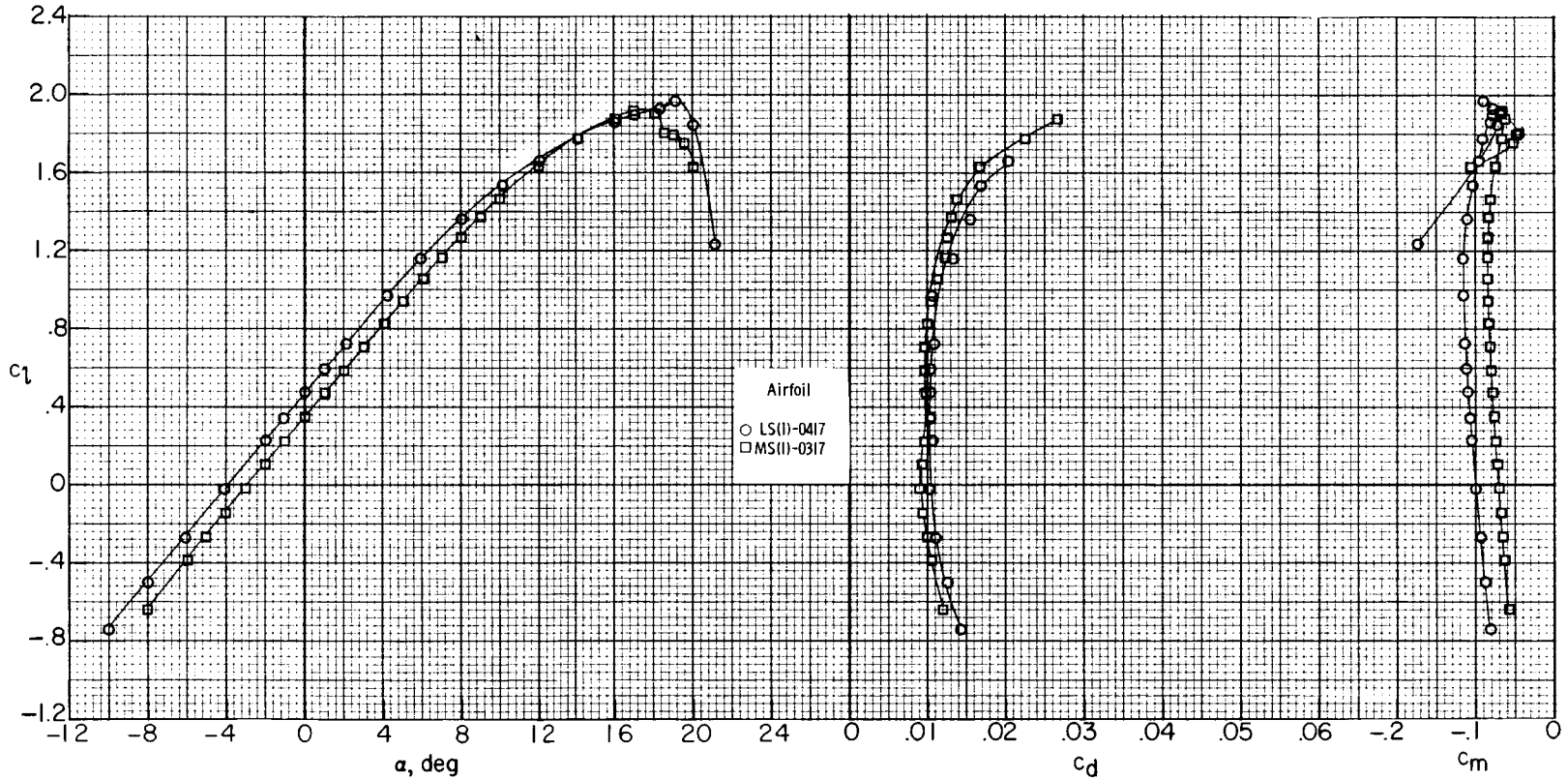

(c) $R = 6.0 \times 10^6$.

Figure 12.- Concluded.

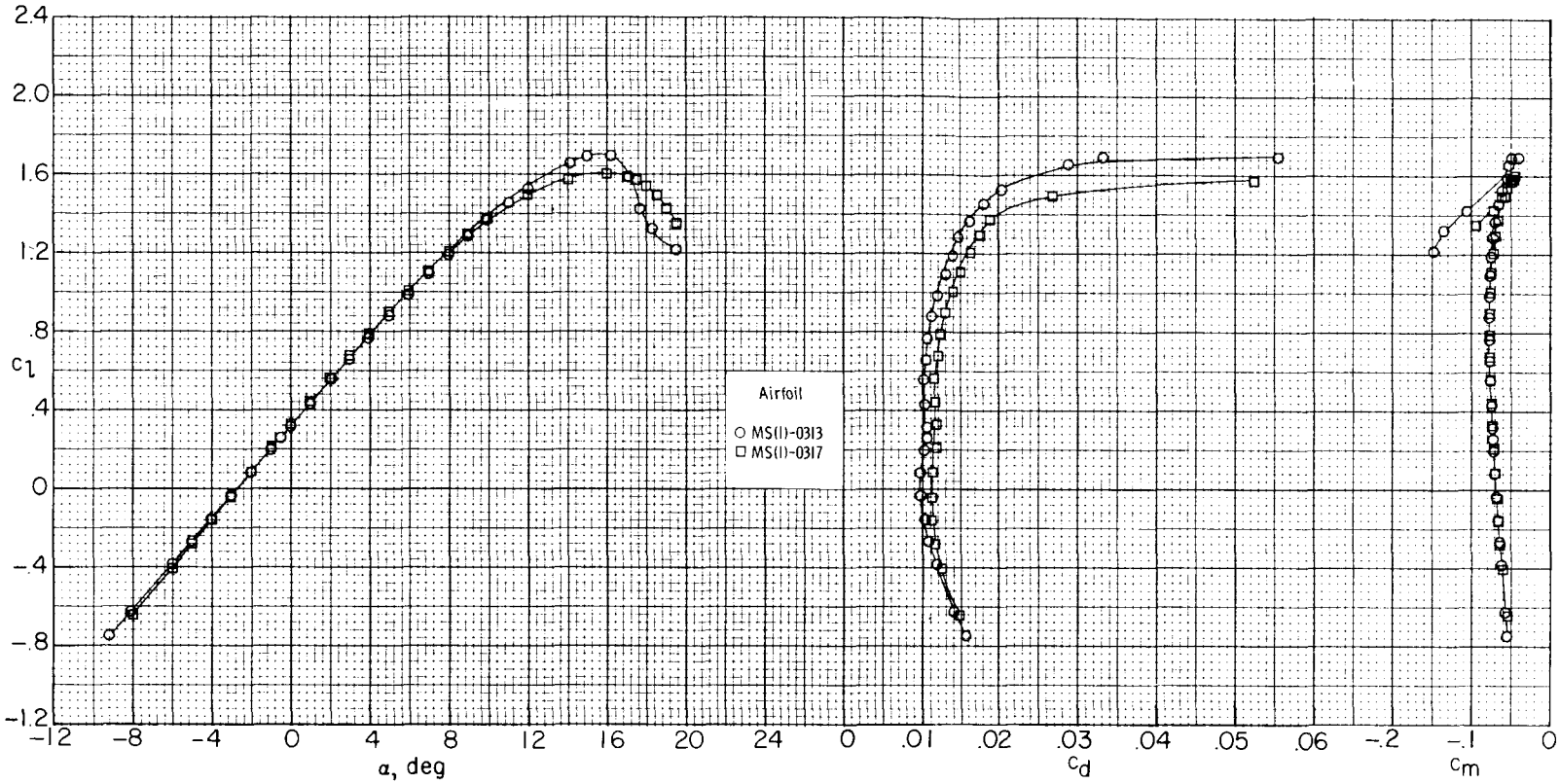

(a) $R = 2.0 \times 10^6$.

Figure 13.- Comparison of section characteristics for MS(1)-0313 and MS(1)-0317 airfoils. Roughness on; M = 0.15.

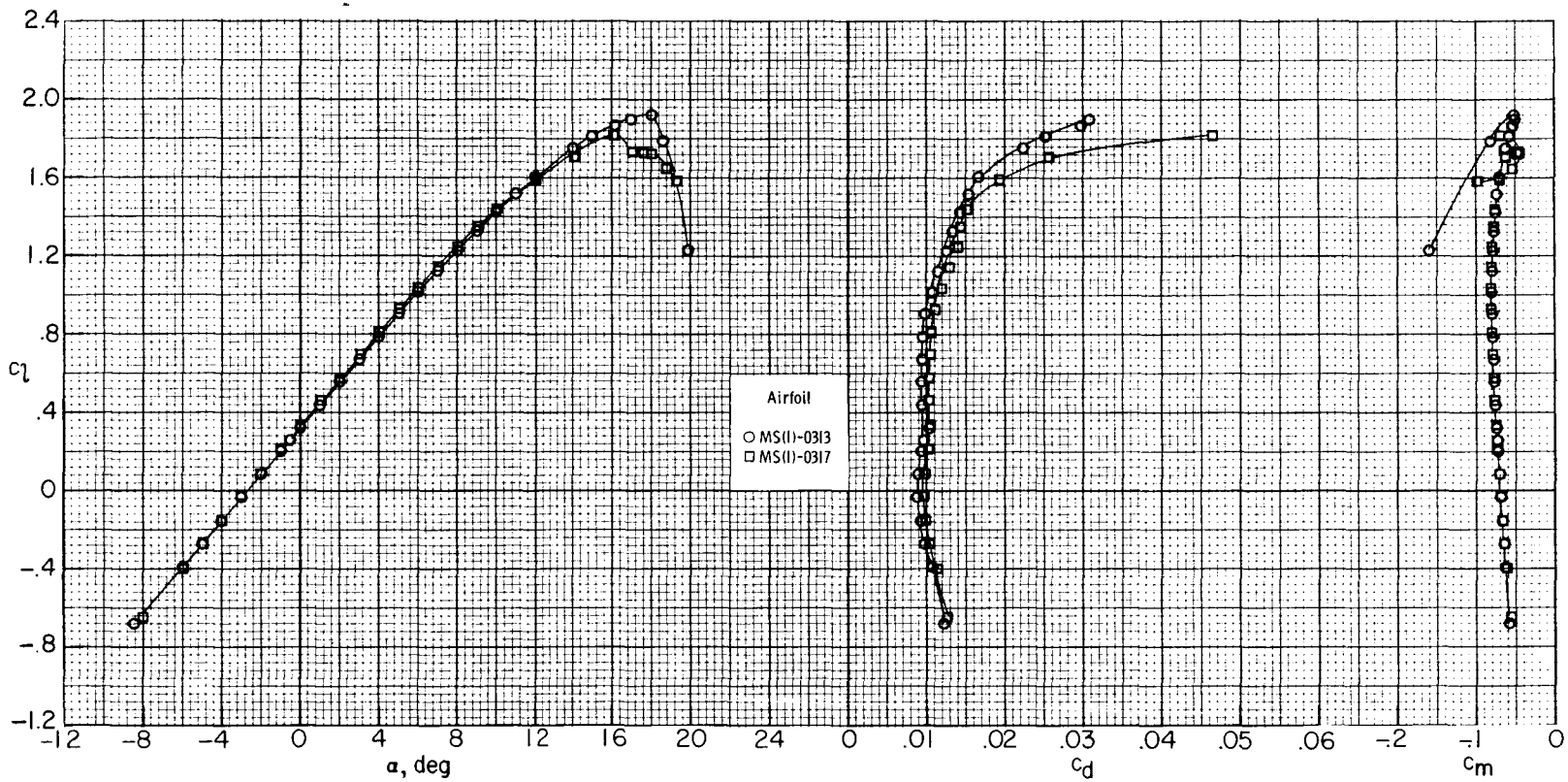

(b) $R = 4.0 \times 10^6$.

Figure 13.- Continued.

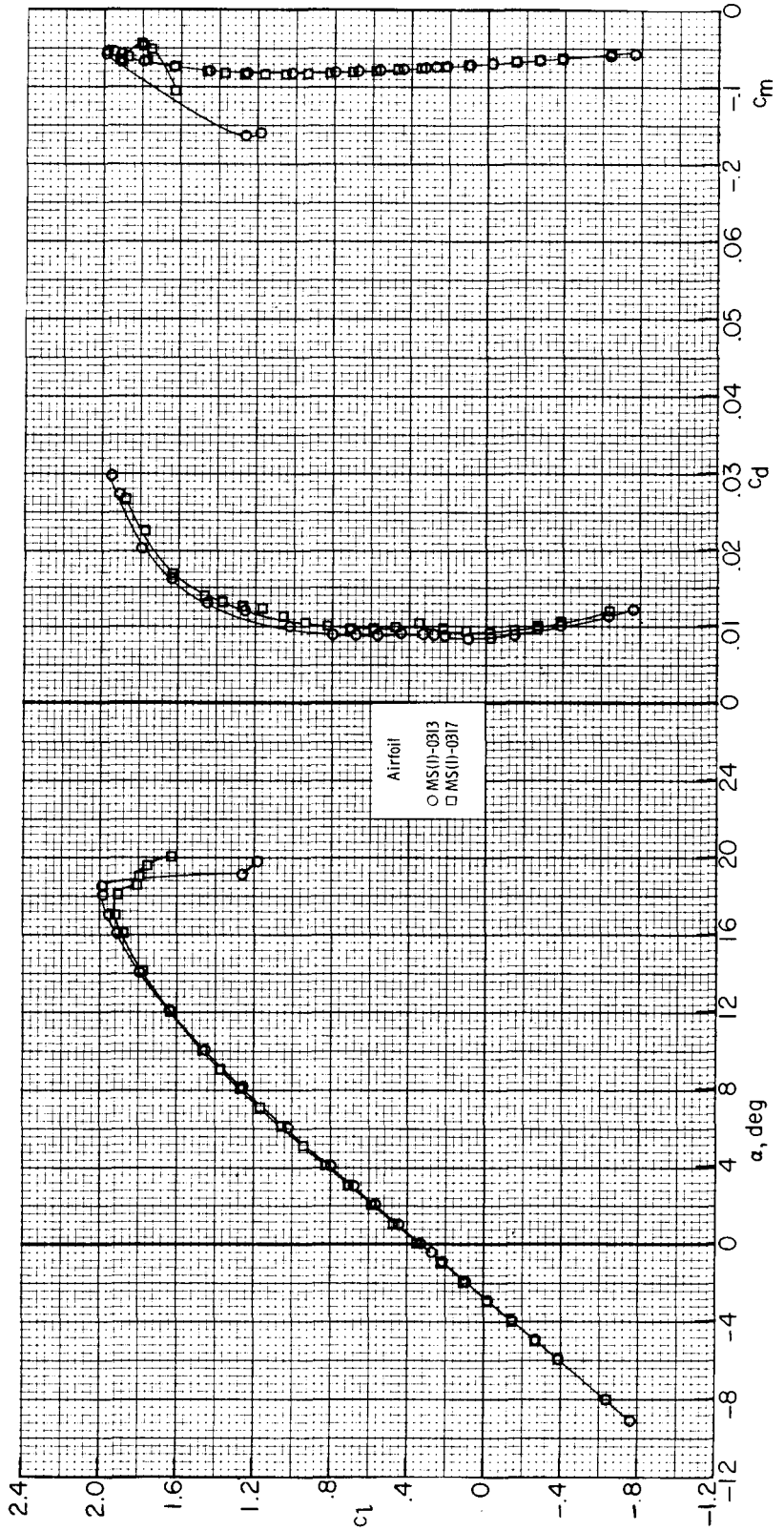

(c) R = 6.0 × 10^6.

Figure 13.- Continued.

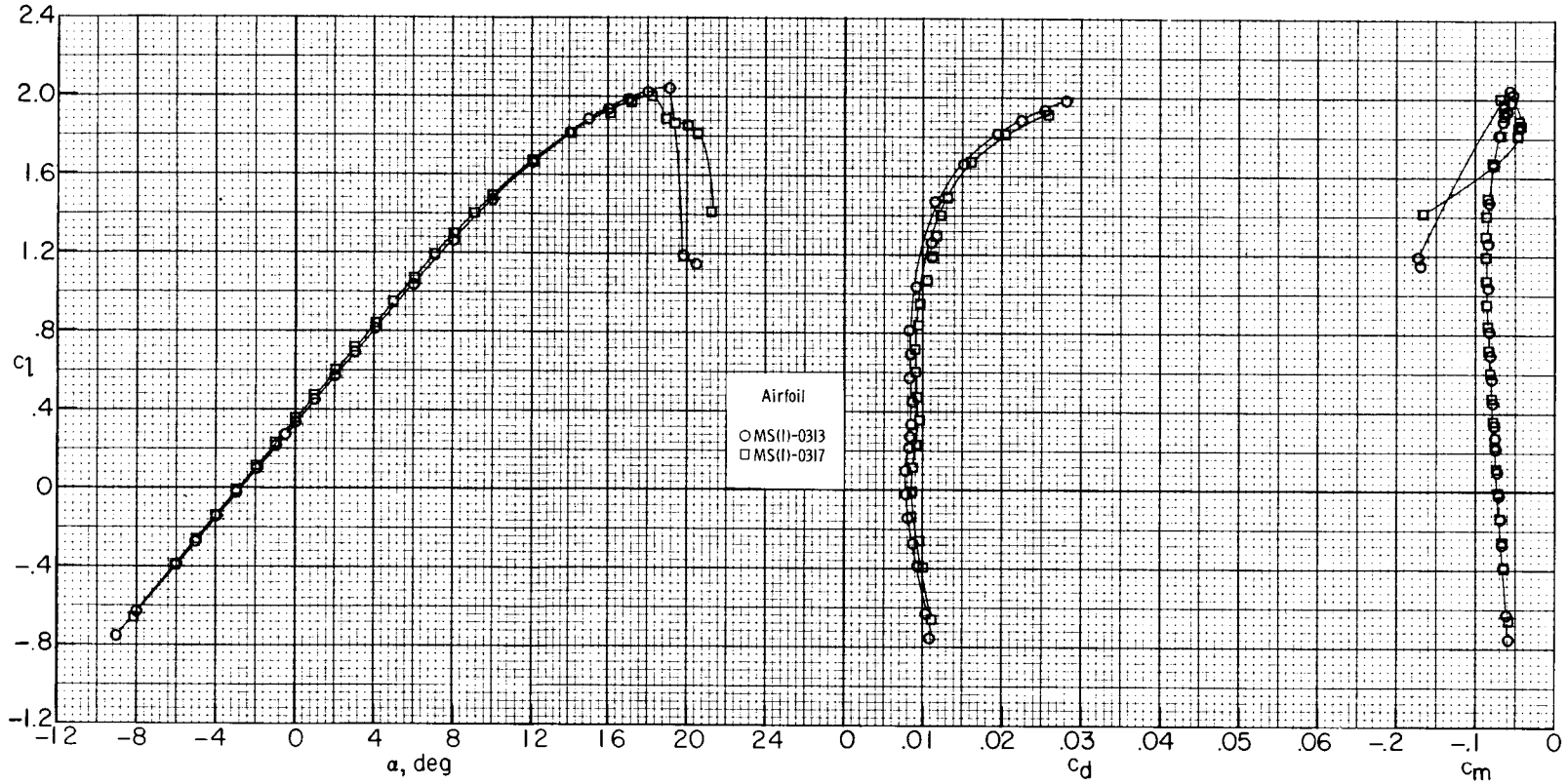

(d) $R = 9.0 \times 10^6$.

Figure 13.- Continued.

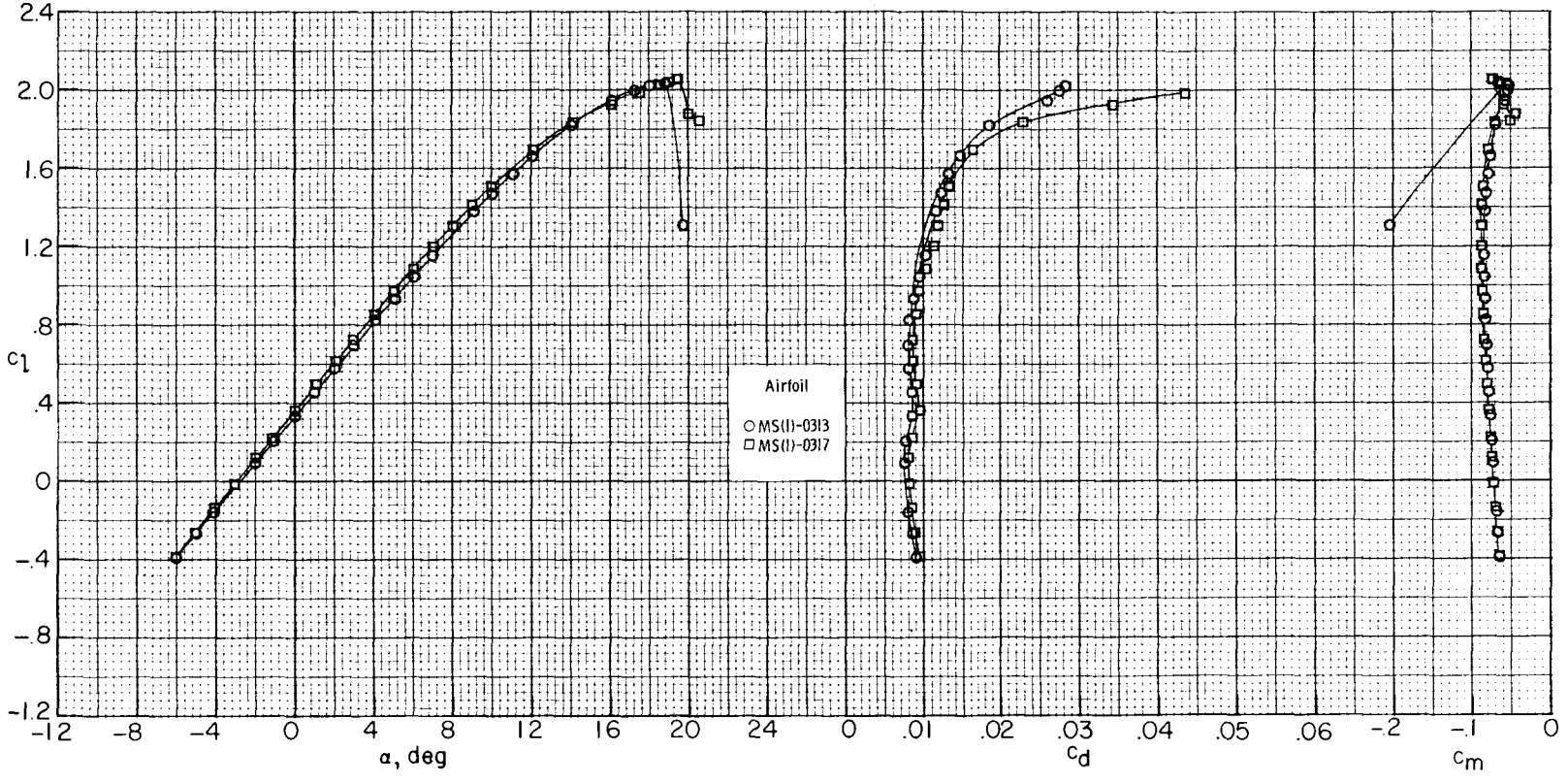

(e) $R = 12.0 \times 10^6$.

Figure 13.- Concluded.

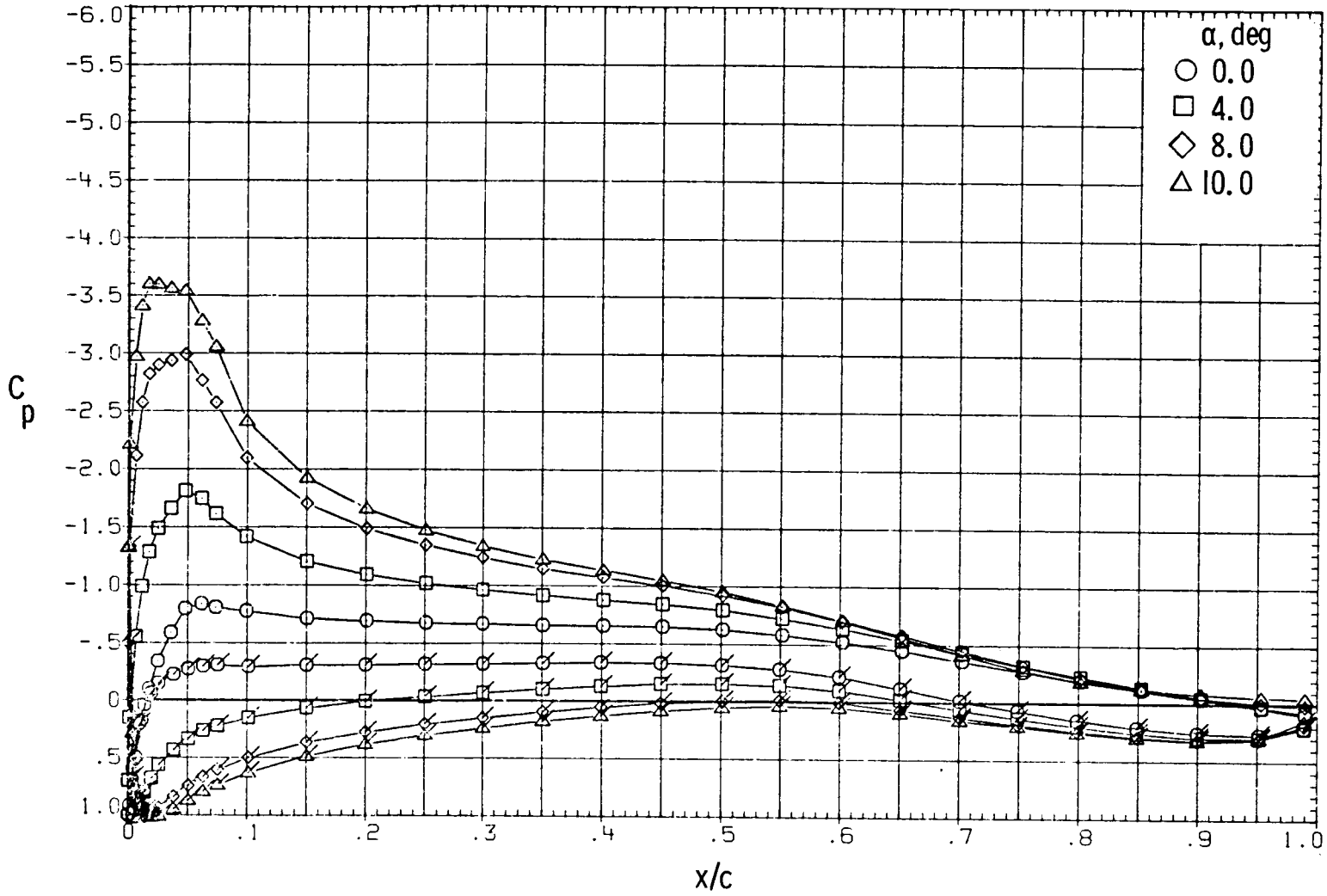

(a) $R = 2.0 \times 10^6$.

Figure 14.- Effect of angle of attack and Reynolds number on chordwise pressure distributions for MS(1)-0317 airfoil. Roughness on; M = 0.15. (Flagged symbols designate lower surface.)

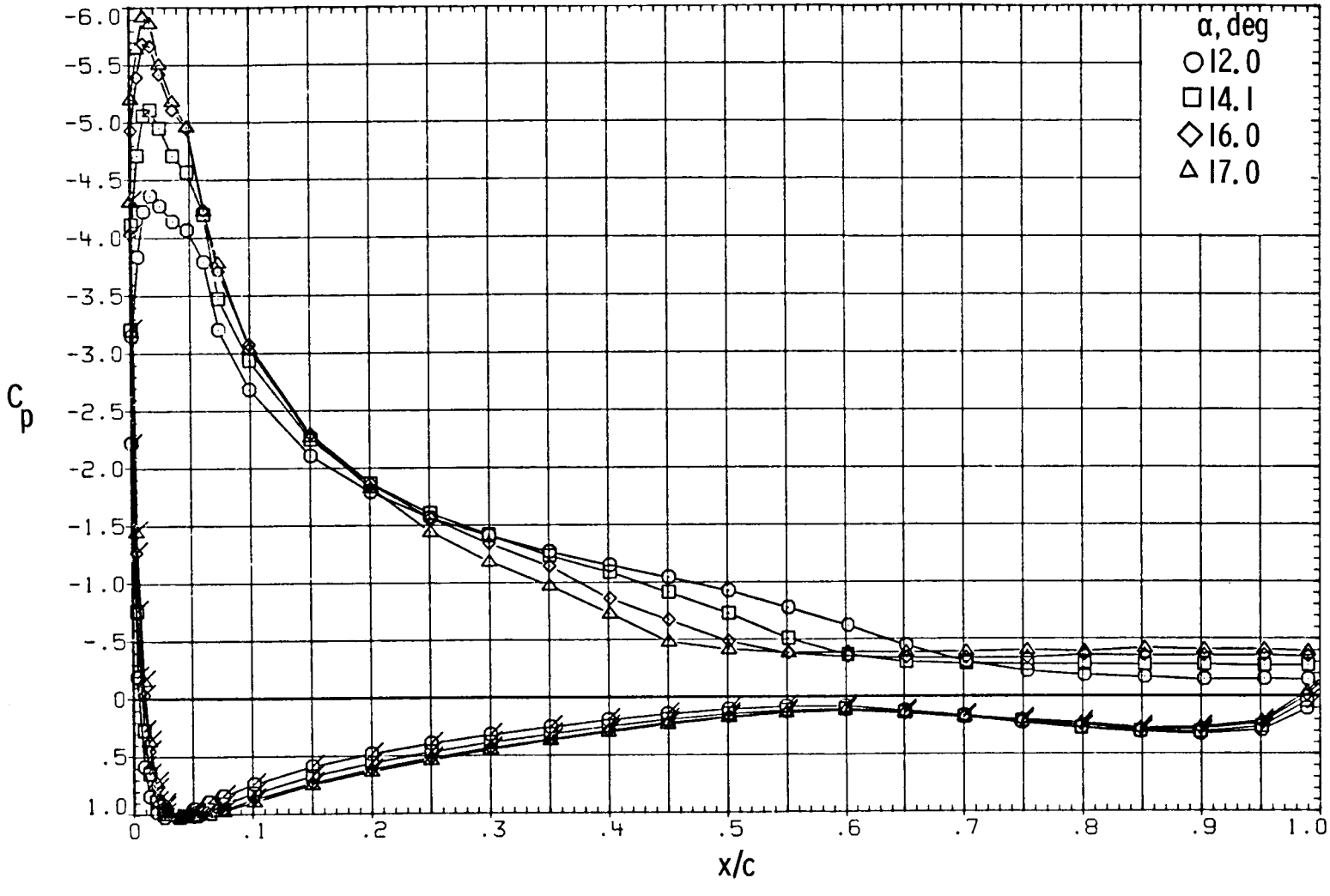

(a) $R = 2.0 \times 10^6$. Concluded.

Figure 14.- Continued.

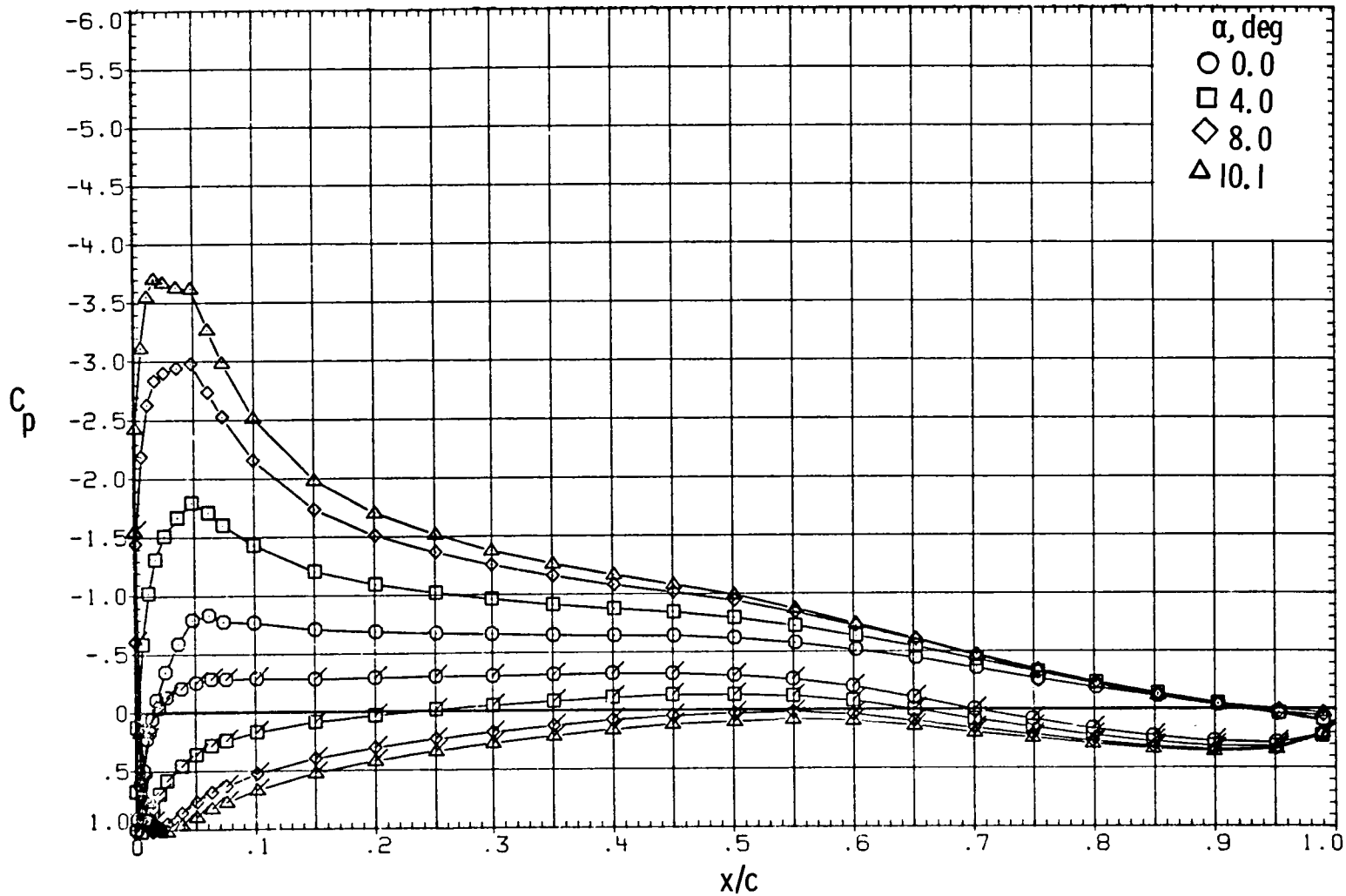

(b) $R = 4.0 \times 10^6$.

Figure 14.- Continued.

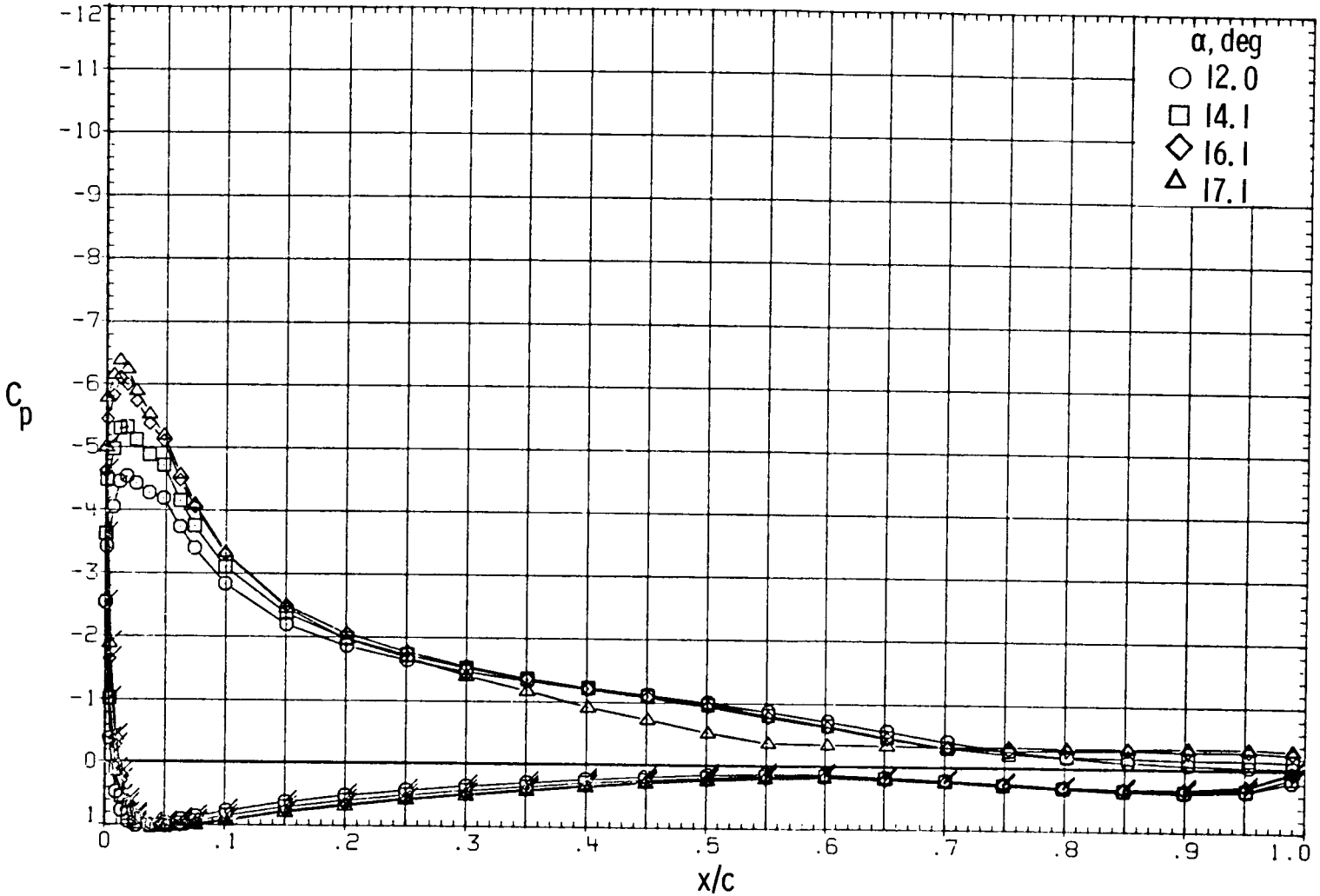

(b) $R = 4.0 \times 10^6$. Concluded.

Figure 14.- Continued.

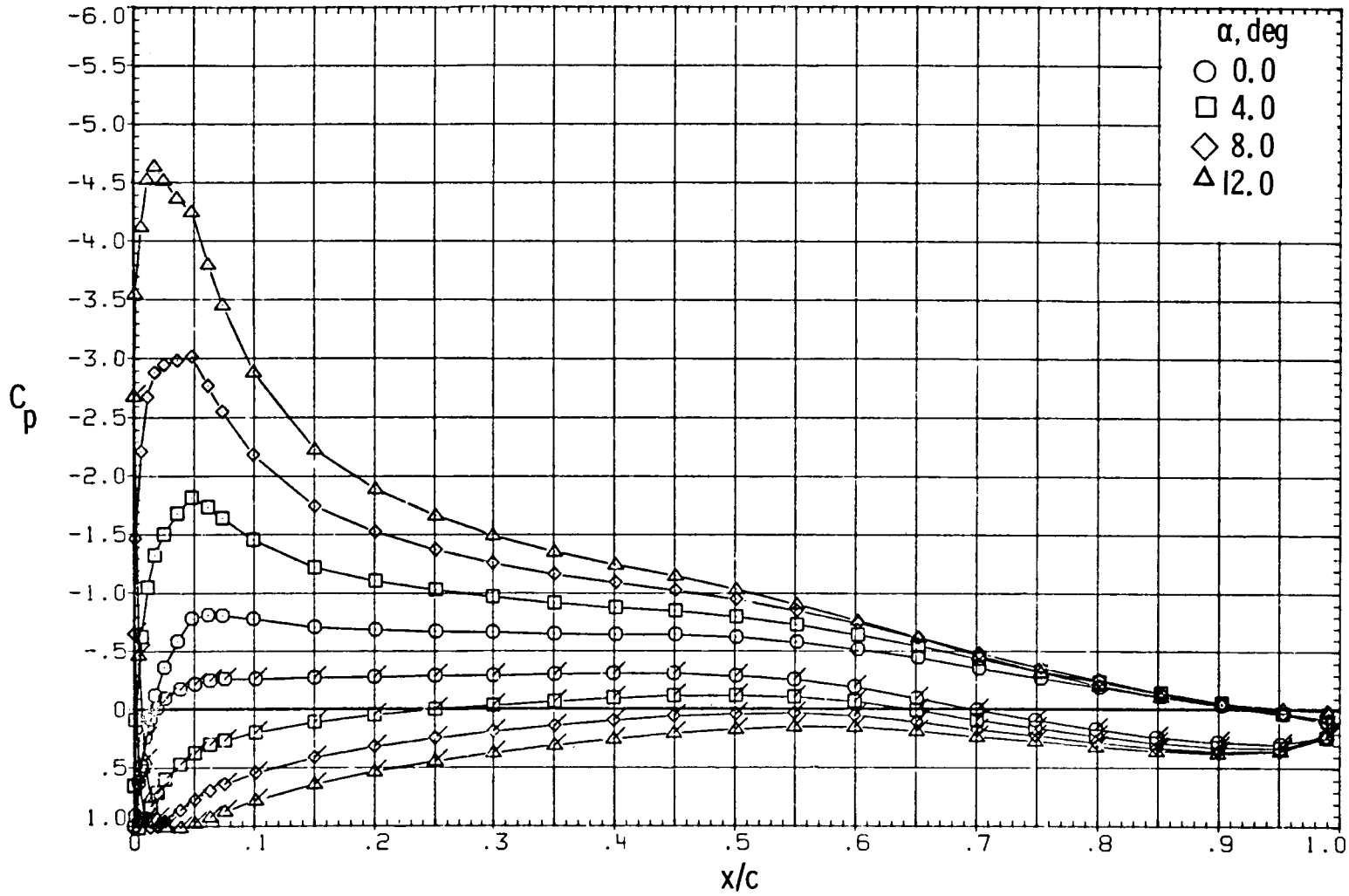

(c) $R = 6.0 \times 10^6$.

Figure 14.- Continued.

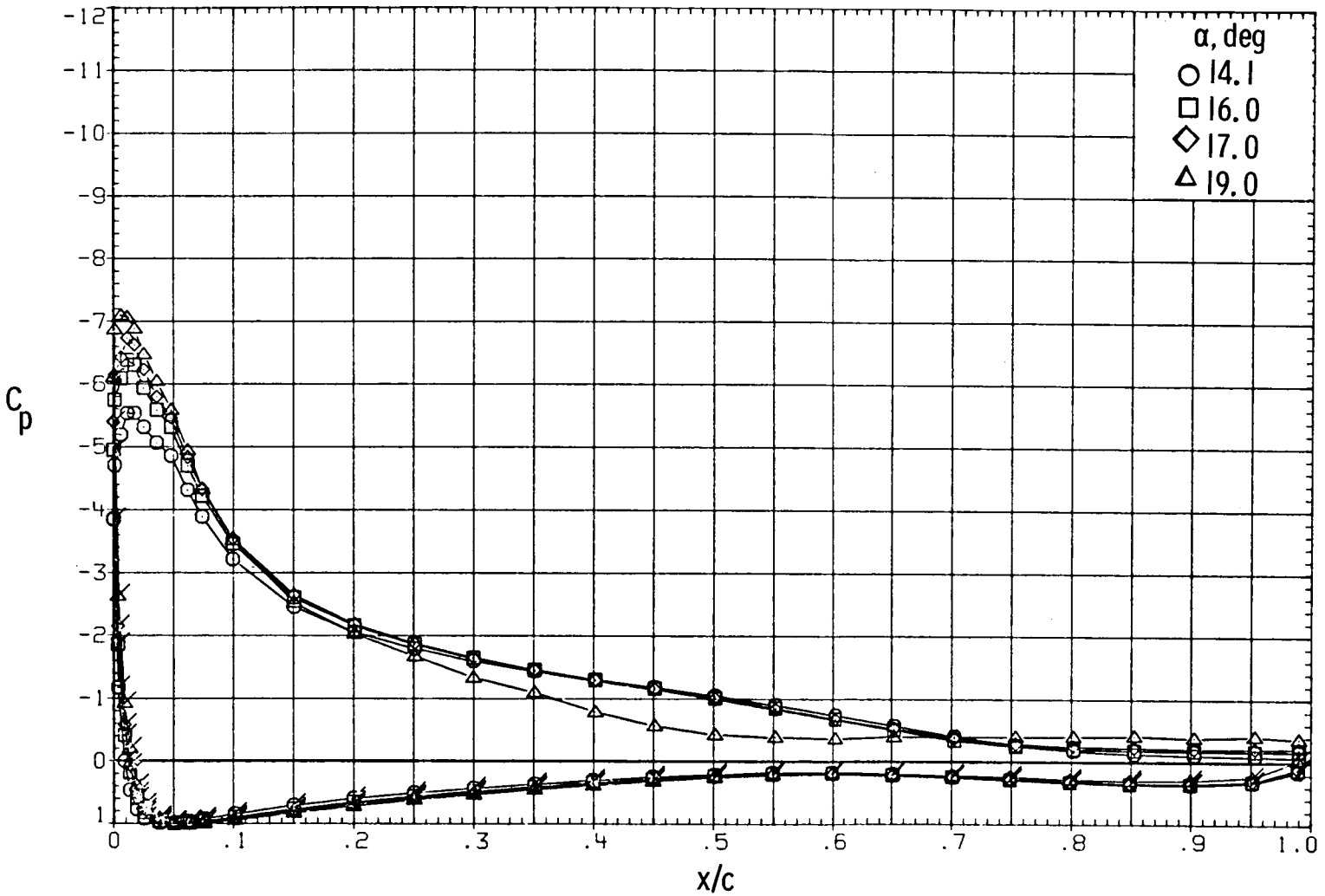

(c) R = 6.0 × 10^6. Concluded.

Figure 14.- Continued.

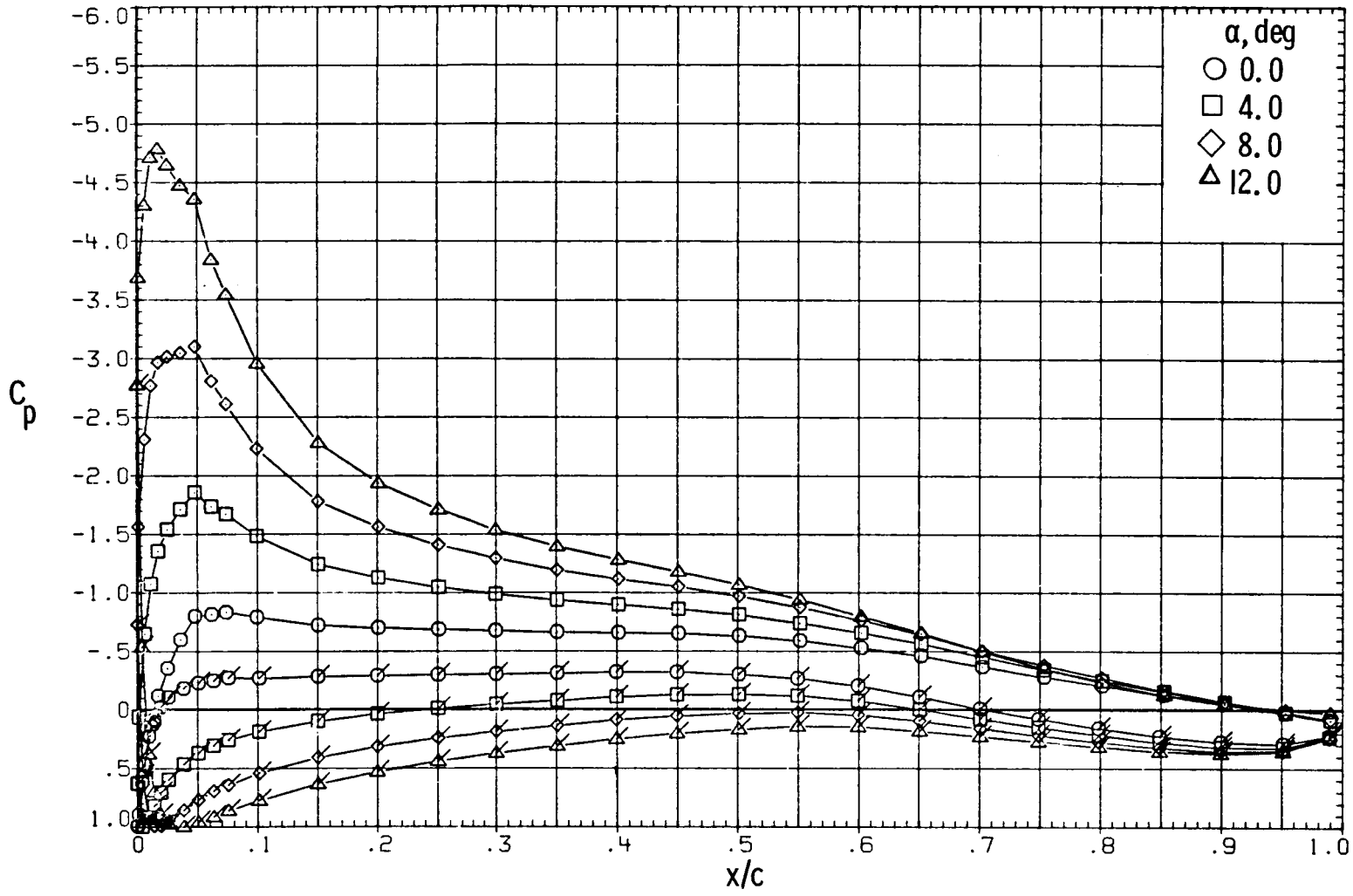

(d) $R = 9.0 \times 10^6$.

Figure 14.- Continued.

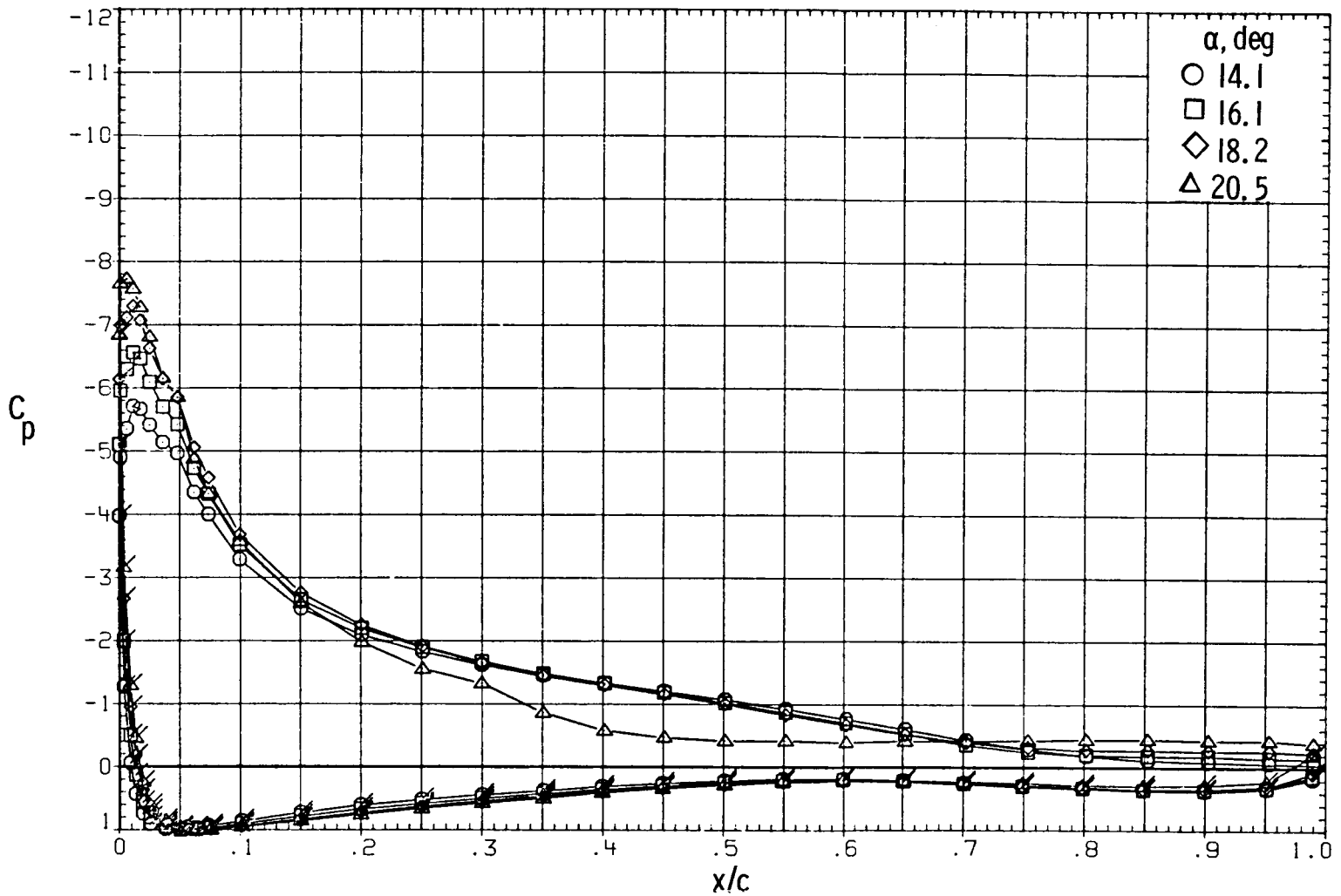

(d) $R = 9.0 \times 10^6$. Concluded.

Figure 14.- Concluded.

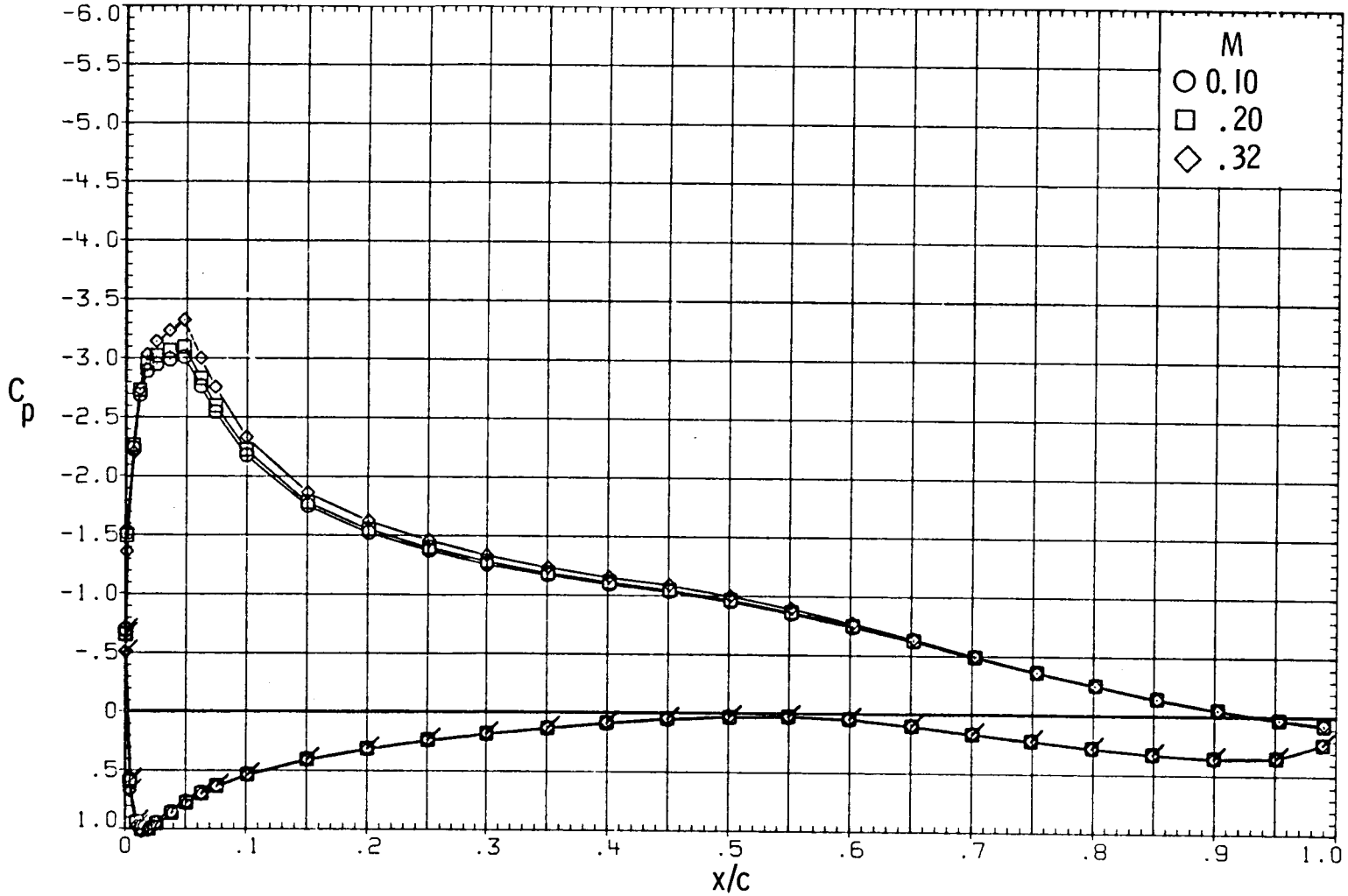

(a) $\alpha = 8^{\circ}$.

Figure 15.- Effect of Mach number on chordwise pressure distributions for MS(1)-0317 airfoil. Roughness on; $R = 6.0 \times 10^6$. (Flagged symbols designate lower surface.)

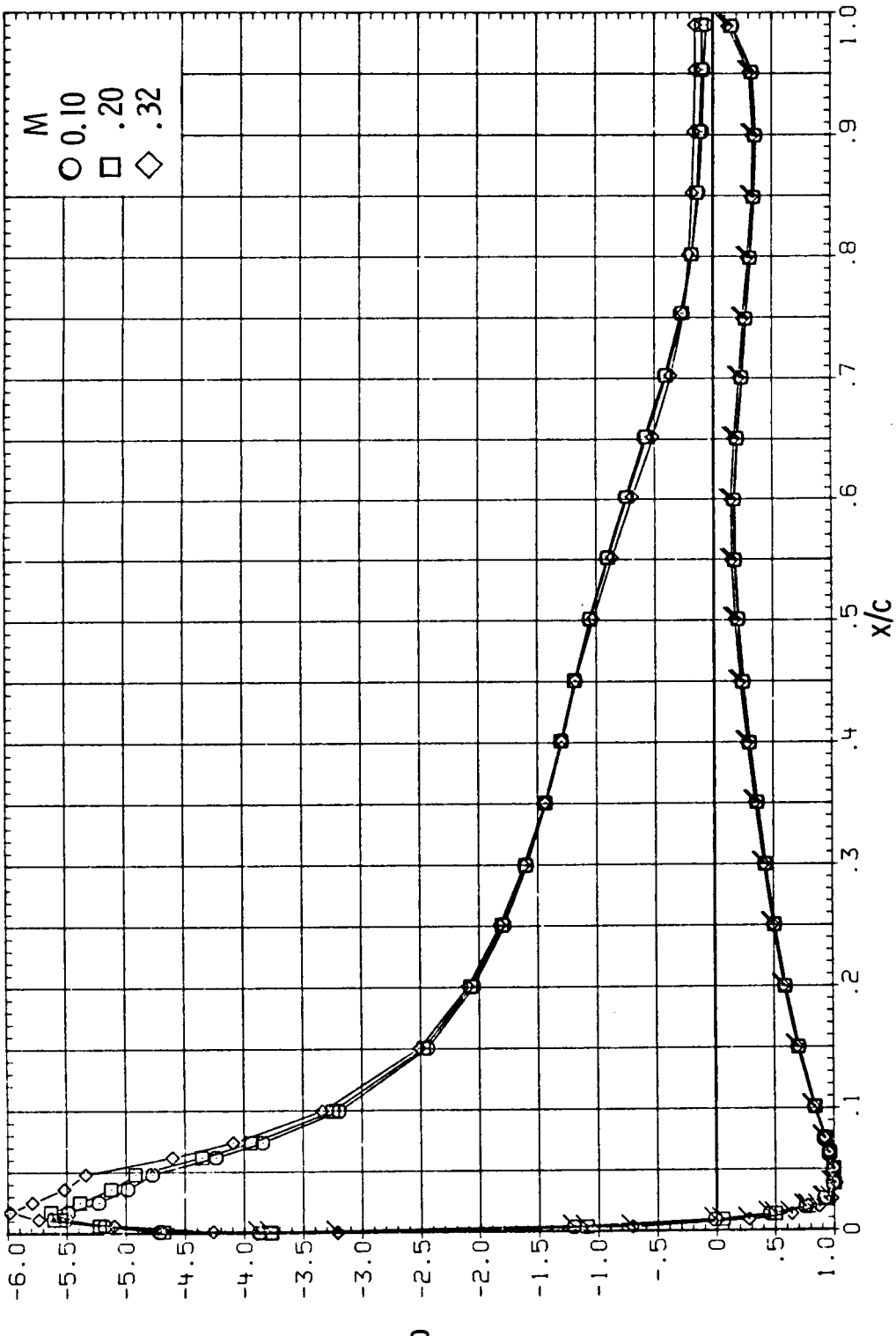

(b) $\alpha = 14°$.

Figure 15.- Concluded.

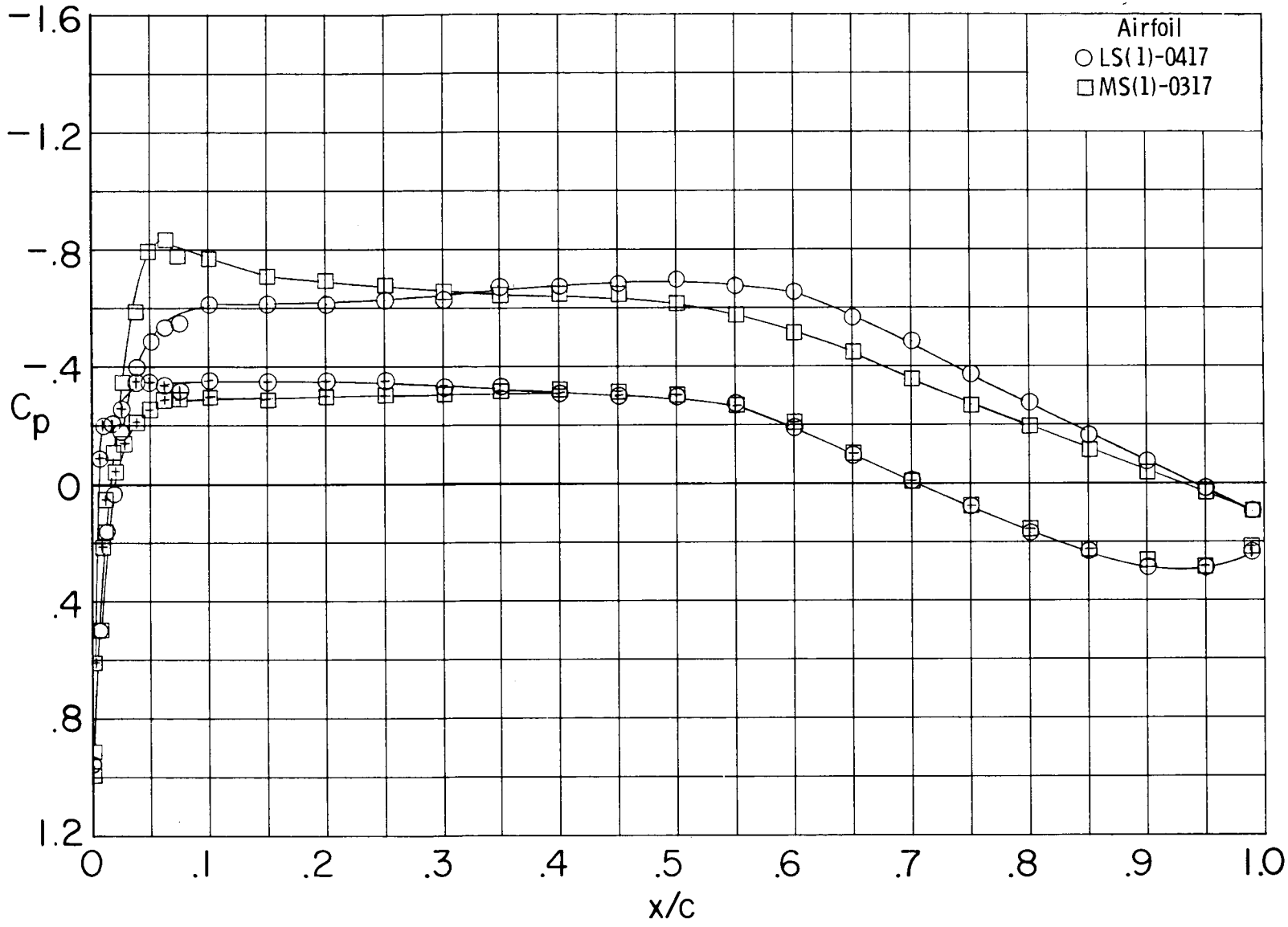

(a) c_l = 0.33.

Figure 16.- Comparison of chordwise pressure distributions for LS(1)-0417 and MS(1)-0317 airfoils. Roughness on; M = 0.15; R = 4.0×10^6. (Symbols with + inside designate lower surface.)

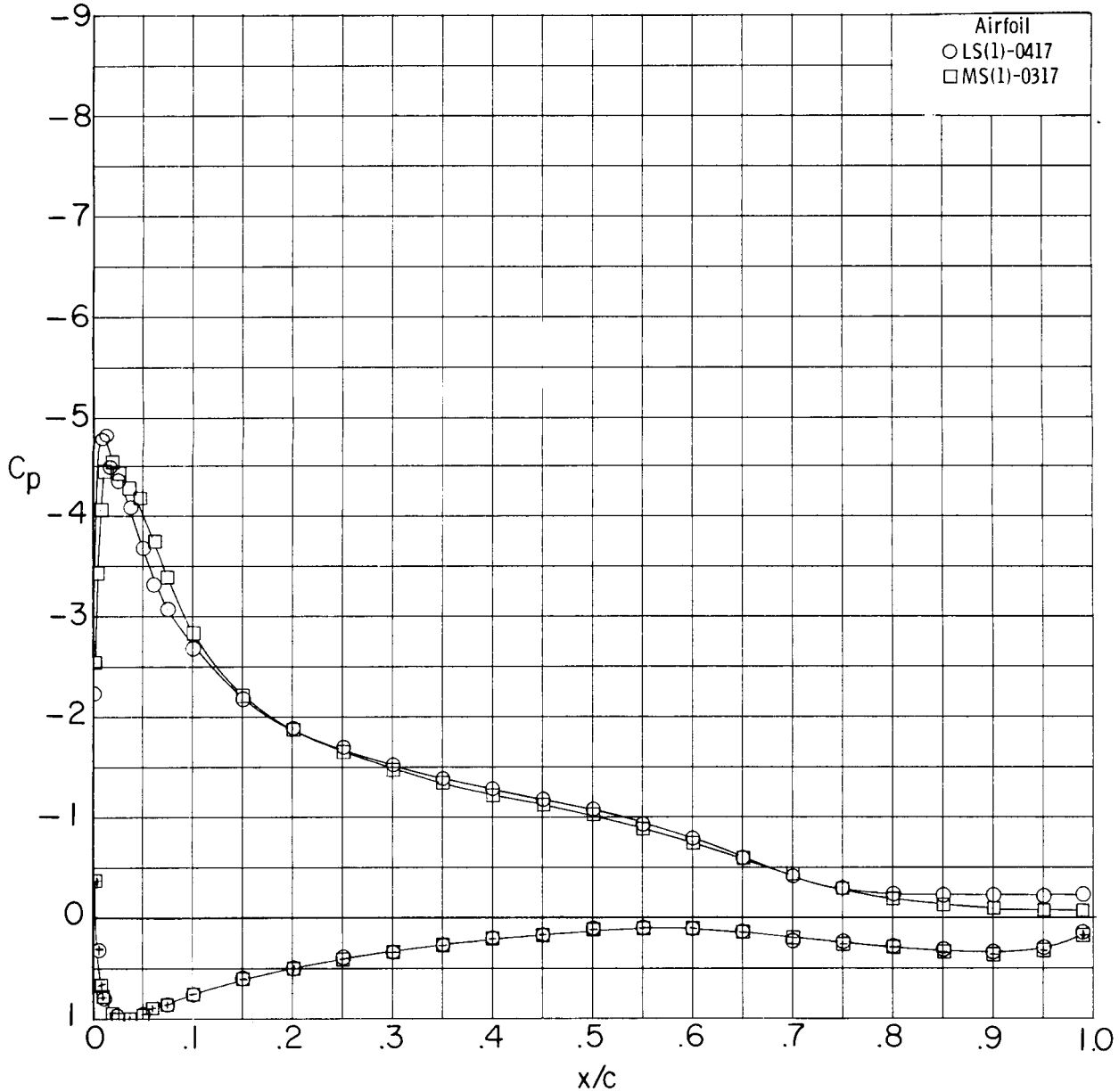

(b) c_l = 1.60.

Figure 16.- Concluded.

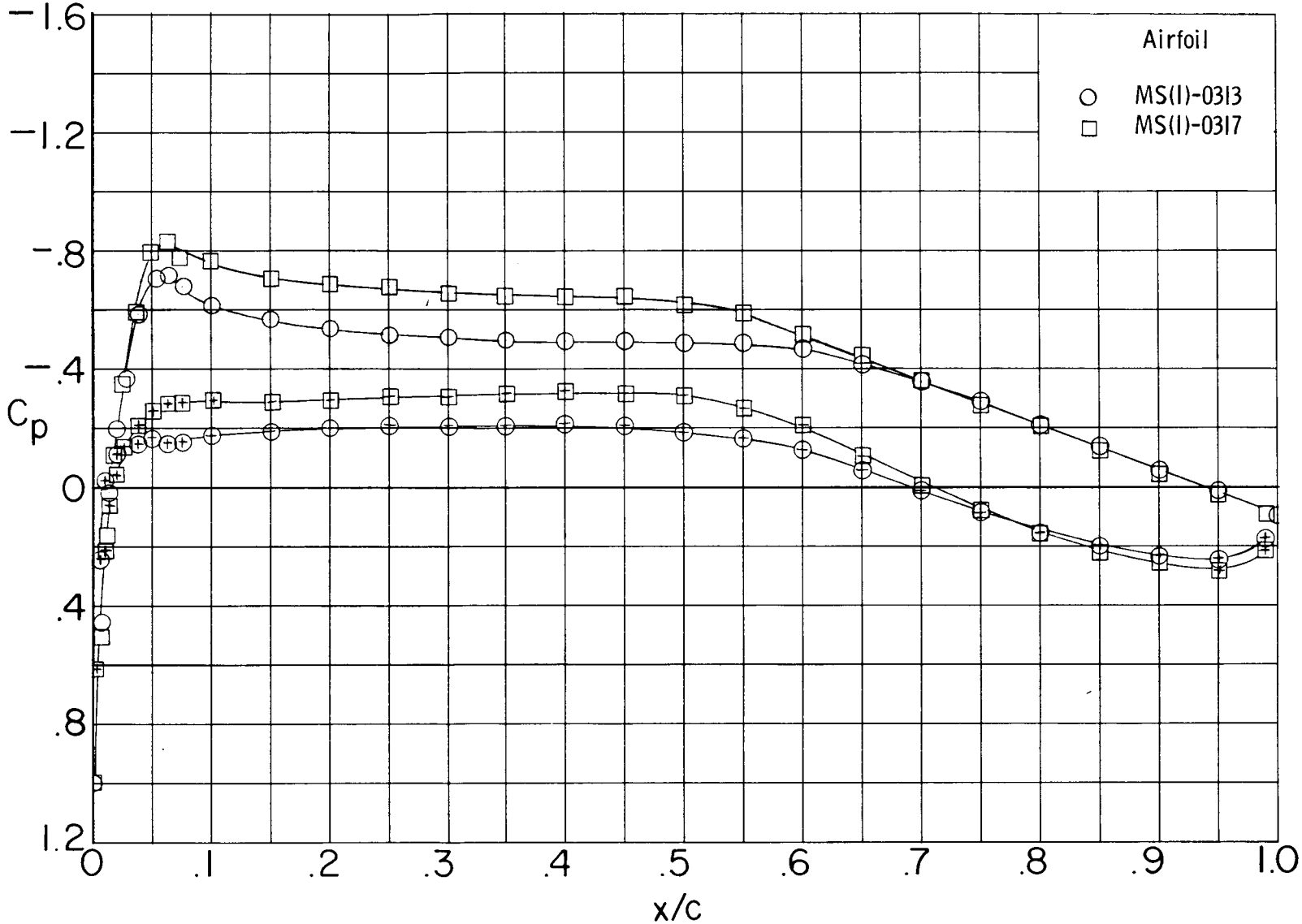

(a) $\alpha = 0^{o}$.

Figure 17.- Comparison of chordwise pressure distributions for MS(1)-0313 and MS(1)-0317 airfoils. Roughness on; $M = 0.15$; $R = 4.0 \times 10^{6}$. (Symbols with + inside designate lower surface.)

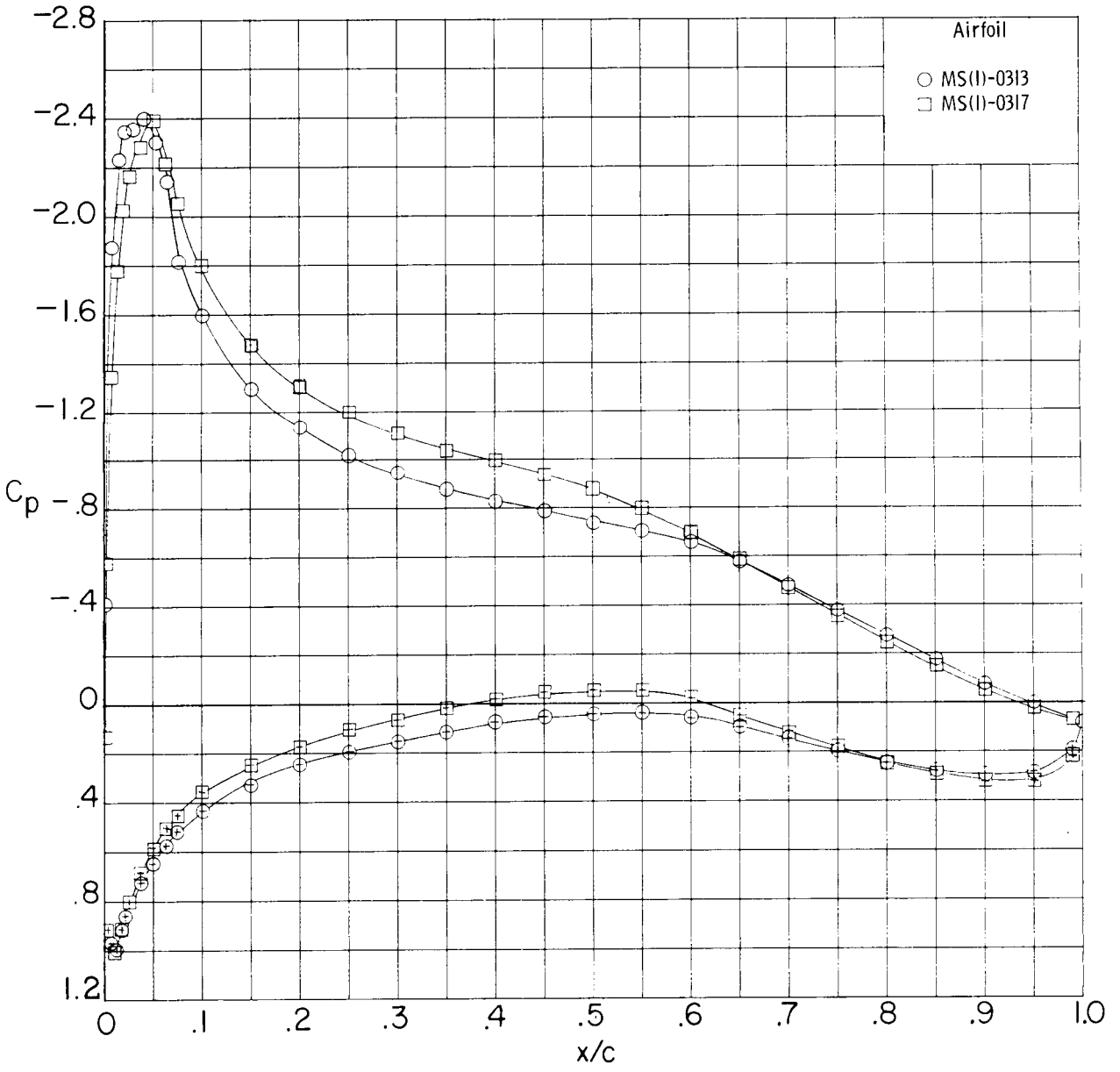

(b) $\alpha = 6^{o}$.

Figure 17.- Continued.

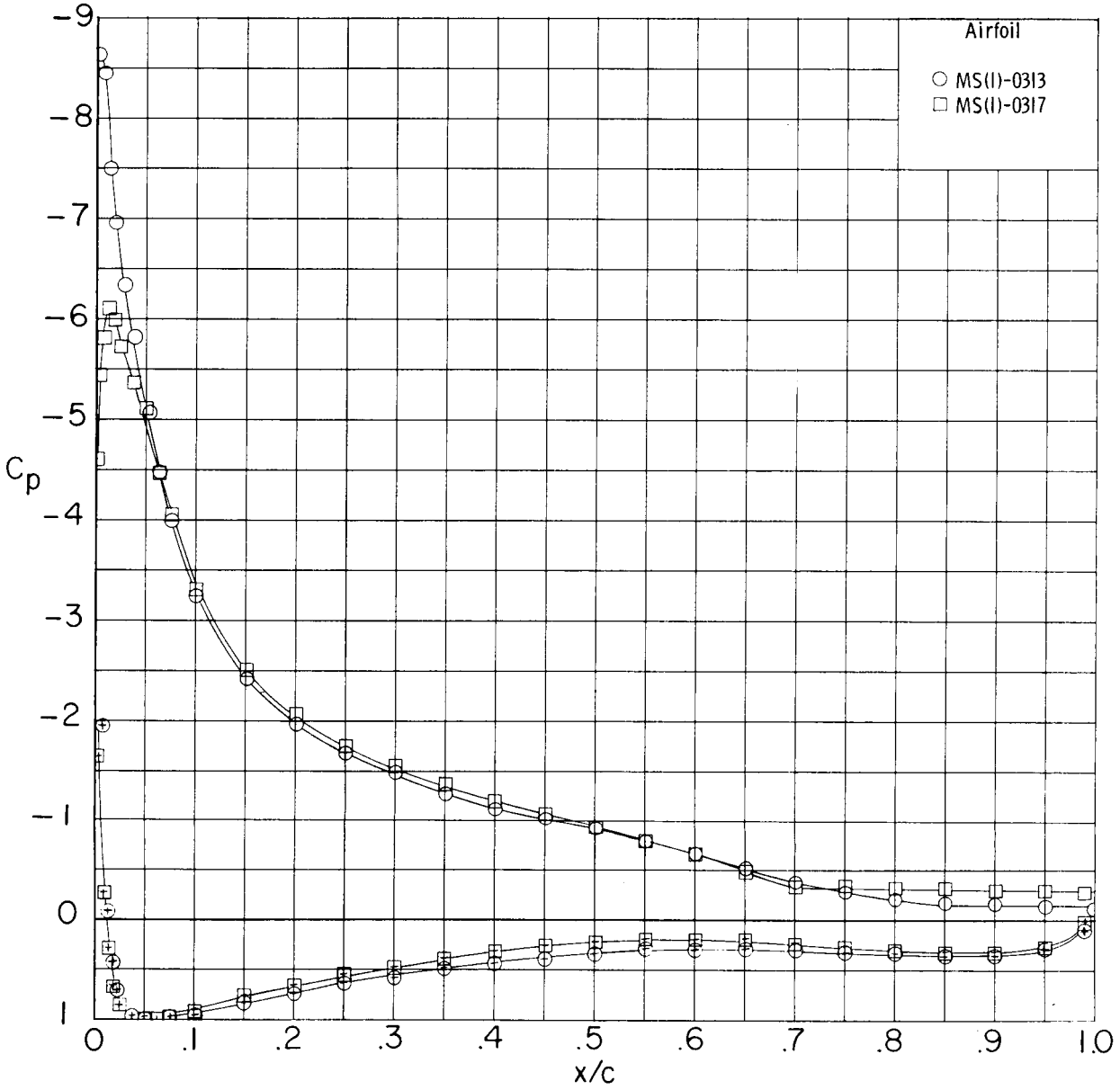

(c) $\alpha = 16^{\circ}$.

Figure 17.- Concluded.

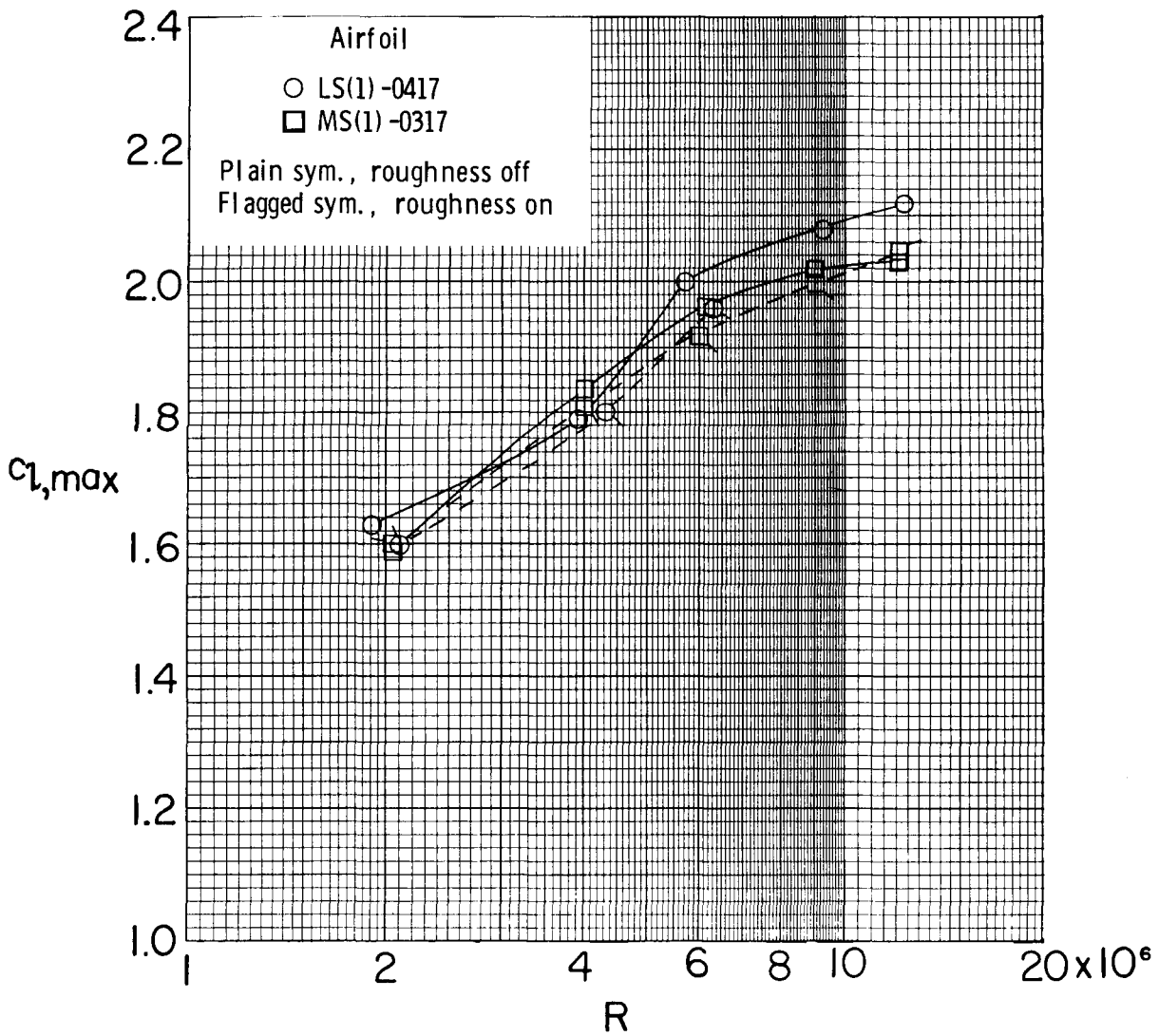

Figure 18.- Variation of maximum lift coefficient with Reynolds number for LS(1)-0417 and MS(1)-0317 airfoils. M = 0.15.

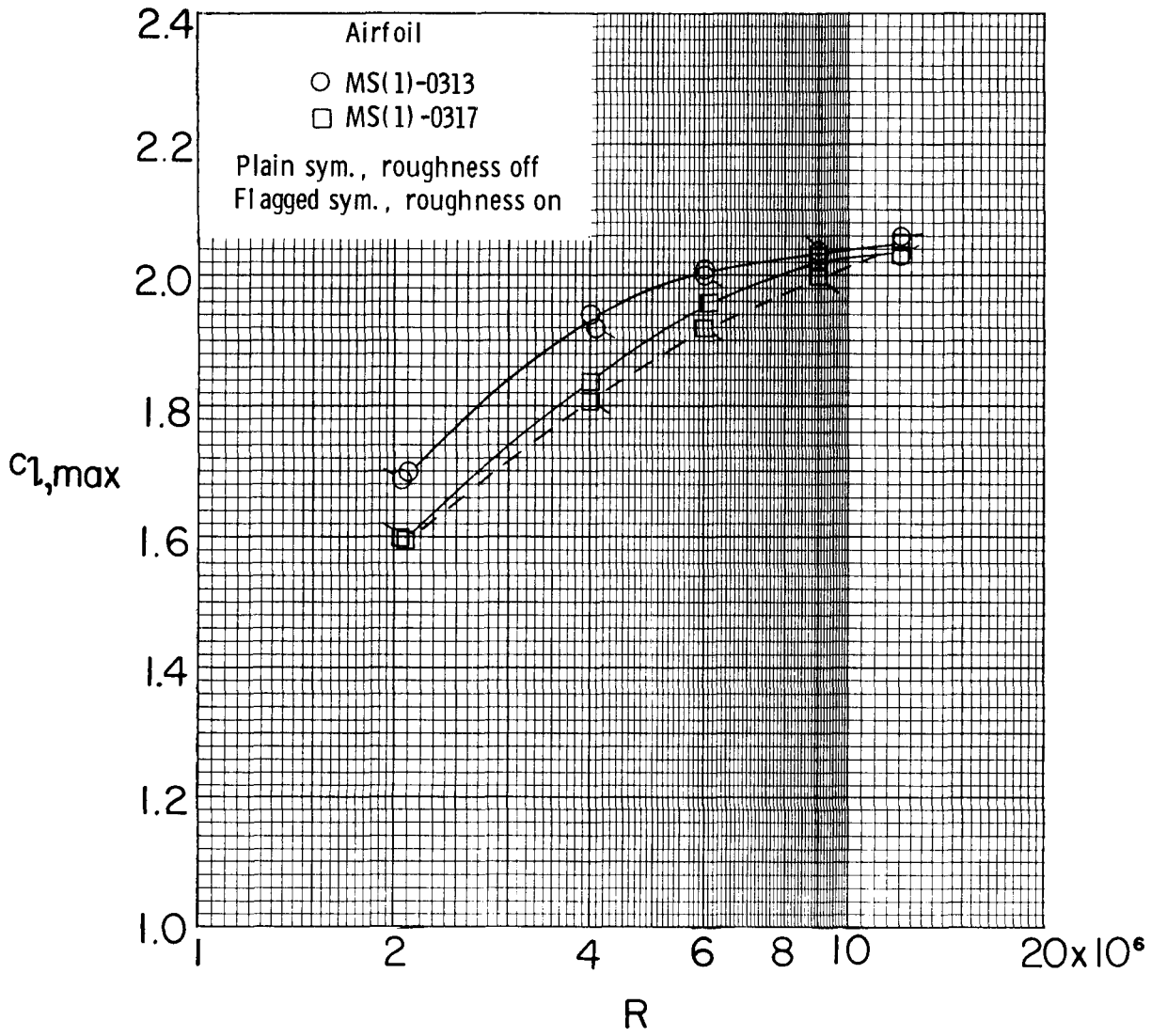

Figure 19.- Variation of maximum lift coefficient with Reynolds number for MS(1)-0313 and MS(1)-0317 airfoils. M = 0.15.

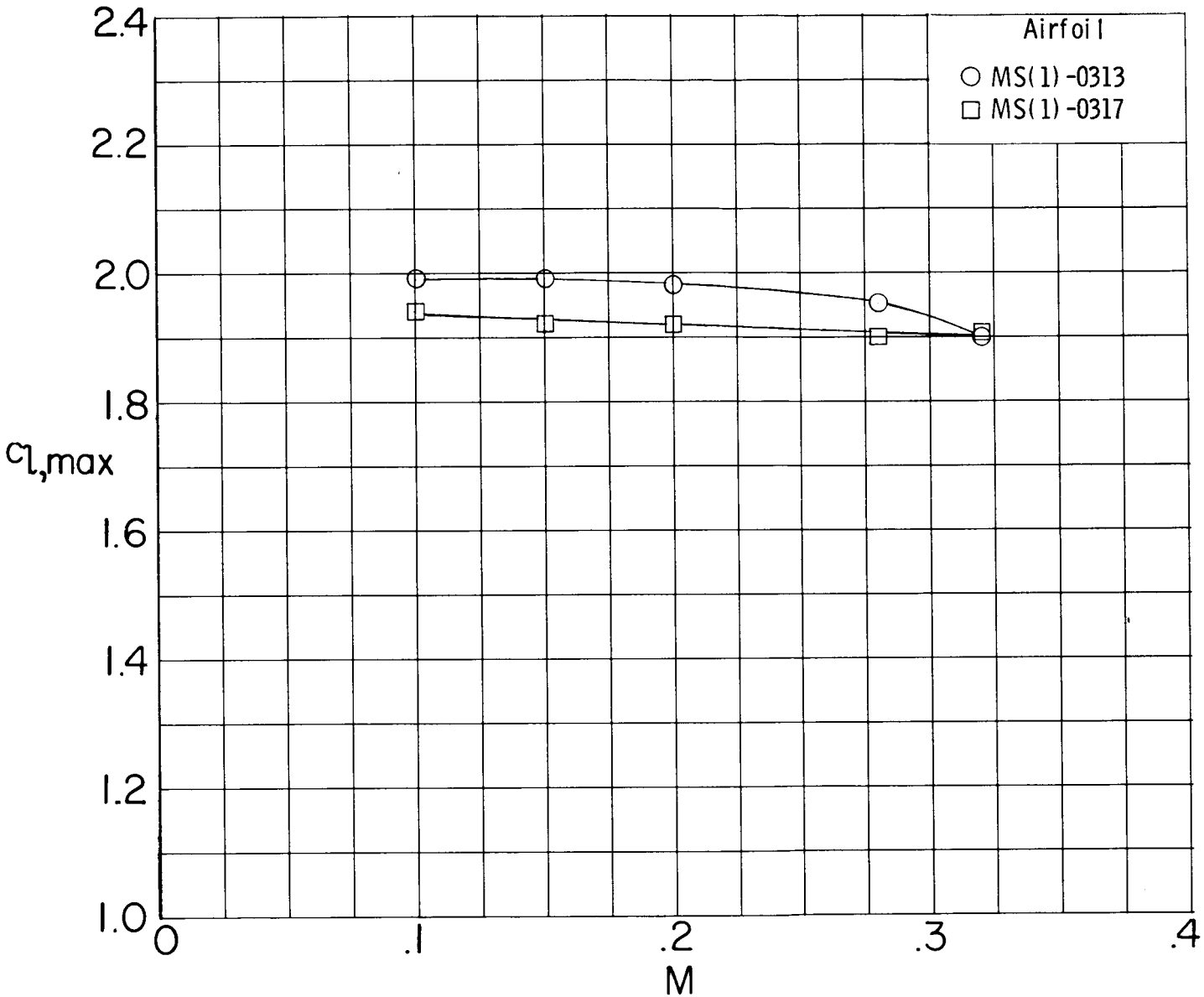

Figure 20.- Variation of maximum lift coefficient with Mach number for MS(1)-0313 and MS(1)-0317 airfoils. Roughness on; $R = 6.0 \times 10^6$.

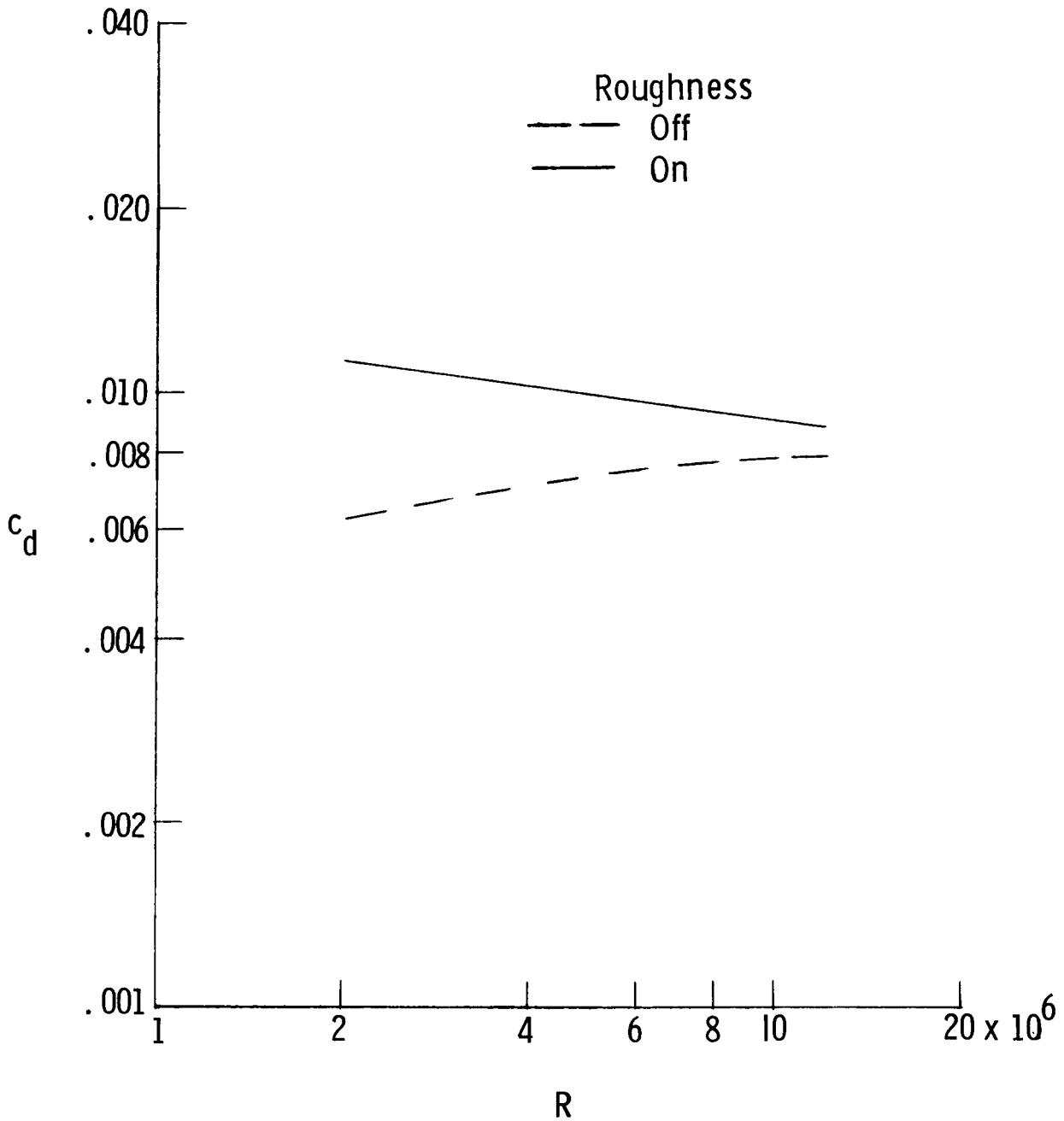

Figure 21.- Variation of drag coefficient with Reynolds number for MS(1)-0317 airfoil. M = 0.15; c_l = 0.30.

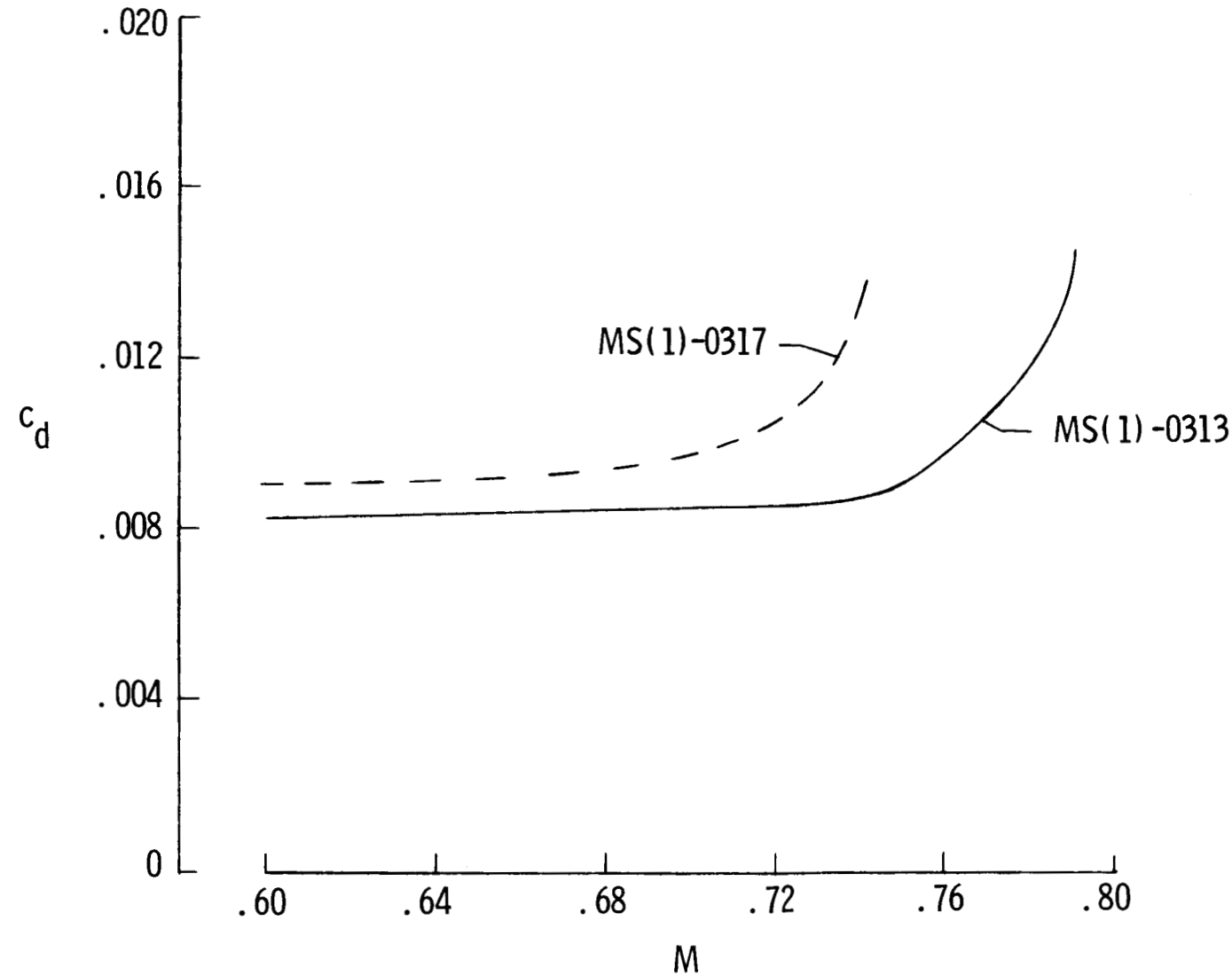

Figure 22.- Calculated drag-rise characteristics for medium-speed airfoils. $R = 14 \times 10^6$. $c_l = 0.30$.

1. Report No.	2. Government Accession No.	3. Recipient's Catalog No.
NASA TP-1786		

4. Title and Subtitle	5. Report Date
LOW-SPEED AERODYNAMIC CHARACTERISTICS OF A 17-PERCENT-THICK MEDIUM-SPEED AIRFOIL DESIGNED FOR GENERAL AVIATION APPLICATIONS	December 1980
	6. Performing Organization Code: 505-31-33-05
7. Author(s): Robert J. McGhee and William D. Beasley	8. Performing Organization Report No.: L-13900
9. Performing Organization Name and Address: NASA Langley Research Center, Hampton, VA 23665	10. Work Unit No.
	11. Contract or Grant No.
12. Sponsoring Agency Name and Address: National Aeronautics and Space Administration, Washington, DC 20546	13. Type of Report and Period Covered: Technical Paper
	14. Sponsoring Agency Code

15. Supplementary Notes

16. Abstract

Wind-tunnel tests have been conducted to determine the low-speed two-dimensional aerodynamic characteristics of a 17-percent-thick medium-speed airfoil (MS(1)-0317) designed for general aviation applications. The results were compared with data for the 17-percent-thick low-speed airfoil (LS(1)-0417) and the 13-percent-thick medium-speed airfoil (MS(1)-0313). Theoretical predictions of the drag-rise characteristics of this airfoil are also provided. The tests were conducted in the Langley Low-Turbulence Pressure Tunnel over a Mach number range from 0.10 to 0.32, a chord Reynolds number range from 2.0×10^6 to 12.0×10^6, and an angle-of-attack range from about -8° to 20°.

17. Key Words (Suggested by Author(s))	18. Distribution Statement
Low-speed characteristics Medium-speed airfoil Reynolds number effects Mach number effects General aviation aircraft	FEDD Distribution Subject Category 02

19. Security Classif. (of this report)	20. Security Classif. (of this page)	21. No. of Pages	22. Price
Unclassified	Unclassified	84	

Available: NASA's Industrial Applications Centers

NASA-Langley, 1980